

**Recent climate variability at the Antarctic Peninsula
and coastal Dronning Maud Land, based on
stable water isotope data**

**Dissertation
zur Erlangung des akademischen Grades
"doctor rerum naturalium"
(Dr. rer. nat.)
in der Wissenschaftsdisziplin "Geowissenschaften"**

**eingereicht an der
Mathematisch-Naturwissenschaftlichen Fakultät
der Universität Potsdam**

von

Francisco Fernandoy

Potsdam, den 21.2.2011

Acknowledgement

I would like to thank Prof. Dr. Hans-Wolfgang Hubberten for the supervision and support to this PhD thesis at the Alfred Wegener Institute for Polar and Marine Research. The generous financial support of the German Academic Exchange Service (DAAD) is greatly acknowledged. The expedition to field supported by the DFG (444CHL-113/40/0-1) and AWI.

This work would not exist without the support of many persons, which in one way or the other helped in the field, the laboratory and in the daily life. To all of them many thanks. A big space in this page belongs to Hanno Mayer, whose support and guidance during this PhD. thesis was beyond of any necessary duty. To Hanno many, many thanks for his sincere friendship and always opportune advice. As well as for the many days expended together in the field. An important place in these lines belongs to all my AWI colleagues, especially to Hans Oerter, Diedrich Fritzsche, Wolf-Dieter Hermichen, Anna Wegner, Thomas Opel and Bernhard Chaplign for the rich scientific and personal discussion in many occasions. I sincerely thank Anna Kloss, Cindy Springer, Eileen Nebel, Lutz Schönicke, Hugues Lantuit, Kasha Fröb and Jennifer Sobiech for their support at work and friendship.

I also would like to thank to my Chilean advisors, who opened the door to the polar research. Especially acknowledged is Dr. José Retamales for his trust and support to our activities in Antarctica, and Dr. Guillermo Alfaro for inspiring me to study abroad. Dr. Carlos Cárdenas and all other members of the Antarctic Department of the Magallanes University are recognized for their crucial help, when organizing the field campaigns. The Antarctic Section of the Chilean Army played a very important role on the realization of this investigation for their logistical and scientific support. To the overwintering crews and exploration personal, who gave us support in the field.

I especially want to acknowledge my family, my parents Cecilia and Luis, and my brother and sister for always take care of my even at long distance.

To the Schrader family, thanks for helping me give my first steps in Germany and the constant words of encouragement and interest in my work. I also want to thank all my friends, who made from Berlin and Potsdam a new home.

Finally, very special thank to my girlfriend Alena Maul, for being very encouraging and patience especially during the time writing this thesis. Thank you very much for the accompany me.

Table of contents

ACKNOWLEDGEMENT.....	I
TABLE OF CONTENTS	II
LIST OF FIGURES.....	IV
LIST OF TABLES	VI
ABSTRACT.....	VII
1 INTRODUCTION.....	1
1.1 SCIENTIFIC BACKGROUND	1
1.2 STRUCTURE AND OBJECTIVES OF THIS INVESTIGATION	4
2 STUDY AREA.....	6
2.1 ANTARCTIC PENINSULA AND SOUTH SHETLAND ISLANDS, WEST ANTARCTICA	6
2.2 COASTAL DRONNING MAUD LAND.....	7
3 STABLE WATER ISOTOPES OF PRECIPITATION AND FIRN CORES FROM THE NORTHERN ANTARCTIC PENINSULA REGION AS A PROXY FOR CLIMATE RECONSTRUCTION.	8
3.1 ABSTRACT	8
3.2 INTRODUCTION	8
3.3 STUDY AREA	10
3.4 METHODS.....	13
3.5 RESULTS AND DISCUSSION	17
3.5.1 $\delta^{18}O$ and δD	17
3.5.1.1 Precipitation samples	18
3.5.1.2 Firn cores.....	22
3.5.2 Deuterium excess	24
3.5.2.1 <i>d</i> excess of precipitation.....	24
3.5.2.2 Deuterium excess of firn cores.....	26
3.5.3 Main δ and <i>d</i> excess forcing.....	30
3.6 BACKWARD TRAJECTORY MODEL.....	33
3.7 CONCLUSIONS.....	35
4 SEASONAL TO DECADEAL CLIMATE VARIABILITY IN THE NORTHERN ANTARCTIC PENINSULA REGION FROM 50 YEARS OF METEOROLOGICAL RECORDS AND ICE-CORE TIME SERIES	37
4.1 ABSTRACT	37
4.2 INTRODUCTION	37
4.3 STUDY REGION:.....	40
4.4 DATA AND METHODS:.....	42

4.4.1	<i>Meteorological data</i>	42
4.4.2	<i>SAM and ENSO indices</i>	42
4.4.3	<i>Stable-water- isotope time series</i>	43
4.4.4	<i>Statistical treatment</i>	44
4.5	RESULTS:	45
4.5.1	<i>Air temperature (T_{air}) trends:</i>	45
4.5.2	<i>Meteorological variability and its relationship to SAM:</i>	48
4.5.3	<i>Stable water isotopes of precipitation and firn cores and their relationship to SAM:</i>	51
4.6	DISCUSSION.....	55
4.7	CONCLUSIONS	61
5	TEMPORAL AND SPATIAL VARIATION OF STABLE ISOTOPE RATIOS AND ACCUMULATION RATES IN THE HINTERLAND OF NEUMAYER STATION, EAST ANTARCTICA	63
5.1	ABSTRACT	63
5.2	INTRODUCTION	63
5.3	STUDY AREA AND BACKGROUND INFORMATION:	65
5.4	METHODS	67
5.5	RESULTS.....	68
5.5.1	<i>Dating of the firn cores:</i>	68
5.5.2	<i>Accumulation:</i>	72
5.5.3	<i>$\delta^{18}O$ and δD</i>	75
5.5.4	<i>Deuterium excess:</i>	79
5.6	DISCUSSION.....	81
5.6.1	<i>$\delta^{18}O$-Temperature relationship:</i>	81
5.6.2	<i>Temporal stable isotope trends:</i>	84
5.6.3	<i>Temporal and spatial variation of the d excess:</i>	87
5.7	CONCLUSIONS	88
6	SYNTHESIS:.....	91
6.1	CHARACTERISTICS OF THE RECENT CLIMATE VARIABILITY OF ANTARCTICA.....	91
6.2	STABLE WATER ISOTOPE COMPOSITION OF RECENT PRECIPITATION AND IMPLICATIONS FOR THE CLIMATE VARIABILITY	93
6.3	STABLE WATER ISOTOPE VARIABILITY OF FIRN CORES	95
6.4	ISOTOPE COMPOSITION OF FIRN CORES AND ITS RELATIONSHIP TO THE CLIMATE FORCING MODES.....	98
6.5	ON THE POTENTIAL OF THE STABLE WATER ISOTOPES AS PROXY FOR CLIMATE-RECONSTRUCTION: CONCLUSIONS, IDEAS FOR FUTURE RESEARCH AND OUTLOOK.....	101
7	REFERENCES	104

List of Figures

FIGURE 1.1: THE ANTARCTIC CONTINENT AND SURROUNDING OCEANS.	1
FIGURE 3.1: MAP OF LOCATIONS MENTIONED IN CHAPTER 3.	11
FIGURE 3.2: MEAN ANNUAL AIR TEMPERATURE OF THE BELLINGSHAUSEN, KING GEORGE ISLAND, AND O´HIGGINS STATION	12
FIGURE 3.3: PICTURE OF THE PLATEAU LACLAVERE (63°27´10´´S, 57°45´32´´W).....	13
FIGURE 3.4: OVERVIEW OF THE STUDY AREA ON KING GEORGE ISLAND	16
FIGURE 3.5: OVERVIEW OF THE STUDY AREA IN THE NORTHERN ANTARCTIC PENINSULA REGION..	17
FIGURE 3.6: ISOTOPIC COMPOSITION OF PRECIPITATION SAMPLES FROM O´HIGGINS STATION.....	19
FIGURE 3.7: MEAN MONTHLY DELTA ¹⁸ O VALUES OF PRECIPITATION FROM O´HIGGINS STATION.....	20
FIGURE 3.8: CO-ISOTOPE RELATIONSHIPS	21
FIGURE 3.9: DELTA ¹⁸ O SIGNAL OF FIRN CORES FROM THE ANTARCTIC PENINSULA AND KING GEORGE ISLAND.....	23
FIGURE 3.10: D EXCESS OF DAILY PRECIPITATION SAMPLES FROM O´HIGGINS STATION	25
FIGURE 3.11: MONTHLY D EXCESS MEAN OF PRECIPITATION SAMPLES FROM O´HIGGINS STATION.....	26
FIGURE 3.12: D EXCESS OF FIRNCORES FROM ANTARCTIC PENINSULA AND KING GEORGE ISLAND.....	28
FIGURE 3.13: SEASONALITY OF D EXCESS PRESENTED BY FIRN CORES FROM KING GEORGE ISLAND AND ANTARCTIC PENINSULA.	29
FIGURE 3.14: SEASONAL VARIATION OF D EXCESS OF CORES FP-1 AND OH-6.	32
FIGURE 3.15: FREQUENCY OF TRACK OF THE SINGLE (3-DAYS) BACKWARD TRAJECTORIES.....	33
FIGURE 3.16: BACKWARD TRAJECTORIES CLUSTERING FOR PRECIPITATION EVENTS AT O´HIGGINS.....	35
FIGURE 4.1: LOCATIONS REFERENCED IN CHAPTER 4.	41
FIGURE 4.2: MONTHLY AIR TEMPERATURES FROM BELLINGSHAUSEN, O´HIGGINS AND ESPERANZA STATIONS	46
FIGURE 4.3: MEAN ANNUAL AIR TEMPERATURE (1960-2009) OF O´HIGGINS , ESPERANZA STATIONS AND THE SAM INDEX	49
FIGURE 4.4: STABLE WATER ISOTOPE COMPOSITION OF MONTHLY MEAN PRECIPITATION SAMPLES FROM BELLINGSHAUSEN, O´HIGGINS AND SAM INDEX.	52
FIGURE 4.5: D EXCESS OF THE CORES OH-6 AND FP-1 CORES AND THE SAM INDEX.	53
FIGURE 4.6: A MEAN ANNUAL AIR TEMPERATURES FROM BELLINGSHAUSEN STATION, SAM INDEX AND ESTIMATED DELTAD MEANS FROM THE FIRN CORE OF SIMÕES ET AL. (2004A)..	54
FIGURE 4.7: SPECTRAL AND CROSS-SPECTRAL ANALYSIS OF THE METEOROLOGICAL TIME-SERIES.....	58
FIGURE 4.8: BANDPASS FILTERED TIME-SERIES OF METEOROLOGICAL DATA AND SAM INDEX.....	59
FIGURE 4.9: COMPARISON OF THE AIR TEMPERATURE FROM O´HIGGINS , ESPERANZA TO DELTA ¹⁸ O TIME SERIES FROM THE GOMEZ PLATEAU ICE CORE.	60
FIGURE 4.10: SPECTRAL DENSITY OF THE DELTA ¹⁸ O TIME SERIES OF THE GOMEZ PLATEAU ICE CORE AND CROSS-SPECTRAL SQUARED COHERENCY AGAINST ENSO AND SAM INDEX.....	61
FIGURE 5.1: GEOGRAPHICAL LOCATION OF THE DRILLING SITES. B38, FB0702 ; B39 AND FB0704.....	67
FIGURE 5.2: TIME SERIES (1960-2007) OF STABLE WATER ISOTOPES FROM THE CORES B38 AND FB0702 (HALVFARRYGGEN) AS WELL AS B39, AND FB0704 (SØRÅSEN).	70
FIGURE 5.3: TRITIUM PROFILE OF FIRN CORES B38 AND B39 TO THE TRITIUM PROFILE OF PRECIPITATION AT KAITOKE.....	71
FIGURE 5.4: DI-ELECTRICAL PROFILES OF THE CORES B38, B39, FB0702, AND FB0704.....	71

FIGURE 5.5: MEAN ANNUAL ACCUMULATION RATES FOR THE CORES B39, FB0704, B38 AND FB0702.	73
FIGURE 5.6: DELTA ¹⁸ O AND D EXCESS DATA OF FRESH-SNOW SAMPLES FROM NEUMAYER STATION AND THE FIRN CORES FB0701, AND FB0703.	75
FIGURE 5.7: CO-ISOTOPE RELATIONSHIP OF THE CORES B38, B39, FB0702 AND FB0704.	77
FIGURE 5.8: HISTOGRAMS SHOWING THE STATISTICAL D EXCESS DISTRIBUTION OF B38, B39, FB0702 AND FB0704.	80
FIGURE 5.9: COMPARISON OF MEAN MONTHLY AIR TEMPERATURES COMPOSITE AT NEUMAYER STATION AND SEASONAL DELTA ¹⁸ O.	81
FIGURE 5.10: CORRELATION OF RE-SAMPLED MEAN DELTA ¹⁸ O VALUES FROM THE FIRN CORES B38 , B39,, FB0702 AND FB0704 TO MONTHLY MEAN AIR TEMPERATURE.	82
FIGURE 5.11: CORRELATION OF DELTA ¹⁸ O VALUES FROM FRESH-SNOW SAMPLES AGAINST AIR TEMPERATURE	83
FIGURE 5.12: DELTA ¹⁸ O ANOMALY INDEX IS SHOWN OF THE FIRN CORNS FROM DRONNING MAUD LAND.	85
FIGURE 5.13: BOREHOLE TEMPERATURE PROFILES FOR CORES B38, B39 AND FB0702.....	86
FIGURE 6.1.: OVERVIEW OF ALL AREAS OF INVESTIGATION FROM THIS THESIS	92
FIGURE 6.2: DENSITY PROFILE OF THE FIRN CORE OH-6 (NORTHERN ANTARCTIC PENINSULA).....	96

List of Tables

TABLE 3.1: GEOGRAPHICAL LOCATION, MEAN ISOTOPE VALUES AND BASIC STATISTICS OF STABLE ISOTOPE ANALYSES OF ALL FIRN CORES RETRIEVED FROM KING GEORGE ISLAND AND THE NORTHERN ANTARCTIC PENINSULA	14
TABLE 3.2: MEAN DELTA ¹⁸ O AND DELTA D VALUES AND BASIC STATISTICS OF PRECIPITATION SAMPLES COLLECTED AT THE STATIONS: FREI AND O’HIGGINS.	15
TABLE 3.3: BASIC STATISTICS OF AIR TEMPERATURE AND AIR PRESSURE AT SEA LEVEL FOR BELLINGSHAUSEN STATION AND O’HIGGINS STATION	18
TABLE 3.4: CORRELATION MATRIX OF MEAN MONTHLY ISOTOPE VALUES: RESAMPLES OF THE HIGH ALTITUDE FIRN CORES (OH-6 AND FP-1), PRECIPITATION (OH) AND MAJOR SEASONAL FORCING OF METEOROLOGICAL VARIABILITY IDENTIFIED FOR THIS REGION	30
TABLE 3.5: CORRELATION MATRIX OF MONTHLY ISOTOPE MEANS OF FIRN CORE FP-1 AND OH-6 (RESAMPLE VALUES) AND PRECIPITATION FROM OH STATION.....	32
TABLE 3.6: SEASONAL FREQUENCIES OF THE BACKWARD TRAJECTORY CLUSTERS CALCULATED FROM SINGLE EVENTS AT O’HIGGINS STATION.....	34
TABLE 3.7: MEAN ISOTOPIC COMPOSITION OF BACKWARD TRAJECTORY CLUSTERS, EACH CLUSTER CONTAINS N SINGLE EVENTS.....	35
TABLE 4.1: BASIC STATISTICS OF THE METEOROLOGICAL RECORD OF THE STATIONS BELLINGSHAUSEN, O’HIGGINS AND ESPERANZA .	45
TABLE 4.2: TEMPERATURE TRENDS OF BELLINGSHAUSEN, O’HIGGINS, AND ESPERANZA STATIONS	47
TABLE 4.3: CORRELATION COEFFICIENTS MATRIX OF AIR TEMPERATURE AND SEASONAL MEANS.....	47
TABLE 4.4: CORRELATION COEFFICIENTS OF THE ANNUAL TEMPERATURE MEANS AND THE SAM INDEX.....	49
TABLE 4.5: SEASONAL CORRELATION COEFFICIENTS BETWEEN SAM AND AIR TEMPERATURES FOR THE PERIOD 1960-2009	50
TABLE 4.6: CORRELATION COEFFICIENTS OF LINEAR REGRESSIONS OF THE SEASONAL D EXCESS VALUES OF THE FIRN CORES FP-1 AND OH-6 TO THE SAM INDEX..	54
TABLE 4.7: CORRELATION MATRIXES BETWEEN AIR TEMPERATURE AND AND SAM INDEX SEASONAL MEANS	56
TABLE 5.1: OVERVIEW DATA SET OF THE CORES B38, B39, FB0702 AND FB0704 ANALYSED IN THIS PAPER,	78
TABLE 5.2: SUMMARY OF STABLE WATER ISOTOPE DATA OF FRESH-SNOW SAMPLES COLLECTED AT THE NEUMAYER STATION	79
TABLE 5.3: CORRELATION MATRIX BETWEEN THE DELTA ¹⁸ O VALUES OF CORES B38, B39, FB0702, AND FB0704.	86
TABLE 5.1: SUMMARY OF THE MEAN ANNUAL AIR TEMPERATURE AND STABLE WATER ISOTOPE COMPOSITION FOR ALL CORES OF THIS THESIS	94
TABLE 5.2: OVERVIEW OF THE ESTIMATED AGES AND STABLE WATER ISOTOPE COMPOSITION OF ALL FIRN CORES	
TABLE 5.3: SUMMER CORRELATION MATRIXES OF MONTHLY ISOTOPE MEANS FROM ALL FIRN CORES FROM COASTAL DML AND SAM AND ENSO MODES.....	100

Abstract

The Antarctic Peninsula (AP) is a hotspot of the recent climate instability of the Antarctic Continent. The highest warming trends are observed at north (Esperanza station $+0.4^{\circ}\text{C decade}^{-1}$) and the west ($+0.6^{\circ}\text{C decade}^{-1}$) of AP. On the other hand, the interior of the continent and most of coastal East Antarctica does not show any clear warming (cooling) trend. Only isolated spots of warming and cooling around the coastal areas are detected. In this thesis, the recent climate variability of two coastal regions of Antarctica is investigated. This study is mainly based on the analysis of stable water isotope of firn cores and precipitation samples from these regions.

First, the northern Antarctic Peninsula and the George Island (South Shetland Islands) are investigated. From the combined isotope composition of precipitation and a backward trajectories model, it was found that the precipitation at this region originates mainly from the South Pacific sector (warmer) and the Amundsen-Bellinghousen Sea (colder). From a firn core retrieved at the AP divide (Plateau Laclavere), a first accumulation rate ($2350 \text{ kg m}^{-2} \text{ a}^{-1}$) has been derived for this unexplored region. The stable water isotope composition of firn cores shows a statistically significant correlation with air temperature (T_{air}), and to relative humidity and sea ice conditions at the nearby Amundsen-Bellinghousen Sea. Moreover, a marked correlation is found between the isotope composition and the Southern Annular Mode (SAM). Hence, SAM is the principal mode of the climate variability on the region in a sub-annual to inter-annual time scale, as observed from the time series analysis of meteorological data and from long ice core records (Gomez Plateau).

The second area investigated is located in coastal Dronning Maud Land (DML), East Antarctica. DML shows no T_{air} trends for the last 20 years from meteorological records. The stable water isotope composition of four cores from the hinterland and one core from Ekströmisen, expand the meteorological record back to ~ 1892 AD. From these records no significant trend is observed from the $\delta^{18}\text{O}$ time series since 1960. According, no temporal changes of the accumulation rates are observed, which strongly vary from the coast ($360 \text{ kg m}^{-2} \text{ a}^{-1}$) to the hinterland ($1260 \text{ kg m}^{-2} \text{ a}^{-1}$). In contrary to AP no consistent correlation are found between SAM and long isotope records, and only sporadic periods (e.g.: 1970-2000) of statistically significant correlations occurs between SAM and $\delta^{18}\text{O}$ (T_{air}). Moreover, the strongest SAM and $\delta^{18}\text{O}$ (T_{air}) correlation are found for the summer season. The recent climate variability of coastal Antarctica is clearly modulated by the major climate mode (SAM and ENSO), however both records for both DML and the AP are too short to reflect a reliable climatic picture of the post-industrial era. Therefore we propose two new localities for coring campaigns aiming to retrieve a medium depth (150-200 m ice) core in AP (Plateau Laclavere) and a medium to depth (>300 m) at DML (Halvfarryggen).

1 Introduction

1.1 Scientific background

The Antarctic continent is the world's largest reserve of freshwater (70%) and expands over $14 \times 10^6 \text{ km}^2$ (Turner et al., 2009). Most of the area is covered by ice (99.1%) with an estimated volume of the ice sheet of around $27 \times 10^6 \text{ km}^3$ (Huybrechts et al., 2000). The Antarctic ice sheet is in average 1900 m thick (reaching up to 4700 m in some locations) with a maximal estimated age of more than 1 million years (Turner et al., 2009). The ice sheet is morphologically divided into three main regions: West Antarctica, East Antarctica and the Antarctic Peninsula (Figure 1.1), which are under the influence of different climatic domains. The East Antarctic Ice Sheet (EAIS) is by far the largest ($10.4 \times 10^6 \text{ km}^2$) and coldest region, whereas the West Antarctic Ice Sheet (WAIS) is smaller ($1.97 \times 10^6 \text{ km}^2$). The WAIS is considered as a marine ice sheet, since it rests on a bed below sea-level (Ainley et al., 2009). Finally, the Antarctic Peninsula is the smallest ice sheet ($0.52 \times 10^6 \text{ km}^2$), with alpine-glacier characteristics and maritime climate regime (King et al., 2003; Pritchard and Vaughan, 2007).

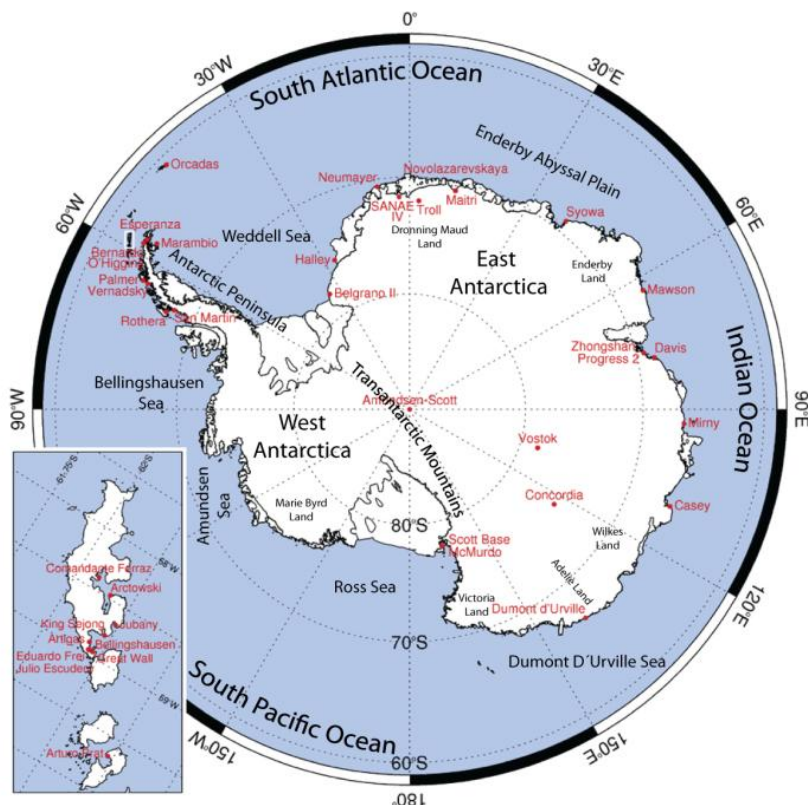


Figure 1.1: The Antarctic Continent and surrounding oceans. The most important geographical features (black labels) and research stations (red labels) are displayed. The small inserted map shows King George Island (South Shetland Islands). Map modified from Turner et al. (2009).

The climatic isolation of Antarctica started with the opening of Tasman Seaway (between Australia and Antarctica) at around 30 to 35.5 Ma. (Wei, 2004), and the opening of the Drake Passage (between South America and Antarctica) at about 40 Ma (Scher and Martin, 2006). The opening of these two passages created the appropriate conditions for the onset of the Antarctic circumpolar current, which isolated and cooled the continent (Abram et al., 2009). The Antarctic continent plays a dominant role in the world's climate regulatory system through the heat exchange from the atmosphere and the ocean between tropical and South Polar regions (Bromwich et al., 1998; Trenberth and Caron, 2000; Lumpkin and Speer, 2007). For this reason, the recent increase of the climate variability and oceanic/atmospheric warming observed especially in coastal West Antarctica and in some specific regions of East Antarctica (Levitus et al., 2005; Chapman and Walsh, 2007), has attracted the scientific interest of many research groups.

The Antarctic climate is modulated by different factors in timescales from millennial (Milankovitch cycles), decadal (El Niño; ENSO) and interannual to seasonal scales (Southern Annular Mode) (Ainley et al., 2009). Recently, it has been suggested that the warming trends at the Antarctic coast are coupled to the intensification of the circumpolar westerlies, which occurs as consequence of the strengthening of the Southern Annular Mode (SAM) (Trenberth et al., 2007; Marshall et al., 2011). However, the exact onset and the cause (natural or anthropogenic) for this warming phenomenon is still matter of debate.

The modern scientific exploration of Antarctica started during the international geophysical year in 1957. Since then, many systematic meteorological records were gained. However, these records just cover the last 50 years and therefore do not include the beginning of the atmospheric warming phenomenon (Steig et al., 2009). Moreover, many of the stations are located in the Antarctic Peninsula region as well as in the coastal regions of the Antarctic continent (Figure 1.1), provoking a geographical bias of the existing information. For this reason, different climate proxies have consequently been used to extend the existing meteorological records into the past. The stable water isotope composition of firn and ice cores is a well-established indicator of air temperature variations, as for atmospheric and circulatory changes from centennial to sub-annual scales (e.g.: EPICA community members, 2004; Masson-Delmotte et al., 2008; Divine et al., 2009; Stenni et al., 2010b). Some ice core evidence suggests that the present warming phenomenon in West Antarctica began in the late 19th Century (Schneider et al., 2006). However, this assumption is not well documented. Since the local climate variability in coastal regions is high, single records (e.g. ice cores) are not well suited to properly capture the regional climate variability. Thus, a broad network of high resolution records is still needed to compile a regional climate variability frame, which is

recognized as a scientific duty to achieve (e.g.: IPICS 2K Network, Brook et al., 2006). The understanding of climatically highly sensitive regions like the west side of the Antarctic Peninsula is an example of a future task to be completed. The west side of the Antarctic Peninsula has been identified as one of worldwide warming hotspots (Vaughan et al., 2003). Nonetheless, not much glaciological work has been done in this relatively warm and humid region so far, and very few ice cores were yet retrieved, e.g.: on James Ross Island (Aristarain et al., 2004) and at Gomez Plateau (Thomas et al., 2008). The scarcity of the data is due to logistical challenges, but also related to the complexity to core in temperate or polythermal ice and to interpret the glaciological proxy data. Main problems may include surface melt and subsequent percolation of melt water (Koerner, 1997). Additionally, a less distinct seasonality due to the proximity of the ocean as well as higher accumulation rates (consequently lower temporal information within one meter of ice core) complicates the interpretation of the obtained geochemical data. However, recent scientific and technical advances allow obtaining reliable and climate-relevant glaciological information from glaciers with evident melt and percolation i.e.: in Spitzbergen (Isaksson et al., 2005), the Siberian Arctic (Weiler et al., 2005; Opel et al., 2009) and Patagonia (Kohshima et al., 2007). Nonetheless, the interpretation of the working area and this kind of proxy is not simple and requires a detailed understanding of the different parameters affecting the isotope composition of precipitation stored in the glacier ice (e.g.: sea surface temperature - SST, sea ice conditions, moisture sources and others). These climatic factors can be unveiled when studying recent precipitation. Precipitation data can be correlated not only with air temperature variations, but also with the climatic conditions at the ocean surface (Uemura et al., 2010), and by this atmospheric (tele) connections and circulation shifts (Divine et al., 2009), as well as local effects may be assessed (Thomas and Bracegirdle, 2009). Therefore, the study of recent precipitation is a key component in this region for understanding the recent climate variability on sub-annual to decadal time scales, which can be used for the interpretation of paleo-precipitation stored in the ice-sheets.

In contrast to the high climate variability from coastal West Antarctica and the Antarctic Peninsula, the coast of East Antarctica presents relatively stable cold climatic conditions and only restricted regions present either negative or positive air temperature trends (Chapman and Walsh, 2007). Of special interest of investigation, is the coastal region of Dronning Maud Land. This area faces the Atlantic Sea, but receives moisture from the Weddell Sea, and the Drake Passage sector to west (Schlosser et al., 2008), which are in part under climatic influence of the Antarctic Peninsula. Moreover high accumulation rates described for this region (Schlosser et al., 2002) ensure that a high resolution paleo-climatic dataset is stored in the ice-sheet.

1.2 Structure and objectives of this investigation

This dissertation is presented in a cumulative structure including three papers (published, in review and in preparation for publication) in international ISI-ranked journal. These manuscripts tackle the recent climate variability of two coastal Antarctic regions: (1) the coastal Dronning Maud Land (DML) and (2) the Antarctic Peninsula area. The study incorporates an extensive set of firn cores (more than 80 m in total) and precipitation samples (in total more 600 daily samples), from both regions collected during field seasons between 2007 and 2010. For DML, precipitation samples are available from 1981 to 2006. The thesis combines data from two different projects: (1) The first expedition (2007) to Halvfarryggen and Søråsen ridges at DML was carried out within the IPICS initiative (Brook et al., 2006), by a German-Swiss team. (2) During 2008 and 2010, three expeditions (API 2008-2010) to the northern region of the Antarctic Peninsula region took place, where several shallow firn cores and snow pits were sampled. Moreover at two stations (O'Higgins and Frei) precipitation samples were continuously collected on a daily basis since 2008 until the present. The project dedicated to the Antarctic Peninsula was organized and carried out with the objective of characterize and select a suitable location for the extraction of a first medium-depth ice core in this region. However, the drilling of the medium-depth ice core is beyond the time frame of this PhD thesis, but is expected to be accomplished in the following seasons (DFG application pending). In order to cover decadal to centennial time scale, this work takes advantage of already available data to draw a broader regional and temporal picture in order to inter-compare the climate variability and its forcing modes, from sub-annual (high resolution) to decadal time scale.

To investigate and understand the recent climate variability of both West and East Antarctica some of following questions lead the direction of this thesis and these are addressed in the following chapters:

(1) Precipitation-meteorology: How is the atmospheric circulation variability related to the observed changes in the isotopic composition of precipitation and, thus, with the isotope-based climate reconstruction of firn/ice cores at both regions?

(2) Spatial climate variability: How different are stable isotope and accumulation trends in a northern Antarctic Peninsula (Laclavere and King George Island) compared to East Antarctica and to other locations such as the Gomez Plateau? What position has the Laclavere Plateau as a divide of the east and west coast of the northern Antarctic Peninsula? How similar are the altitudinal isotope (temperature) and accumulation gradients at the Antarctic Peninsula and coastal East Antarctica? Is the intensification of westerlies detectable in the stable isotope signal of both regions?

(3) Temporal climate variability: When did the climate warming start and reached significance at the northern tip of the Antarctic Peninsula? Did the climate variability have a seasonal component different than today throughout the last decades?

(4) Main drivers for climate change: Is SAM also the main driver for climate variability in pre-instrumental times as well as on longer time scales or are there other dominant forcing modes? How different is the signature of the modes over the northern Antarctic Peninsula and East Antarctica? Is that influencing the present temperature trends of both regions?

This investigation was based mainly on the analysis of the stable-water isotope composition of firn cores and recent precipitation samples. The stable isotope data was statistically compared through time series analyses techniques to the main climatological factors that dominate this region: surface air temperature, air pressure, sea ice extent, relative humidity and SST. The central objective of this work is to characterize the recent climate variability of the coastal Antarctica and understand the influence of the main climate drivers of this region (i.e.: SAM and ENSO oscillations) under the present scenario of strong warming in the Antarctic Peninsula area and the relative stability of coastal East Antarctica.

Chapter 3 of this thesis summarizes the results and interpretation of firn cores and precipitation samples collected in the Antarctic Peninsula area (Fernandoy et al., in review). The potential of the stable water isotope composition of the cores from different localities is discussed and confirmed. The paper includes a detailed description of the atmospheric circulation and is based on the isotopic variability as well as on a backward air parcel trajectory model, describing the moisture source and the air paths of the humidity transport of the precipitation arriving at this region. Chapter 4 extends the observations and conclusions of the previous chapter to a longer (decadal to centennial) time scale (Fernandoy et al., in preparation for submission). For this purpose, our data was complemented by and compared to climate records from earlier investigations. The dominant influence of SAM, as well as the sporadic influence of ENSO oscillations on the climate variability of the region was studied. Chapter 5 is based on the analysis of four firn cores from DML and on precipitation samples collected at the Neumayer Station. The potential for a high-resolution paleo-climate record of up to 1.9 ka was assessed (Fernandoy et al., 2010). Chapter 6 discusses the statistical inter-comparison of the stable isotope composition of firn cores from coastal West and East Antarctica, using cross time-series analyses methods and the different response of both regions to climate oscillations is analyzed and discussed. This chapter synthesizes all the data and summarizes the principal results discussed in this thesis.

2 Study Area

The coastal region of Antarctica is particularly sensitive to the changing climate conditions due to the circumpolar wind regime currents and off-pole displacement of the continent (Turner et al., 2009). The combined effect of the wind and geographical factors, has lead to a strong warming) effect especially in West Antarctica (Steig et al., 2009). Coastal East Antarctica shows no defined warming (or cooling) patterns, and significant warming and cooling has been detected only in specific locations of the coastal region (Chapman and Walsh, 2007). The areas studied in this thesis represent two key locations to understand the recent climate variability. Both regions face in part the same sector of the Southern Ocean, where much of the warming is taking place, therefore likely to reflect the change on the southern oceans.

2.1 Antarctic Peninsula and South Shetland Islands, West Antarctica

The Antarctic Peninsula and the sub-Antarctic Islands comprise a long (>1000 km) and narrow (~100 km, excluding the ice shelf) mountain chain (Pritchard and Vaughan, 2007), that connects the Pacific Ocean in the north with the continental ice sheet in the south (Figure 1.1). Due to its geographical position, and characteristics this area is dominated by a strong maritime climate regime at the west side and drier and colder regime at the east side (Peel et al., 1988; King, 1994). It is the only Antarctic region that undergoes substantial melting in summer, especially in areas of low altitude (Pritchard and Vaughan, 2007). The ice sheet that covers the Antarctic Peninsula is composed by more than 400 individual glaciers and receives around 8% of the total precipitation of the Antarctic Continent (Cook et al., 2005).

During the field work (2008-2010), two localities in the region were visited. These areas include the ice cap covering King George Island (KGI) (62°23'S/58°27'W), and the ice sheet at the northern Antarctic Peninsula close to the Chilean Antarctic Station "Bernardo O'Higgins" (63.3° S, 57.9° W) (Figures 1.1), both located at the west side of the Antarctic Peninsula. KGI is the largest of the South Shetland Islands (1250 km²), covered by an ice cap by more of 90% of its extension. The annual surface temperature is around -2.3°C at sea level, as measured at different ground stations. The KGI area has been studied to some extent from a glaciological point of view (e.g.: Wen et al., 1998; Simões et al., 2004a; Blindow et al., 2010; Rückamp et al., 2010). The second locality investigated is the ice sheet situated near the Chilean O'Higgins Station. This region has been much less explored than KGI and no glaciological investigations have been carried out before this work. The meteorological conditions are similar to that of the KGI with slightly lower mean air temperatures at sea level (-3.8°C). Both localities display a similar air temperature trend of about +0.02°C a⁻¹ for the

last 40 years (Zitat). Throughout the field campaigns, fresh snow samples, surface snow from several snow pits and a total of 9 firn cores (up to 16 m depth) were collected and retrieved.

2.2 Coastal Dronning Maud Land

Dronning Maud Land (DML) is located in the sector of East Antarctica that faces the South Atlantic Ocean located between the meridians 20°W and 44°E and has a no defined south border (Figure 1.1). The total area of DML is of around 2.5×10^6 km². The coastal region extends to from the ice shelf border to the southern mountain ridges (200-350 km to the south), dividing this region from inland. The area under investigation in this work is located in the coastal western sector of DML and comprehends the Ekströmsen ice shelf and the surrounding ice ridges from Halvfarrygen (East) and Søråsen (West). Ekströmsen is a smallest ice shelf of DML, with an area of 8.7×10^3 km² (Schlosser et al., 1999). In this ice shelf area the German Neumayer station (as well as the old stations) is situated. For this reason, this area has been intensively investigated since the 1980s until the present. First exploration of the area dates back to the beginning of the 20th century (Schlosser et al., 1999). At the Neumayer Station continuous meteorological observations were carried out since 1981 (including precipitation collection). Moreover, periodic observations of accumulation rates and the compactation process took part near the Neumayer station (Schlosser et al., 2002). The area is characterized by a mean annual temperature of -16°C, with precipitation occurring mainly as moderate fall of snowflakes. Since Ekströmsen is located at the southern edge of the circumpolar low-pressure belt (König-Langlo and Loose, 2007), the troposphere is dominated by easterly winds. The ice shelf extends about 130 km to the south, being limited by Halvfarrygen and Søråsen. These ridges rise above 1000 m a.s.l. and separate the coastal from the interior region. In selected locations of Halvfarrygen and Søråsen, 4 firn cores (2 at each ridge) were extracted during the summer of 2007 in frame of the pre-IPICS activities by a German-Swiss expedition. Accumulation rates at the ridges are estimated to be high and the thickness of ice at this area reaches more than 800 m (Steinhage et al., 1999)

3 Stable water isotopes of precipitation and firn cores from the northern Antarctic Peninsula region as a proxy for climate reconstruction.

F. Fernandoy, H. Meyer and M. Tonelli

(The Cryosphere, Especial issue: "Ice and climate change: a view from the south", submitted)

3.1 Abstract

In order to investigate the climate variability in the north Antarctic Peninsula region, this paper focuses on the relationship between stable isotope content of precipitation and firn, and main meteorological variables (air temperature, relative humidity, sea surface temperature, and sea ice extent). Between 2008 and 2010, we collected precipitation samples and retrieved firn cores from several key sites in this region. We conclude that the deuterium excess oscillation represents a robust indicator of the meteorological variability on a seasonal to sub-seasonal scale. Low absolute deuterium excess values and the synchronous variation of both deuterium excess and air temperature imply that the evaporation of moisture occurs in the adjacent Southern Ocean. The $\delta^{18}\text{O}$ –air temperature relationship is complicated and significant only at a (multi)seasonal scale. Backward trajectory calculations show that air-parcels arriving at the region during precipitation events predominantly originate at the South Pacific Ocean and Bellingshausen Sea. These investigations will be used as a calibration for on-going and future research in the area, suggesting that appropriate locations are located above 600 m a.s.l. We selected the Plateau Laclavere, Antarctic Peninsula as the most promising site for a deeper drilling campaign.

3.2 Introduction

It is well known that Antarctica plays a key role in the earth's climate regulation. The influence of the Antarctic Circumpolar Current over the ocean and atmosphere in the Southern Hemisphere demonstrate the strong interconnection of the climate dynamics (White and Peterson, 1996). Lately, Antarctica has been in the focus of scientific attention, due to the elevated rate of atmospheric warming during the second half of the 20th century. The warming rate of $0.082^\circ\text{C decade}^{-1}$ as a mean value for whole Antarctica (Chapman and Walsh, 2007) is in fact close to the rate for the Southern Hemisphere warming (IPCC, 2007). However, the strong atmospheric warming detected over West Antarctica ($0.14^\circ\text{C decade}^{-1}$), especially over the western Antarctic Peninsula (WAP) ($0.4^\circ\text{C decade}^{-1}$), has no counterpart in any other region of the world (Vaughan et al., 2003; Turner et al., 2005; 2009;

Steig et al., 2009). The strongest trends were detected at coastal ground stations (e.g.: Vernadsky Station (formerly Faraday): $0.56^{\circ}\text{C decade}^{-1}$ 1951-2000), and especially during winter seasons in the 1990s. Since then the temperature trend seems to be at least stabilized or decreased (Turner et al., 2005; Chapman and Walsh, 2007). Until now the consequences of the present elevated temperature conditions are not fully understood. The South Pacific and Atlantic ocean's surface (0-300 m depth) have raised in temperatures by 0.13°C and 0.23°C , respectively, for the period 1955-2003 in response to the elevated air temperatures (Levitus et al., 2005). Moreover, the sea surface temperature increase at the WAP reached more than 1°C for the period 1955-1998 during summer season (Meredith and King, 2005), and coincident retreat of the sea ice extent since 1958 (Abram et al., 2010). Warmer oceanic water triggers the melting of the base of ice shelves (Shepherd et al., 2004), leading to events like the disintegration of the Wordie ice shelf (Rignot et al., 2005). Thus, these events facilitate an accelerated discharge flow of inland glaciers to the ocean (De Angelis and Skvarca, 2003). The retreat of the ice shelves and sea ice acts as a feed-back mechanism of atmospheric warming and a clear anti-correlation of the sea ice extent and surface air temperature at WAP exists (Weatherly et al., 1991; Turner et al., 2005; Bracegirdle et al., 2008). Up to 87% of 244 marine glacier fronts from the whole Antarctic Peninsula are presently retreating (Cook et al., 2005) and the height line of permanent dry snow has clearly ascended over the last decades (Rau and Braun, 2002; Tedesco et al., 2007). The warming of both the atmosphere and the ocean has been producing an increase of humidity, leading to raised snow accumulation rates in the southern WAP as shown by Thomas et al. (2008). However, the mass balance of the Antarctic Peninsula is negative with a loss of $\sim 38.1 \text{ Gt a}^{-1}$, mostly concentrated in the central and north regions ($\sim -28.6 \text{ Gt a}^{-1}$) according to Chen et al. (2009). Nonetheless, Hall (2009) shows that the ice shelf grounding line of the Antarctic Peninsula has constantly retreated since the Last Glacial Maximum and reached its approximate present position during the early Holocene time, with some glacier advances at around 7 ka, 5 ka, 2 ka and 0.7 ka in the Holocene. According to Hall (2009) the present overall glacier retreat in the area of the Antarctic Peninsula is not unique in recent periods, but is now reaching warm conditions similar to those of the mid-Holocene within a short period of time (decades). Moreover, the ice-shelve disintegration has not been detected even during the warm Holocene phases.

The rapid warming of the WAP most likely originated from the intensification of the westerly circumpolar trough and increasing transport of heat from the ocean at lower latitudes, which has been related to the positive shift of the Southern Annular Mode (SAM) index (Marshall, 2003) since the 1960's (Thompson and Solomon, 2002; Gillett et al., 2006; Marshall et al., 2006). The

intensification of SAM has recently been related to anthropogenic causes like increased concentration of greenhouse-gases in the atmosphere and ozone's stratospheric depletion (Gillett et al., 2008). Little is known about when these processes started and their evolution through the industrial period. Additionally, the existing scarce meteorological data (~50 years) is often interrupted and clearly geographically-biased, because most of the stations are located at coastal regions. For these reasons, a better and deeper understanding of the climate variability of the last decades to centuries is still urgently needed for the region. The stable-isotope composition of Antarctic ice offers a unique proxy to extend the existing meteorological records well beyond the pre-instrumental times. The interpretation of this of proxy is not straight forward and requires a detailed study of the different parameters affecting the isotope composition of precipitation stored in the glaciers. It has been demonstrated that precipitation reflects not only air temperature variations, but also conditions at the ocean surface, atmospheric teleconnections and circulation shifts, as well as other local effects (Ichiyanagi et al., 2002; Uemura et al., 2008; Thomas and Bracegirdle, 2009). In this paper we aim to construct a comprehensive isotope geochemical and hydrological data set to characterize the present climate and hydrological situation at the northern Antarctic Peninsula, a basis needed for on-going and future research in this region. This work is also aimed to contribute to the objectives of the newly created initiative of the Tropical to Polar Connections Institute (www.polar-tropical.org)

3.3 Study Area

Our study focuses mainly on the northern Antarctic Peninsula and the South Shetland Islands. Two key regions were selected for our field work due to their glaciological potential, relatively easy access, adequate logistical facilities and previous work. These two areas are the ice cap covering King George Island (KGI), South Shetland Islands, and the region south-east of the Chilean Antarctic Station "Bernardo O'Higgins" (later referred to as O'Higgins - OH) at the Antarctic Peninsula (API) (Figure 3.1).

KGI is a 1250 km² island covered by an ice cap with an extension of more than 1158 km² (>90% of KGI) (Simões et al., 1999). The climate regime of the island is characterized by maritime conditions. The surface mean annual air temperature (MAAT) recorded at the Russian Station Bellingshausen is -2.3°C for the period 1968-2009. A clear positive temperature trend of 0.025°C a⁻¹ is observed since the beginning of the meteorological record (Figure 3.2). According to Blindow et al. (2010) and Rückamp et al. (2010), the ice cap of KGI displays a polythermal regime, with a lower temperate part and a cold part above 400 m a.s.l. However, the exact line of transition between temperate and cold

regime is still a matter of discussion. The altitude of the ice cap reaches the 700 m a.s.l. in the central region of KGI (Blindow et al., 2010). Rückamp et al. (2010) and Wen et al. (1998) estimate that the MAAT at the highest point of the ice cap should be around -6 to -6.6°C. This implies that the KGI ice cap is very sensitive to climate variability. The firn/ice transition was identified by radio echo sounding profiles at a depth of 35 m (Blindow et al., 2010) and by density profiles of ice cores retrieved at the main glacier dome (700 m a.s.l.) in this island (Simões et al., 2004a). Both studies detected a water table above the firn/ice transition. As a consequence of the climatic conditions of the region, strong melting, melt water percolation, and refreezing processes are evident, thus making the drilling process and interpretation of the isotope signal in the temperate part of the ice cap complicated.



Figure 3.1: Map showing all locations mentioned in this paper, as stations in Antarctica (yellow dots), ice/firn core retrieve locations (red points), and on-going and future research areas (orange dots).

The second study region at the API had been much less explored and the scientific background is scarce. The coastal region displays similar meteorological conditions as for KGI, however, the MAAT at sea level is slightly lower (-3.8°C) for the period 1963-2008 at the O'Higgins Station, which is located 140 km to the south of KGI (Figure 3.1). The trend of the air temperature registered at this station is similar to that from KGI, with an increase of $0.022^{\circ}\text{C a}^{-1}$ (Figure 3.2). The nearby Laclavere Plateau (1030 m a.s.l.), around 19 km to the south-east of OH (Figure 3.1), was reached and explored for the first time during the austral summer 2010. The plateau has a flat surface of approximate 6 km

long and 3 km wide (Figure 3.3) and divides the warmer and moist west side from the colder and drier east side of API. Therefore, this plateau represents a key location to investigate the recent climate variation of the region. Using the same temperature gradients invoked by Rückamp et al. (2010) and Wen et al.(1998), the MAAT at Laclavere should be around -10°C, since the temperature oscillation recorded at OH are in the range of +/- 3.6°C, the air temperature should stay the whole year below the freezing point, making this area ideal for glaciological investigations.

In addition to the ice-coring work a network for collecting precipitation samples was established in cooperation with the Chilean Meteorological Service (DMC) and the Antarctic Department of the Chilean Army (DAE). Two stations collect precipitation samples and provide the meteorological record on a daily schedule since 2008 until present. These are located at the Antarctic Chilean Stations Eduardo Frei (FP) and Bernardo O’Higgins (OH), situated on Fildes Peninsula, KGI, and the API, respectively (Figure 3.1).

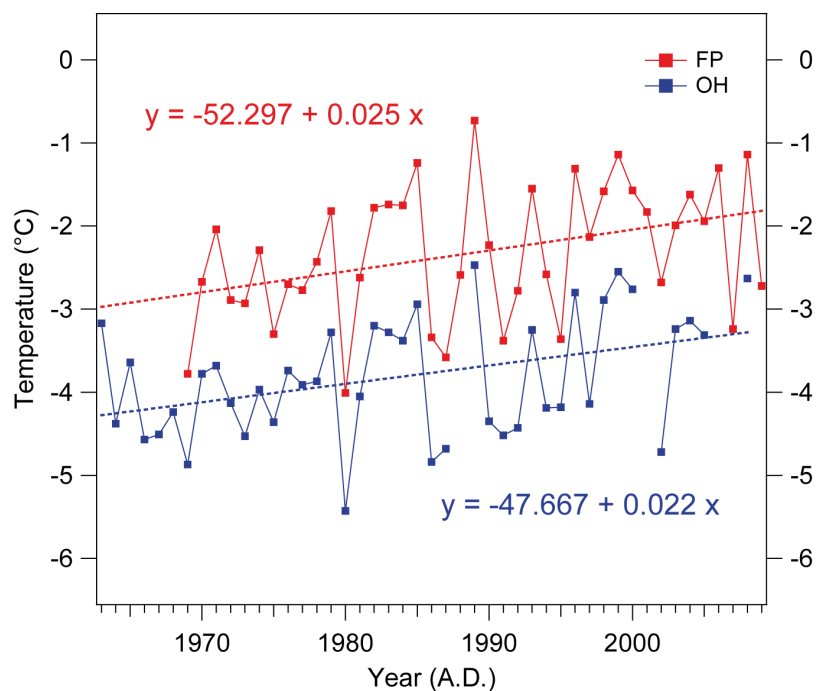


Figure 3.2: Mean annual air temperature (MAAT) of the last 4 to 5 decades from Bellingshausen station (FP, red line), King George Island, and O’Higgins station (OH, blue line), Antarctic Peninsula. For both stations linear regression (dotted lines) are presented, as well as the annual air temperature trend (equations).



Figure 3.3: Picture of the Plateau Laclavere ($63^{\circ}27'10''S$, $57^{\circ}45'32''W$, 1030 m a.s.l.) reached the first time on the 31st January 2010 with a Twin-Otter aircraft of the Chilean Air Force. From this location a firn core of 11m depth was extracted (OH-6).

3.4 Methods

During three consecutive summer campaigns (2008-2010), several firn cores (more than 80 meters in total) were retrieved from KGI and the northern part of API. At both localities, an altitudinal profile was completed from sea level up-to 1030 m a.s.l. A total of 7 firn cores is included in this paper: FP-1, FP-3 and FP-4 from KGI (Figure 3.4), and OH-1, OH-4, OH-5 and OH-6 from API (Figure 3.5); coordinates and further details of the firn cores are given in Table 3.1. At both stations of the precipitation collection network more than 300 samples were gathered (Table 3.2). The firn cores were retrieved using a mechanical drilling device (Rufli auger), stored frozen at O'Higgins and Chilean scientific station Escudero (King George Island) and later transported to the ice core processing facilities of the Alfred Wegener Institute in Bremerhaven, Germany. There, the cores were sampled with a 5 cm resolution for stable-isotope analyses. A visual logging and description of the cores was carried out to identify melt layers. Thereafter, firn and recent precipitation samples were analysed by Finnigan Delta-S mass spectrometers, following the gas equilibration technique as described by Meyer et al. (2000). Stable-isotope data is later compared to major meteorological and synoptic features of the region. For this purpose different data sets are incorporated to our analysis.

Core	FP-1	FP-3	FP-4	OH-1	OH-4	OH-5	OH-6
Site	KGI	KGI	KGI	API	API	API	API
Coordinates	62.13°S, 58.67°W	62.13°S, 58.77°W	62.16°S, 58.89°W	63.33°S, 57.84°W	63.36°S, 57.80°W	63.38°S, 57.62°W	63.45°S, 57.76°W
Drilling date	11.01.2009	06.02.2009	08.02.2009	23.01.2008	19.01.2009	31.01.2009	30.01.2010
Altitude (m a.s.l.)	620	440	130	220	350	620	1030
Depth (m)	15.56	15.28	1.42	14.96	15.75	10.6	11.02
<hr/>							
δ¹⁸O ‰							
Mean	-9.2	-9.7	-7.8	-9.7	-10.4	-10.2	-12.0
Sdev	1.5	0.9	0.4	0.4	1.2	1.5	2.5
Min	-18.2	-13.7	-8.5	-11.3	-14.1	-14.2	-19.8
Max	-5.2	-6.8	-6.6	-8.7	-7.0	-7.2	-6.5
δD ‰							
Mean	-70.2	-73.7	-61.4	-75.3	-78.9	-78.1	-91.4
Sdev	12.1	6.9	3.5	2.9	9.7	12.0	19.4
Min	-142.8	-105.8	-65.8	-88.9	-108.2	-111.2	-154.9
Max	-40.3	-43.9	-50.1	-67.4	-54.0	-52.1	-53.2
d excess							
Mean	3.8	3.8	1.2	2.2	4.0	3.9	4.4
Sdev	2.5	1.9	0.6	0.8	1.5	1.7	2.8
Min	-3.3	-2.3	0.2	0.0	0.5	-0.6	-2.6
Max	13.7	11.0	2.6	5.0	8.6	8.2	15.0
n (samples)	308	303	27	256	318	213	124

Table 3.1: Geographical location, mean isotope values and basic statistics of the high resolution (5cm) stable isotope analyses of all firn cores retrieved from King George Island (FP) and the northern Antarctic Peninsula (OH).

Station:	Frei (FP)	O'Higgins (OH)
Coordinates:	62.2°S, 58.96°W	63.32°S, 57.9°W
m a.s.l.:	45	13
$\delta^{18}\text{O}$ ‰		
Mean	-7.9	-9.2
Sdev	2.6	3.3
Min	-15.7	-19.4
Max	-1.8	-3.8
δD ‰		
Mean	-62.3	-70.5
Sdev	20.8	26.4
Min	-126.5	-150.6
Max	-10.7	-21.8
<i>d</i> excess		
Mean	0.6	2.7
Sdev	2.5	4.2
Min	-5.0	-6.6
Max	6.9	22.3
n (samples)	66	139

Table 3.2: Mean $\delta^{18}\text{O}$ and δD values and basic statistics of precipitation samples collected between February, 2008 and March 2009, and geographical coordinates of the corresponding collection stations: Frei (Fildes Peninsula, King George Island, South Shetland Islands) and O'Higgins (North Antarctic Peninsula).

Meteorological data at daily and monthly resolutions are available from the Global Summary of the Day (GSOD) data sets of the National Climatic Data Center (NCDC) (available at: www.ncdc.noaa.gov), the SCAR Reference Antarctic Data for Environmental Research (READER) (available at: www.antarctica.ac.uk/met/READER/) (Turner et al., 2004), respectively. Sea ice index and sea surface temperature (SST) time series were extracted from the Hadley Centre Sea Ice and Sea Surface Temperature data set (HadISST) (<http://www.metoffice.gov.uk/climatechange/science/monitoring/hadisst.html>). The HadISST provides SST on a global 1° to 1° grid and sea ice coverage fields were derived from in situ sea surface observations and satellite derived estimates. Sea ice coverage and SST fields are provided in monthly means from 1973 to the present (Rayner et al., 2003). NCEP/NCAR reanalysis data (Kalnay et al., 1996) was used to estimate the relative humidity (*h*) of the region. This reanalysis uses a state-of-the-art analysis/forecast system to perform atmospheric data assimilation from 1948 to the present.

Datasets are provided in a 2.5° to 2.5° latitude-longitude regular grid. HadISST and NCEP/NCAR fields were resampled to a regional scale in a Bellingshausen component (West Antarctic Peninsula), Weddell Sea component (East Antarctic Peninsula) and a whole region component (Bellingshausen and Weddell composite). The fields were resampled bordered by 85°W to 40°W longitude and 60°S to 90°S latitude limits. A field horizontal mean was computed to construct the time series used. Additionally, for each precipitation event registered at O'Higgins station, a 3-day air parcel backward trajectory was calculated to identify the moisture mass provenance. For this purpose, we used the free accessible Hybrid single-particle Lagrangian integrated trajectory (HYSPLIT) model (Draxler and Hess, 1998) (available at <http://ready.arl.noaa.gov/HYSPLIT.php>). This 3-D model was fed with the global data assimilation system (GDAS) archives from NOAA/NCEP (Kanamitsu, 1989). GDAS offers a global 1° to 1° latitude-longitude spatial coverage with a 6-hour temporal resolution and is available from 2004 to the present (for more details visit <http://ready.arl.noaa.gov/gdas1.php>). Single trajectories were later grouped in 4 major clusters for each station, following a statistical treatment that calculates the spatial variance of the trajectories.

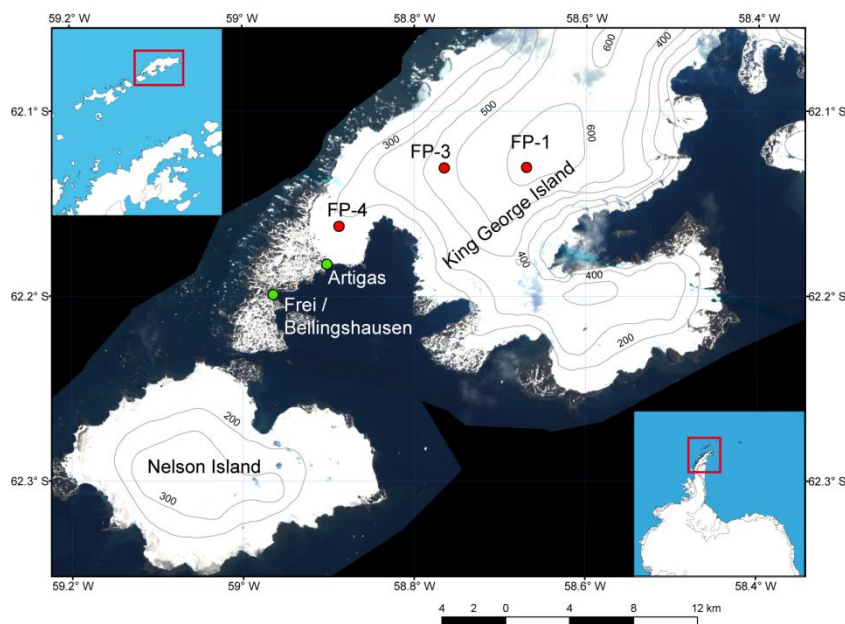


Figure 3.4: Overview of the study area on King George Island (KGI), South Shetland Islands. Precipitation samples and meteorological data were collected at the Chilean station Frei and the neighbouring Russian station Bellingshausen; expeditions to the KGI glacier were organized from the Uruguayan station Artigas (green dots). Three firn cores (red dots) were retrieved from this area between the local Bellingshausen dome (FP-4) and the main dome of KGI (FP-1).

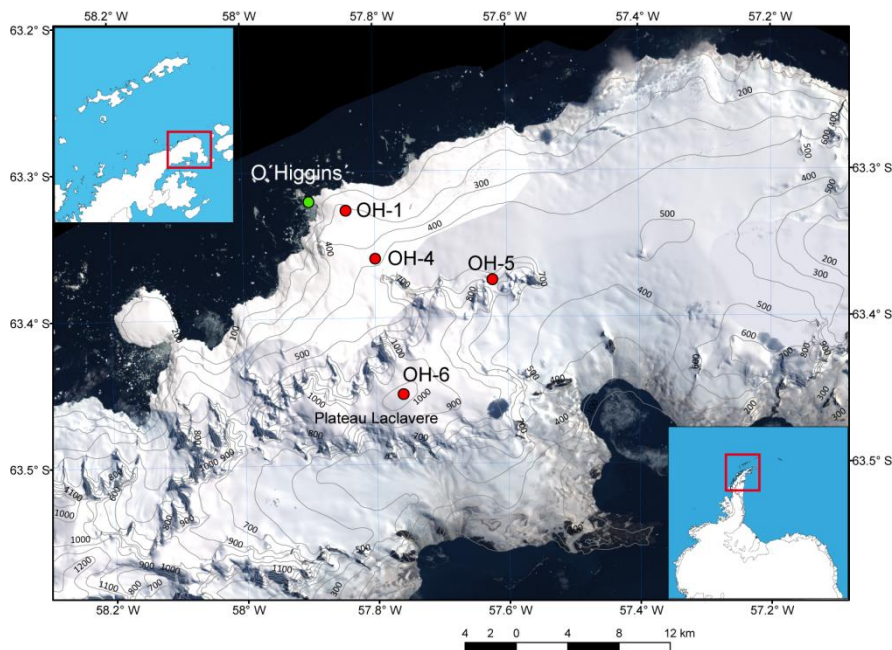


Figure 3.5: Study area in the northern Antarctic Peninsula region. The Chilean station O'Higgins (green dot) is located at the west side of the Antarctica Peninsula on the Isabel Riquelme Islet facing the Bransfield strait. At this station precipitation samples and meteorological data were collected. Between the O'Higgins station and the Plateau Laclavere (1030 m a.s.l.) four firn cores (red dots) were retrieved during 2008 and 2010. The Landsat 7 satellite image is available at the LIMA website (<http://lima.usgs.gov/>). Contour lines shown are from the Antarctic Digital Database (ADD) (www.add.scar.org:8080/add).

3.5 Results and discussion

3.5.1 $\delta^{18}\text{O}$ and δD

Stable isotopes (oxygen and hydrogen) content of water molecules in precipitation are considered as an excellent proxy to trace seasonal changes in air temperatures, especially in Polar Regions (Dansgaard, 1964; van Ommen and Morgan, 1997). Thermodynamic differences between the natural oxygen and hydrogen stable isotopes lead to the fractionation of water molecules ($^{18}\text{O}/^{16}\text{O}$ and $^2\text{H}/\text{H}$ ratios) during water phase changes (such as evaporation). Moreover a continuous depletion of the heavy isotopes occur relative to the temperature variation and trajectory of air masses during condensation (Dansgaard, 1964). Distillation of the heavy isotopes from an air mass will follow approximately a Rayleigh-type process (Dansgaard, 1964; Gat, 1996). In-cloud condensation of moisture occurs in an approximately closed system and therefore the isotopic composition at the moment of precipitation will depend mainly on the local air temperature (Rozanski et al., 1993; Gat, 1996; Clark and Fritz, 1997). This makes the isotope composition of precipitation suitable to identify air temperature fluctuations (e.g.: summer and winter oscillations) and changes in the air masses pathways and moisture sources. In the next section, oxygen and

hydrogen stable water isotopes of precipitation and firn core samples are presented, compared and discussed. All results are referred to the Vienna Standard Mean Ocean Water Standard (VSMOW) in ‰, as $\delta^{18}\text{O}$ and δD for oxygen and hydrogen isotopes, respectively.

3.5.1.1 Precipitation samples

Table 3.2 shows the results and basic statistics for the precipitation samples collected at FP and OH stations. At both stations the collection period was 14 months (February, 2008 to March, 2009). Unfortunately an extended gap in time during the collection in winter occurs at FP, as consequence of logistic difficulties linked with meteorological conditions and organization. Therefore, we base our analysis mainly on the samples collected at OH and transfer the conclusions to KGI, since meteorological conditions like mean air temperature (here referred to as T_{air}) of both localities highly correlate on a daily to seasonal time scale ($r = 0.89$, $p < 0.01$; February 2008 to March 2010). From the OH meteorological record, the mean daily air temperature T_{air} during the whole sampling period (-2.1°C) is around 0.3°C lower than the mean daily air temperature T_p calculated only for days with precipitation events. In parallel, a lower mean air pressure at sea level is observed during days with precipitation events compared to the whole period ($\text{MSLP}_p = 983.2$ mbar is 5 mbar lower than MSLP_{air}) (Table 3.3).

Bellingshausen - Daily					Bellingshausen - Monthly means				
	$T_{\text{air}} (^\circ\text{C})$	$T_p (^\circ\text{C})$	$\text{SLP}_{\text{air}} (\text{mbar})$	$\text{SLP}_p (\text{mbar})$		$T_{\text{air}} (^\circ\text{C})$	$T_p (^\circ\text{C})$	$\text{SLP}_{\text{air}} (\text{mbar})$	$\text{SLP}_p (\text{mbar})$
Mean	-0.7	0.5	990.1	985.7	Mean	-0.4	-0.1	988.4	984.9
Sdev	3.1	2.7	12	11.0	Sdev	2.3	2.9	4.8	6.8
Min	-12.8	-9.6	951.7	956.1	Min	-5.1	-8.0	982.2	975.6
Max	3.8	3.7	1025.3	1015.2	Max	2.1	2.2	1001.3	1001.1
n (events)	406	62	402	61	n (events)	12	12	12	12

O'Higgins - Daily					O'Higgins - Monthly means				
	$T_{\text{air}} (^\circ\text{C})$	$T_p (^\circ\text{C})$	$\text{SLP}_{\text{air}} (\text{mbar})$	$\text{SLP}_p (\text{mbar})$		$T_{\text{air}} (^\circ\text{C})$	$T_p (^\circ\text{C})$	$\text{SLP}_{\text{air}} (\text{mbar})$	$\text{SLP}_p (\text{mbar})$
Mean	-2.3	-2.0	988.7	983.2	Mean	-2.1	-1.6	989.0	983.3
Sdev	3.6	3.7	12.0	11.7	Sdev	2.6	2.8	5.2	6.2
Min	-13.8	-14.0	949.2	949.2	Min	-7.1	-7.3	979	974.7
Max	3.4	2.5	1022.4	1011.6	Max	1.3	1.4	999	996.2
n (events)	372	136	356	135	n (events)	14	14	14	14

Table 3.3: Basic statistics of air temperature and air pressure at sea level for Bellingshausen Station at Fildes Peninsula (FP) and O'Higgins Station (OH), separately calculated for days with precipitation (T_p and SLP_p) and for the whole collection period (T_{air} , SLP_{air}).

It should be noted that the year 2008 was around 0.8°C warmer than the average of the past 2 decades (1989-2009), but an anomaly in MSLP has not been detected. The collected precipitation samples show almost no seasonal difference in the distribution of the precipitation events during 2008-2009. 33, 35, 36 and 35 precipitation events were registered during summer (DJF), autumn (MAM), winter (JJA) and spring (SON), respectively. On a monthly scale, a semi-annual behaviour in the number of events is apparent with maxima at the end of summer and during spring, and an extreme peak in June 2008 (16 events). The semi-annual distribution at OH is coincident with long-term meteorological observations at FP (Carrasco and González, 2007). These characteristics reflect mainly the frontal-system origin of the precipitation events for this area and a constant year-round approach of fronts reaching this station.

The isotope analysis of the precipitation samples show that mean $\delta^{18}\text{O}$ value of OH (-9.2‰) is more depleted than mean value of FP $\delta^{18}\text{O}$ (-7.9‰). It is likely that this marked difference is not completely caused by a latitudinal effect (temperature difference) between both stations, but may rather be explained by a biased sampling due to the lack of winter samples at FP. As mentioned before, usually a correlation between air (condensation) temperature and $\delta^{18}\text{O}$ (δD) composition of precipitation exists, yet the observed relationship is not easy to understand (Figure 3.6).

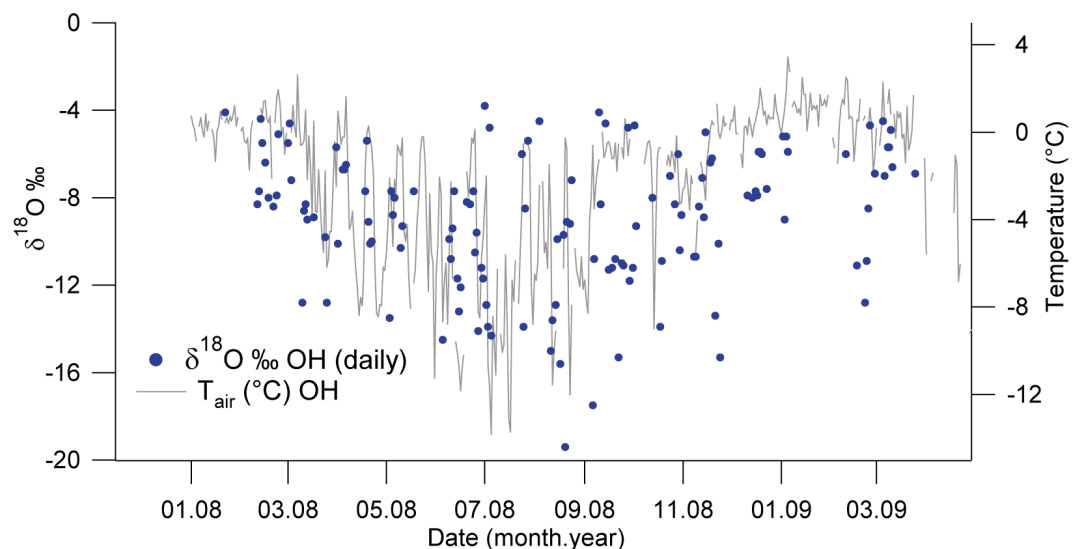


Figure 3.6: Isotopic composition of precipitation samples (blue dots) collected at O'Higgins station in a daily schedule during February 2008 and March 2009. The mean daily temperatures (light grey line) for O'Higgins are displayed as well. A high variability of air temperature and isotope data is observed, especially during the winter season.

The isotope composition of precipitation at daily resolution correlates relative poorly with T_p ($r = 0.35$, $p < 0.01$). This is mostly related to the meteorological instability and low temperature oscillation (standard deviation, $\sigma_{air} = 3.5^\circ\text{C}$), typical for the maritime influence and for the complexity of the isotope fractionation process at coastal regions (Carrasco et al., 2003; Noone, 2008; Sime et al., 2009). On the other hand, monthly averages calculated from daily events, significantly improve the $\delta^{18}\text{O}/T$ correlation coefficient ($r = 0.79$, $p < 0.01$) (Figure 3.7): this improvement of the $\delta^{18}\text{O}/T$ correlation is produced by the smoothing of (high) daily variability, and therefore enhance of the seasonal T_{air} oscillation. This confirms that $\delta^{18}\text{O}$ composition of precipitation, at least on a seasonal scale, indeed captures the T_{air} variations of the region, despite of the limited seasonal temperature fluctuations. The temperature difference between monthly T_{air} and T_p (Table 3.3) at a monthly scale is around $T_p = T_{air} + 0.5^\circ\text{C}$. For these reason a correction has to be applied for the $\delta^{18}\text{O}/T_{air}$ relationship. From the monthly means a $\delta^{18}\text{O}/T$ gradient of $0.41\text{‰ }^\circ\text{C}^{-1}$ has been calculated, being quite similar to that determined for the station Vernadsky (formerly Faraday). The Ukrainian Vernadsky Station has an extensive isotopic data base of more than 40 years, which started in 1964 and finished in 2005, while the meteorological record expands from 1947 to the present.

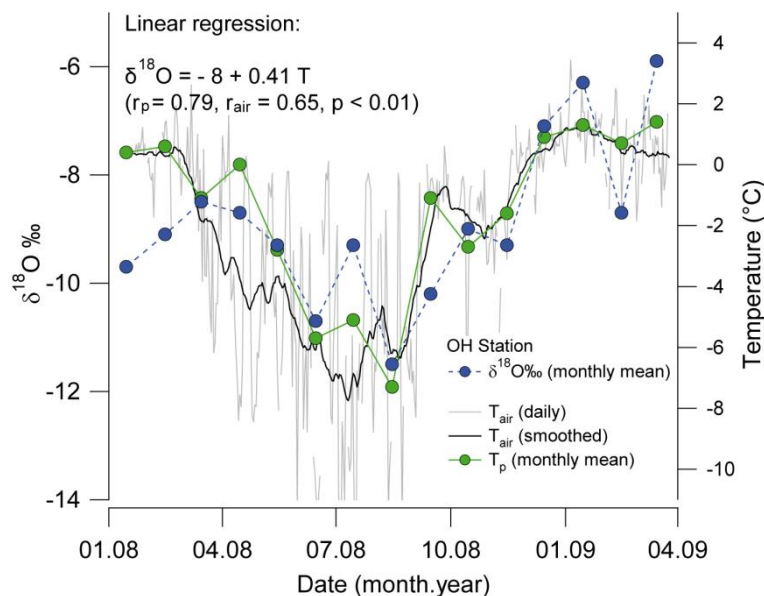


Figure 3.7: Mean monthly $\delta^{18}\text{O}$ values (blue dots) of precipitation samples collected at O'Higgins station. Also shown are data of mean monthly air temperature during precipitation days only (T_p , green dots), daily record (T_{air} , light grey) and smoothed record T_{air} (30 day smoothing, black line) at this station. A clear seasonal variability of $\delta^{18}\text{O}$ is observed, linear regression of the $\delta^{18}\text{O}$ and T correlation is presented in the figure.

From the $\delta D/\delta^{18}O$ relation (Craig, 1961; Rozanski et al., 1993), known as meteoric water line (MWL), more detailed conclusions on the origin and evolution of the moisture masses can be drawn. Slope and δD intercept of the Local MWL (LMWL) result from the evaporation setting at the moisture source and the local condensation conditions. The slope of the LMWL at OH ($m = 7.89$) is very close to the Global MWL ($m = 8.13$) (Rozanski et al., 1993), indicating that condensation process occurs in equilibrium conditions. Additionally, no seasonal variations of the condensation conditions (seasonal effect) are interpreted from our data. The similar slopes of both lines but lower intercept of the LMWL (1.2‰) than that of the GMWL (Figure 3.8a), indicates slightly differences of evaporation conditions in the moisture source with respect to the global average. This point will be discussed in greater detail in the following sections.

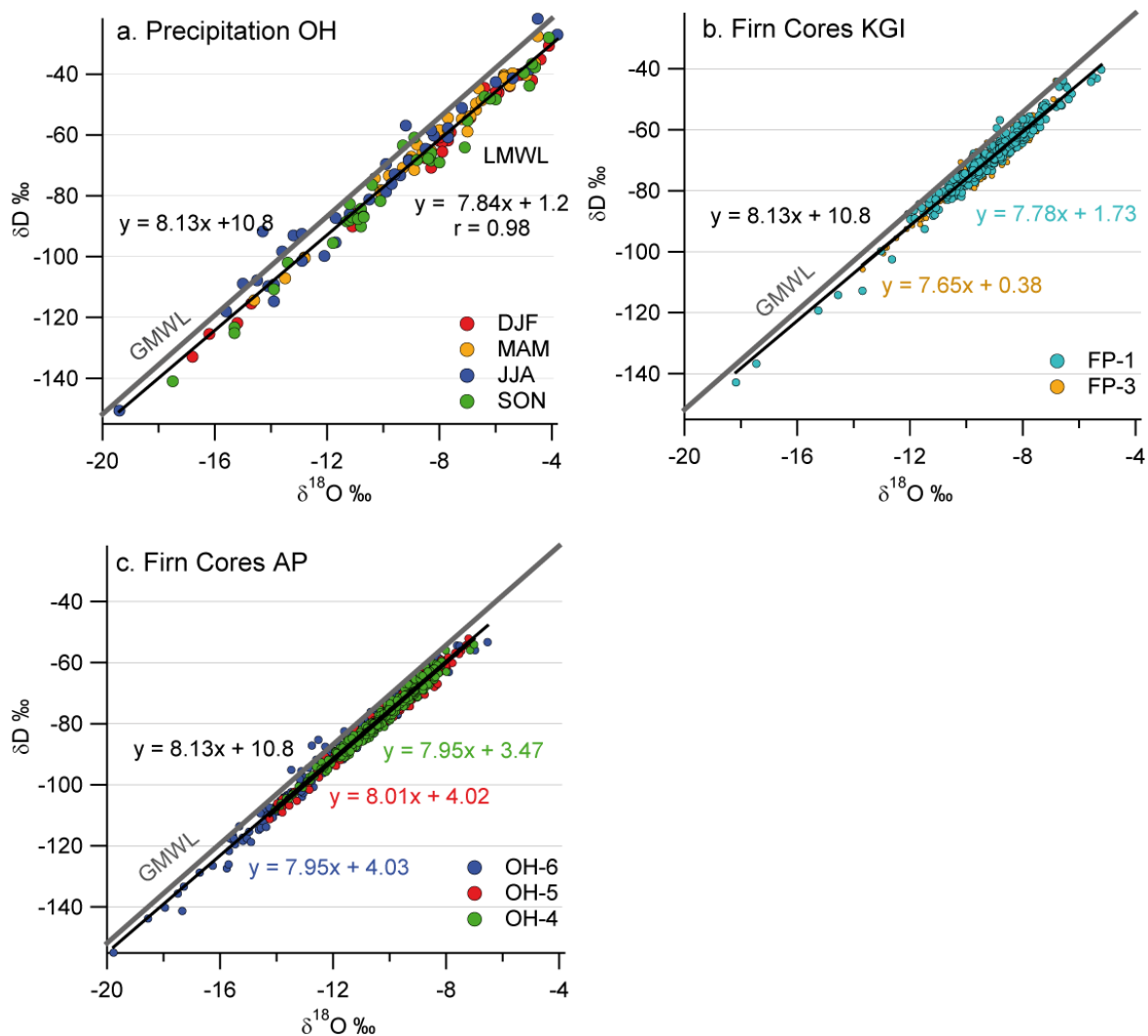


Figure 3.8: Co-isotope relationships for: a. Precipitations samples collected in O’Higgins showing the Local Meteoric Water Line (LMWL) defined for this location (black line), b. Firn cores retrieved from King George Island (FP cores) and c. Firn cores from the Antarctic Peninsula (OH). For all correlations the equation of the best linear fit is presented, additionally the Global Meteoric Water Line (GMWL) is showed for all three figures (dark grey line).

3.5.1.2 Firn cores

Measurements of $\delta^{18}\text{O}$ and δD were performed for all cores at 5 cm resolution. In Table 3.1, a detailed description of the results from all firn cores is displayed. The location of the 7 cores described here is shown in Figure 3.4 and 3.5 for FP and OH, respectively. The most negative mean $\delta^{18}\text{O}$ value (-12‰) is found for core OH-6. The location of core OH-6 corresponds with the highest altitude of the study area (1030 m a.s.l.). On the other hand, the cores OH-1, OH-4 and OH-5 show only a slight difference of their $\delta^{18}\text{O}$ mean, as well as compared to precipitation $\delta^{18}\text{O}$ mean values, despite of the altitude differences between the coring locations. This implies that an isotopic altitude effect is visible only above 600 m a.s.l. (i.e.: between the location of OH-5 and OH-6). Unfortunately no direct comparison within the cores from FP is possible, since only 2 of the 3 cores are suitable but located too closely to each other, thus no altitude effect is visible. Co-isotope $\delta\text{D}/\delta^{18}\text{O}$ diagrams of the cores allow comparing recent precipitation samples to samples from firn cores, similar to the LMWL explained in section 4.1.1. From Figure 3.8b, it is observed that all firn cores have a slope close to 8 and intercepts between 0.4 and 4, and are therefore quite similar to the precipitation LMWL (below the GMWL). From this observations, it can be derived that (1) the fractionation during the condensation process is common for the whole region, and (2) that post-depositional effects (e.g.: diffusion and/or sublimation) do not play an important role for the snow/firn isotopic composition of the area.

It is widely accepted that annual $\delta^{18}\text{O}$ and δD maxima (minima) occur in summer (winter) coincident with highest (lowest) air temperature in the southern high latitudes. The counting of alternation of these peaks is the most common method used for dating of firn and ice in regions with high accumulation (Legrand and Mayewski, 1997). However, this is not an easy task in our study area. As seen in Table 3.1, all firn cores below 600 m a.s.l. show a strong smoothing of the isotopic signal that can be visualized from the $\delta^{18}\text{O}$ and δD standard deviation values (σ_{cores}), caused by the summer melt of the surface snow and firn. The σ_{cores} for both FP and OH locations are clearly dependent on the altitude, with constrained σ_{cores} for the cores in lower altitudes and increasing σ_{cores} in high locations. Moreover, the deviation of the isotope composition of OH-6 ($\sigma = 2.5\text{‰}$) is almost identical to that of OH precipitation ($\sigma = 3.3\text{‰}$), pointing out that at this location, melt is absent or strongly reduced. These observations are also confirmed by the visual inspection of the firn cores OH-1, OH-4, FP-3 and FP-4, which displays several ice layers caused by melt and refreezing up to several centimetres thick. In the case of these cores retrieved more close to the coast, the infiltration and refreezing is especially strong with up to 0.5 m thick melt/refreeze sections. In contrast, the core OH-6 does not show any major ice layers. The few ice layers in this core are all less than 1 cm thick and

rather representing wind-glazed crusts. An exception was observed at around 0.5 m depth (snow) where a clear melt-refreeze ice layer is visible with a thickness of around 2 cm. This layer has a clearly defined upper surface, and was then covered by snow. Despite of the fact that the cores above 600 m a.s.l. (FP-1, OH-5 and especially OH-6) are most likely not (or only rarely) affected by melt-percolation processes, no clear seasonality in the $\delta^{18}\text{O}$ (δD) record can be seen (Figure 3.9). Thus, the dating and estimation of accumulation rate is not a straight forward procedure. The explanation for this feature is linked to the meteorology of the region, with restricted seasonal temperature oscillations. Sime et al. (2009), described that the $\delta^{18}\text{O}$ (δD) signal reflect only between 11% and 30% of the MAAT for the James Ross Island area, north-east Antarctic Peninsula (Figure 3.1). The isotope/temperature relation varies along the Antarctic Peninsula improving to the south-west (explaining up to 70% of local MAAT variation), depending on local daily, synoptic and seasonal atmospheric and meteorological characteristics. The isotope seasonality signal of our study region is further discussed in the following deuterium excess section.

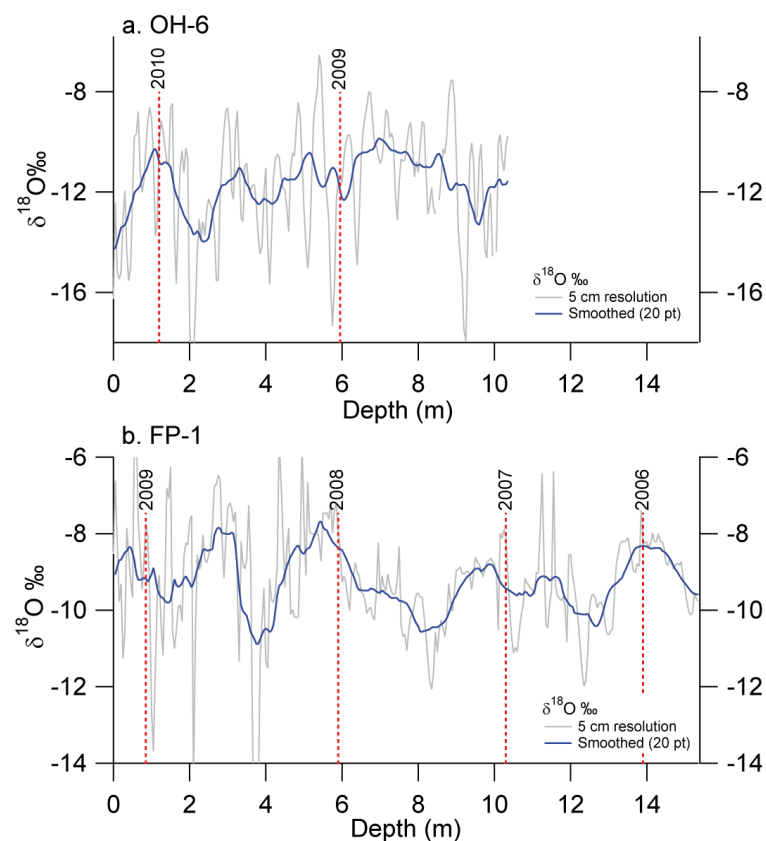


Figure 3.9: High resolution (5 cm, light grey lines) and smoothed (20 points, blue line) $\delta^{18}\text{O}$ signal of firn cores: a. OH-6 and b. FP-1. OH-6 was retrieved from Laclavere Plateau (Antarctic Peninsula) in 2010; FP-1 was retrieved from the main dome of King George Island (South

Shetland Islands), in 2009. Note that none of the cores show defined seasonal cycles, as seen from the year of deposition (dashed red lines).

3.5.2 Deuterium excess

The secondary isotopic parameter deuterium excess (d excess), was defined by Dansgaard (1964) in the following relationship: $d = \delta D - 8 \delta^{18}O$. This parameter refers to the fractionation rate difference (or excess) of $HD^{16}O$ and $H_2^{18}O$ during the evaporation of water vapour from the ocean (kinetic evaporation process). Since the posterior in-cloud condensation is considered to occur in equilibrium conditions (Dansgaard, 1964; Gat, 1996), the d excess generally does not undergo further modifications during the rain-out process. Therefore, d excess will depend mainly on the conditions at the evaporation moment, i.e.: relative humidity (h), sea surface temperature (SST) and wind speed at the moisture source. Because of these characteristics, d excess is useful to identify the moisture source conditions and to reconstruct variations of these conditions in time, a tool broadly accepted and well-suited for glacio-geochemical investigations (e.g.: Stenni et al., 2010b). Uemura et al. (2008) made direct measurements of water vapour above the sea level at southern high latitudes, as one of the first empirical validations of the d excess variability in response to sea surface conditions. They found that d excess negatively correlates with h and positively correlates with SST, however, a strong and random variability is observed close to the Antarctic coast region. Here, we present and discuss the results of the high-resolution measurements of d excess calculated from $\delta^{18}O$ and δD values.

3.5.2.1 d excess of precipitation

From all 139 samples collected at OH between February, 2008 and March, 2009 singles d excess values have been calculated (Figure 3.10). A mean d excess value of 2.7‰ (Table 3.2) suggests that the evaporation of the moisture reaching this station occurs in conditions of relatively high h , most probably with origin in the adjacent Southern Ocean. According to the relationship defined by Uemura et al. (2008): $d = -0.61h + 55.7$, the evaporation of moisture that arrives at OH should occur under conditions of ~87% relative humidity, close to the global mean of 85% (Clark and Fritz, 1997) calculated for the GMWL of Craig (1961) and the GNIP data base (available at: <http://www-naweb.iaea.org/napc/ih/index.html>) (Rozanski et al., 1993). The disagreement between global mean values and precipitation at OH (contrasting d excess but similar h), indicates that the use of the GMWL for Antarctic coastal regions is not precise, since evaporation and condensation occurs under different conditions than those from tropical and sub-tropical regions. Therefore, we introduce a local MWL, which should better fit for these purposes.

Daily d excess values are shown in Figure 3.10, displaying a large variability, especially in winter. A very similar, but inverse pattern is seen for the T_{air} (Figure 3.10, light grey line), therefore suggesting that local T_{air} controls the d excess variability. This is a substantial observation of this investigation, because: (1) this gives the possibility to use the d excess variability as geochemical proxy for local T_{air} and (2) the synchronous (inverse) variation of T_{air} and d excess implies that the moisture source should be located relatively near, since a longer path of moisture masses arriving at OH, will cause a lag on $T_{\text{air}} - d$ excess oscillations. Furthermore, the single events reveal that d excess is a good indicator of extreme meteorological conditions, as observed in fast drops of T_{air} , e.g.: on July 4th ($T_p = -14^\circ\text{C}$), August 5th ($T_p = -9^\circ\text{C}$) and August 23rd ($T_p = -12^\circ\text{C}$) reflected in a strong increase of d excess (22.3‰, 13.8‰ and 14.6‰), respectively (Figure 3.10), which is characteristic for input of Antarctic continentally originated moisture.

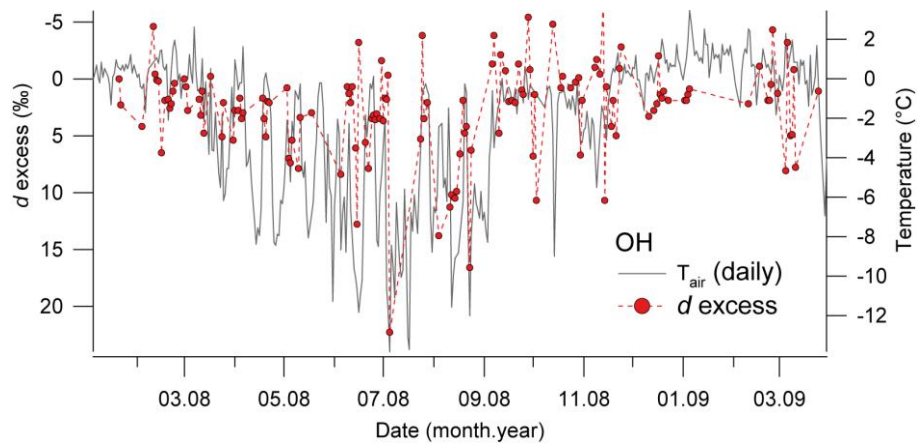


Figure 3.10: d excess (red dots) values of daily precipitation samples collected at O'Higgins stations and daily air temperature record (light grey lines) from this station. For visualization purposes the d excess axis has been inverted.

The increase of d excess has been related to changes in the fractionation rates at extreme low temperatures and to the kinetic fractionation produced by the ice-crystal formation from super-cooled air masses. This effect is mainly visible above 2000 m a.s.l. (Jouzel and Merlivat, 1984; Masson-Delmotte et al., 2008). Nonetheless, the general negative correlation of daily d excess values and T_p is relatively low ($r = -0.42$, $p < 0.01$), due to the instability of meteorological conditions. This correlation greatly improves on a monthly to seasonal scale, as for $\delta^{18}\text{O}$, mostly because the extreme and fast changes in temperature are smoothed, and by this revealing a more realistic relationship between d excess and T_{air} (and T_p). The winter temperature drop of the precipitation site is then linked with an increase of d excess. The physical explanation is most likely the decrease of h and/or

SST at the moisture source. Figure 3.11 shows a summary of the monthly mean values of d excess, T_{air} and T_p . Linear regressions demonstrate that the correlation coefficients (r) are high between both, T_{air} and T_p relative to d excess values. Regressions and r are given for monthly mean values by the expressions:

- 1) $d = 1.54 - 0.54 T_{\text{air}}$ ($r = -0.61, p < 0.01$) and
- 2) $d = 1.73 - 0.59 T_p$ ($r = -0.72, p < 0.01$)

The linear regression equations demonstrate that the isotopic composition of precipitation from this region reflects most of the meteorological variability at seasonal and even sub-seasonal scales. Therefore, we conclude that the isotope composition of precipitation represent a suitable proxy for T_{air} and climate parameters reconstruction.

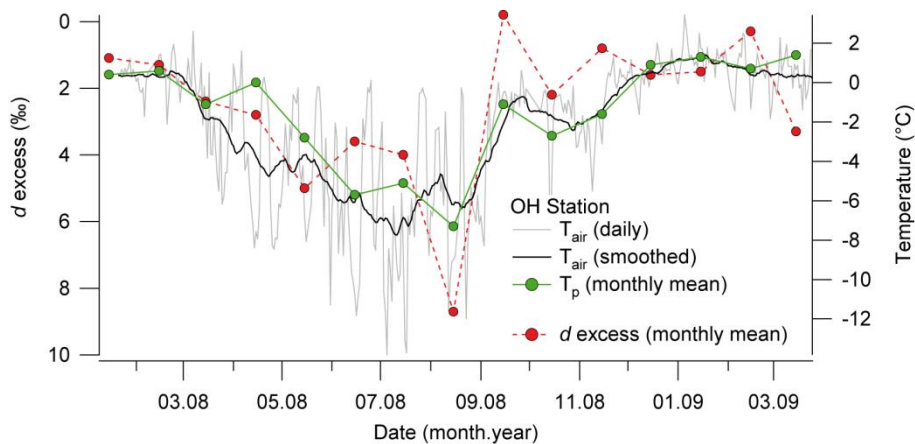


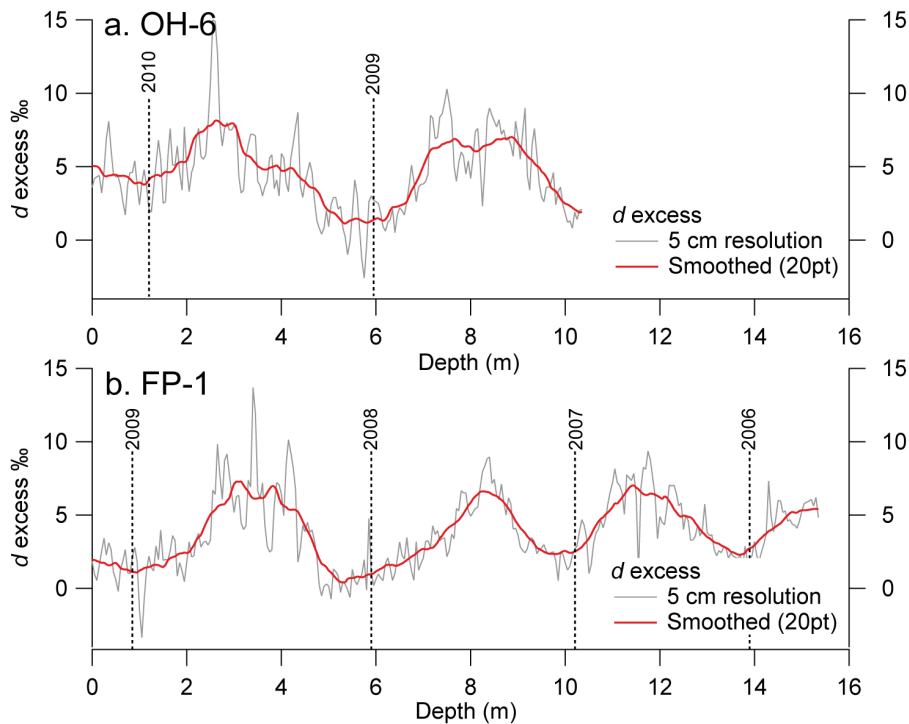
Figure 3.11: Monthly d excess mean (red dots) of precipitation samples from O’Higgins station and daily air temperature (T_{air} , light grey). The smoothed T_{air} (black line) correspond to a 30 day running mean function. For visualization purposes the d excess axis has been inverted.

3.5.2.2 Deuterium excess of firn cores

The d excess of most of the firn cores show mean values close to 4‰ (Table 3.1), with values around 1.3‰ above the mean d excess value for precipitation (OH = 2.7‰), an exception are the cores OH-1 and FP-4 (d excess of 1.2‰ and 2.2‰, respectively). Despite the slight difference of d excess values between OH station and firn core values, both are clearly under the GMWL (d excess = 10‰). At this step, some influence of moisture of continental provenance cannot be discarded for high altitude locations of KGI and API. As demonstrated above, both high-altitudes cores (OH-5, OH-6 and FP-1) do not indicate major signs of melting and/or percolation. Furthermore OH-6 show the highest d excess value of all cores (4.4‰). Thus, the d excess values in high altitude locations could

reflect a slightly different moisture composition as compared to the coastal area. Moreover, at both areas (OH and KGI) the d excess of the cores systematically decreases towards low altitudes. Therefore, the d excess difference between firn cores and precipitation values is likely not to be related to post-depositional effect. Additionally, melt and/or infiltration of lower d excess (summer) precipitation can be discarded as the main cause of the lower values with decreasing altitude, since d excess of OH-1 (220 m a.s.l.) is similar to that of precipitation at OH station. As previously mentioned, at this station year-round well distributed precipitation events were sampled and a seasonal bias of isotope composition can for this reason be rejected. Other local effects like diffusion within the snow cover or preferential removal of low d excess layers cannot be ruled out without direct observations (e.g.: wind drift or sublimation), but these have been considered to be not significant for the API region, due to the high precipitation rates, and therefore not having a great impact on the isotope composition (van Lipzig et al., 2004). The comparison of the d excess standard deviation (σ_{excess}) of firn cores and precipitation demonstrate that closer to the coast firn display a strong homogenization of the isotope composition, where σ_{excess} for OH station ($\sigma_{\text{excess}} = 2.7$) is clearly larger than coastal cores OH-1 ($\sigma_{\text{excess}} = 0.8$) and FP-4 ($\sigma_{\text{excess}} = 0.6$). Larger values of σ_{excess} are found only at the high altitudes regions (>600 m a.s.l.) of OH and FP (see Table 3.1). Lower d excess values, as mentioned above, are associated with more humid conditions at the moisture source. This supports the assumption that the coastal regions are influenced by a stronger maritime regime, which slightly decreases towards the higher altitudes.

Similar to the observed seasonal variations of the OH data, the d excess of firn cores presents a marked seasonality (Figure 3.12), hence allowing the use of the d excess seasonal variability as an instrument for dating of the accumulated snow and firn.



1

Figure 3.12: Firn cores d excess high resolution (5 cm samples, red line) and smoothed (20 points, red line) signal of: a. OH-6, retrieved in January 2010 at the Laclavere Plateau (Antarctic Peninsula); and FP-1, retrieved in January 2009 at the main dome of King George Island (South Shetland Islands). A clear seasonality is visible for both cores, however a decrease of the amplitude is observed for the core FP-1 in depth, showing some post-depositional effects. The deposition year of firn for both cores are showed (black dashed lines).

In Figure 3.13, the smoothed d excess of cores OH-6, OH-1 and FP-1 are compared to the T_{air} from FP. The smoothing of the d excess signal was done using a special moving average function (box function), considering a similar number of points before and after the smoothed value (21 points, ~ 1 meter firn depth). In this case the FP record has been used because of gaps in the monthly and daily meteorological record of OH station during some periods between 2005 and 2010. This visual comparison underlies a correlation between T_{air} and d excess. Moreover, assuming that accumulation is approximately constant through all seasons, re-sample to monthly means of the isotope data of firn cores can be performed. This allows a direct comparison of monthly T_{air} and d excess values (monthly re-sampled). Correlation coefficients for monthly means are given in Table 3.4. Additionally, the $\delta^{18}\text{O}$ re-sample value is presented for comparison, reaffirming the complexity to directly infer T_{air} from oxygen and deuterium data. From generated age model, it can be preliminary concluded that both locations have high accumulation rates. Wen et al. (1998) and Simões et al. (2004a) retrieved ice cores from the main plateau area at KGI during different field seasons. Density of snow/firn of

these cores show a compactation with an approximately linear tendency in the first 20 meters and an increase step of 4.5 kg m^{-3} per meter, the surface snow density is estimated to be around 490 kg m^{-3} . Using these density profiles combined with our age model of FP-1, accumulation rates of 2542, 2296 and $1935 \text{ kg m}^{-2} \text{ a}^{-1}$ are estimated for 2008, 2007 and 2006, respectively for this location. These rates are similar to the mean accumulation of $2480 \text{ kg m}^{-2} \text{ a}^{-1}$ described by Wen et al. (1998), but much higher than accumulation rates calculated by Simões et al. (2004a). However, the snow/firn cover of KGI includes several ice layers, which are the product of percolation and refreezing. These may lead to overestimated density values, which would therefore correspond to higher accumulation rates. In general, the Antarctic coast exhibits elevated accumulation rates (van den Broeke et al., 2006; Masson-Delmotte et al., 2008). Hence, we conclude that Simões et al. (2004a) underestimated the accumulation rates of this location.

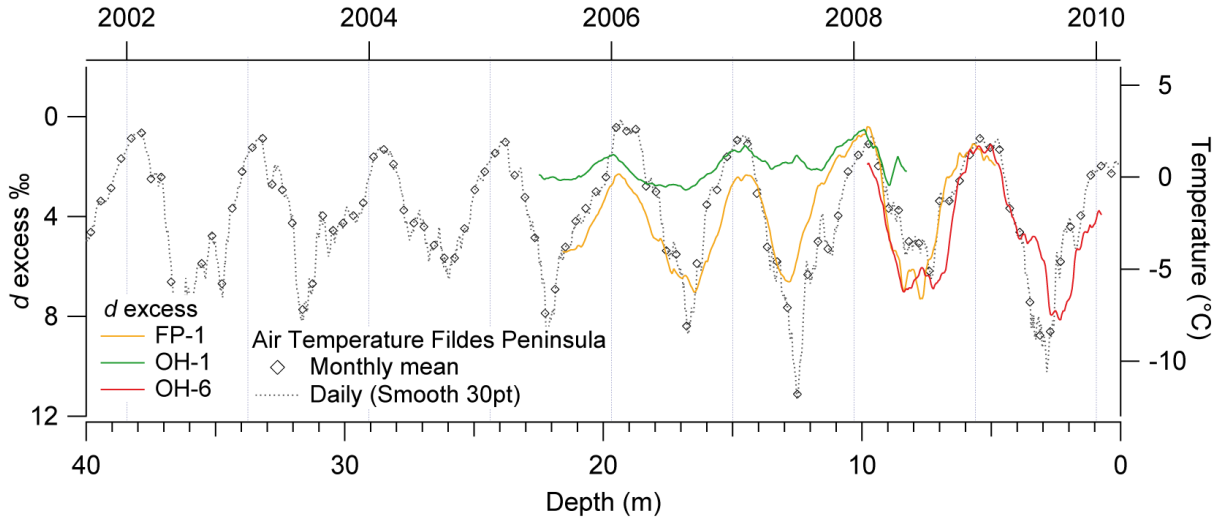


Figure 3.13: Seasonality of d excess presented by three firn cores: FP-1 (King George Island), OH-1 and OH-6 (Antarctic Peninsula). The cores were retrieved in different field campaigns during 2008 and 2010, therefore the depth axis is only referential, note as well that the d excess axis has been inverted for better comparison of the data. Air temperature (dashed black line and diamonds) is from Bellingshausen Station, Fildes Peninsula (King George Island).

	T_{air} OH	T_{air} FP	SIF	SST	h	
FP-1						
$\delta^{18}O$	0.386	0.354	-0.032	0.322	0.277	n = 42
	p=0.012	p=0.022	p=0.839	p=.038	p=.076	
d excess	-0.6561	-0.7298	0.5229	-0.6096	-0.7104	
	p=0.000	p=0.000	p=0.000	p=0.000	p=0.000	
OH-6						
$\delta^{18}O$	0.0633	-0.001	-0.1053	0.0157	-0.1509	n = 23
	p=0.774	p=0.996	p=0.633	p=0.943	p=0.492	
d excess	-0.5948	-0.6066	0.7596	-0.7231	-0.3394	
	p=0.003	p=0.002	p=0.000	p=0.000	p=.113	
OH						
$\delta^{18}O$	0.6954	0.8429	-0.7669	0.7067	0.644	n = 14
	p=0.008	p=0.000	p=0.002	p=0.007	p=0.018	
d excess	-0.5882	-0.6976	0.4888	-0.3208	-0.7833	
	p=0.034	p=0.008	p=0.090	p=0.285	p=0.002	

Table 3.4: Correlation matrix of mean monthly isotope values: resamples of the high altitude firn cores (OH-6 and FP-1), precipitation (OH) and major seasonal forcing of meteorological variability identified for this region. Significant p-level ($p < 0.05$) are marked in red letters for easier recognition.

3.5.3 Main δ and d excess forcing

In the preceding sections the relationship of stable water isotopes and T_{air} has been largely discussed. Nonetheless, correlation coefficients of this relationship are statistically significant but in some cases relatively low. The relationship between $\delta^{18}O$ (δD) from firn cores and T_{air} is complicated, and probably suitable only to study inter-annual variability; in contrast monthly $\delta^{18}O$ means from precipitation events may reproduce well the T_{air} variability. On the other hand d excess (from cores and precipitation) turns out to be significantly suitable to study the regional climatic variability, because it does not directly depend on local conditions. The synchronicity of T_{air} and d excess variation, with low d excess values, suggest a (humid) nearby oceanic source of the moisture precipitating at the study region. The d excess depends primarily on the h and SST of the moisture source, moreover h and SST seasonal oscillation are linked and influenced by the sea ice cover. During winter, the sea ice cover can obstruct the contact between the water surface and atmosphere, therefore influencing T_{air} , h and SST. Weatherly (1991) proved the interdependency of T_{air} and sea ice cover, acting as inverse feed-back mechanisms of each other, i.e.: an extended sea ice cover in winter will cause a decrease of T_{air} , and on the other hand T_{air} in summer will predispose the following season's sea ice genesis. This mechanism is strong at the API region, since most of the local

oceanic moisture is transported by the westerlies and then trapped by the natural barrier of the API range; therefore directly influencing the isotope composition of coastal precipitations. Similar conclusion on the effect of sea ice over the isotope composition of moisture were drawn by Noone and Simmonds (2004), recognizing the potential of water isotope (particularly the d excess) for paleo-climate reconstruction.

In our study, the local isotope variability is evaluated for T_{air} , SST, h and sea ice cover (expressed as sea ice fraction – SIF) as the main drivers of the seasonal to sub-seasonal isotope composition of moisture masses (Figure 3.14). Table 3.5 displays a correlation matrix for $\delta^{18}O$ and d excess values of two firn cores (OH-6 and FP-1) monthly resample and of monthly mean precipitation, compared with the meteorological time series. High correlation coefficients are found for d excess of both firn cores with T_{air} from FP and OH stations (note that the OH station shows slighter lower coefficients probably related to the data gaps of the time series). As expected from our previous observations $\delta^{18}O$ from firn cores do not correlate well with T_{air} . However, SIF, SST and h time series correlate fairly well to the d excess of both cores, confirming the dependency of the isotope composition from the moisture source conditions. The only exception to this assumption is the firn core OH-6, where the h / d excess correlation coefficient is low and not significant. Nevertheless, this is forced by two high d excess values, because of the low number of observations ($n = 23$). High d excess values most likely do not represent oceanic moisture and are linked to more continental influenced moisture. If these two peaks are removed, the correlation improves to $r = -0.46$ and become significant at p -level <0.05 . OH monthly mean $\delta^{18}O$ and d excess of precipitation correlate very well to T_{air} from both stations with a very high correlation coefficient with respect to FP station. The relationship between isotope composition and SIF, SST and h is more complicated to interpret since the number of valid observation is very restricted. In any case again the correlation between h and d excess remains strong. On the other hand, several studies showed that NCEP/NCAR reanalysis overestimate some of the meteorological parameters (Hines et al., 2000; Smith et al., 2001). From our observation a relative humidity for the moisture source of about 84% (cores OH-6 and FP-1) to 87% (OH precipitation) was estimated. NCEP/NCAR reanalysis for the corresponding locations and time periods estimates a slightly higher $h = 89\%$ for all cases. The inter-comparison between the two different locations with respect to the precipitation samples in a common time-span (Table 3.5), i.e.: the period of common overlap of the two firn cores and precipitation collection (12 months in total, March 2008 to March 2009), allows to test the strength of the regional isotope signal. The $\delta^{18}O$ correlation for the firn cores and precipitation shows no coherent pattern, reflecting the high spatial variability of local meteorological (e.g.: T_{air}) conditions. On the other hand, from this matrix is again

confirmed that the d excess signal correlates for all data sets, with coefficients close or higher than 0.7, reaffirming the robustness of the monthly d excess signal.

	FP-1		OH-6		n= 12
	$\delta^{18}\text{O}$	d excess	$\delta^{18}\text{O}$	d excess	
OH Prec					
$\delta^{18}\text{O}$	0.0615	-0.7427	-0.422	-0.7238	n= 12
	p=0.849	p=0.006	p=0.172	p=0.008	
d excess	0.1411	0.7621	-0.1171	0.2963	n= 12
	p=0.662	p=0.004	p=0.717	p=0.350	
FP-1					
$\delta^{18}\text{O}$	1	-0.0479	-0.1103	-0.2311	n= 12
	p=---	p=0.883	p=0.733	p=0.470	
d excess	-0.0479	1	0.0316	0.6869	n= 12
	p=0.883	p=---	p=0.922	p=0.014	
OH-6					
$\delta^{18}\text{O}$	-0.1103	0.0316	1	0.0515	n= 12
	p=0.733	p=0.922	p=---	p=0.874	
d excess	-0.2311	0.6869	0.0515	1	n= 12
	p=0.470	p=0.014	p=0.874	p=---	

Table 3.5: Correlation matrix of monthly isotope means of firn core FP-1 and OH-6 (resample values) and precipitation from OH station for the 12 months common period (March 2008 to March 2009). Significant p-level ($p < 0.05$) are marked in red for easy recognition.

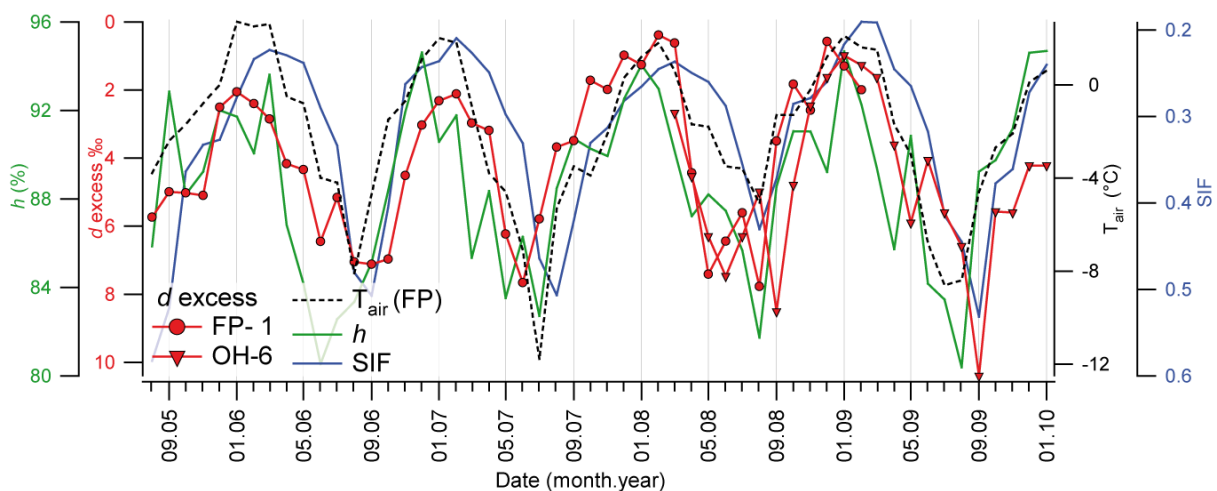


Figure 3.14: Seasonal variation of monthly means of excess d of cores FP-1 and OH-6 compared to the meteorological variables: relative humidity (h , green line), T_{air} Bellingshausen station (FP, dashed black line) and sea ice fraction (SIF, blue line) for the Bellingshausen Sea. Note that the d excess and SIF axes are inverted for visualization purposes.

3.6 Backward trajectory model

With the objective to further investigate the (physical) source of moisture masses that arrive to the study area, the air parcels circulation model Hysplit (Draxler and Hess, 1998) (available at: <http://www.arl.noaa.gov/ready/hysplit4.html>) has been used to reconstruct a 3-day backward circulation path of every single precipitation event registered at OH station arriving at 1500 m a.s.l. (850 mb approximately). Figure 3.15 presents a frequency chart of all paths that arrived during daily precipitation events between February, 2008 and March, 2009 (139 events). This figure shows a wide distribution of the trajectories varying in their origin from South Pacific in the north to the Bellingshausen Sea in the south, from the east (Weddell Sea and South Atlantic) some sporadic events are seen as well. Most of the trajectories follow a clear pattern following a restricted pathway between latitudes 60° and 65°S.

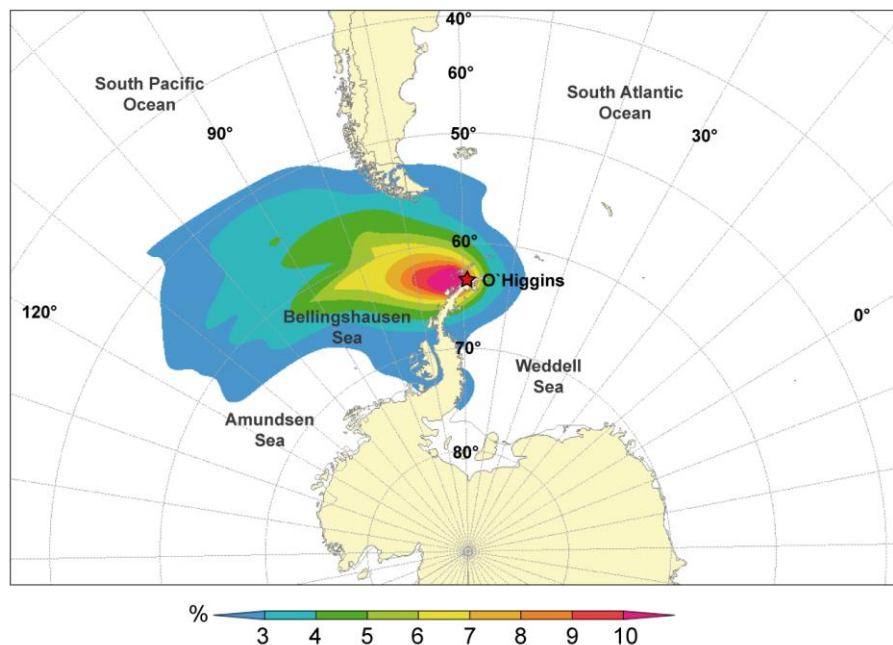


Figure 3.15: Frequency of track of the single (3-days) backward trajectories calculation of air parcels arriving at OH station (1500 m a.s.l. level) during precipitation events. The red star show the location of O'Higgins Station. A total of 139 single trajectories were calculated in total.

Following a statistical treatment, all trajectories were clustered in 4 main paths to identify the regions, from where the events preferentially originated (Figure 3.16). The statistical treatment consists of clustering the trajectories with the lower spatial variance. Initially all trajectories are considered independent clusters (as many cluster as trajectories), consecutive passes will group the two clusters with the absolute lowest spatial variance, repeating this iteration as many times as trajectories to finally calculate only one cluster and calculating a total spatial variance (TSV) at each

step. The optimal number of clusters is finally chosen arbitrarily observing when the TSV approached a flat maximum. For further details visit the Hysplit website (<http://ready.arl.noaa.gov/HYSPLIT.php>). After running the cluster analysis an optimal number of 4 cluster was recognized (Figure 3.16). The most common direction (cluster 3) is found at around 55°S (47%), followed by two southern clusters (1 and 2) that together gather almost 40% of all events originating south of latitude 60°S (Bellingshausen Sea). The seasonal distribution (Table 3.6) of the clusters reveals a migration pattern with a preferential South Pacific origin (cluster 3) in summer (DJF) and autumn (MAM), and preferential Bellingshausen Sea direction (Cluster 2) in winter (JJA) and spring (SON). Later the clusters were combined with the stable water isotope information to identify difference in the composition of precipitation events under the influence of different sources. As seen in Table 3.7, both northern clusters (3 and 4) are composed by events with less negative $\delta^{18}\text{O}$ (δD) and tending to lower d excess values. The southern clusters (1 and 2) present lower $\delta^{18}\text{O}$ (δD) and higher d excess. Both southern clusters are also associated with lower temperatures and atmospheric pressures. In contrast, the cluster 3 is associated with higher temperatures and pressure. Cluster 4, the less common, represents especially high pressures containing all trajectories with an east component occurring most frequently in winter. This could reflect some influence of continental moisture or katabatic winds; however this is not reflected in the isotopic composition. Finally two main origins of the air parcels arriving at O'Higgins can be concluded: one between latitudes 50°S and 60°S (South Pacific), representing the most common one; and a second origin south of the latitude 60°S (Bellingshausen-Amundsen Sea).

	Cluster				n
	1	2	3	4	
DJF	21.2%	24.2%	51.5%	3.0%	33
MAM	21.2%	12.1%	60.6%	6.1%	33
JJA	28.6%	45.7%	5.7%	20.0%	35
SON	29.4%	32.4%	29.4%	8.8%	34

Table 3.6: Seasonal frequencies (in percentage) of the backward trajectory clusters calculated from single events at OH station. The right column indicates the number (n) of singles events recorded in each season.

Cluster	n	$\delta^{18}\text{O}\text{‰}$	$\delta\text{D}\text{‰}$	<i>d</i> excess	T_p (°C)	SLP _p (mbar)
1	27	-10.2	-78.1	3.2	-2.2	979.4
2	26	-10.1	-76.1	5.0	-4.1	979.3
3	65	-8.7	-67.8	1.6	-0.9	983.9
4	17	-8.4	-64.8	2.5	-3.3	992.0

Table 3.7: Mean isotopic composition of backward trajectory clusters, each cluster contains *n* single events. Temperature (T_p) and air pressure (SLP_p) correspond to the precipitation day only.

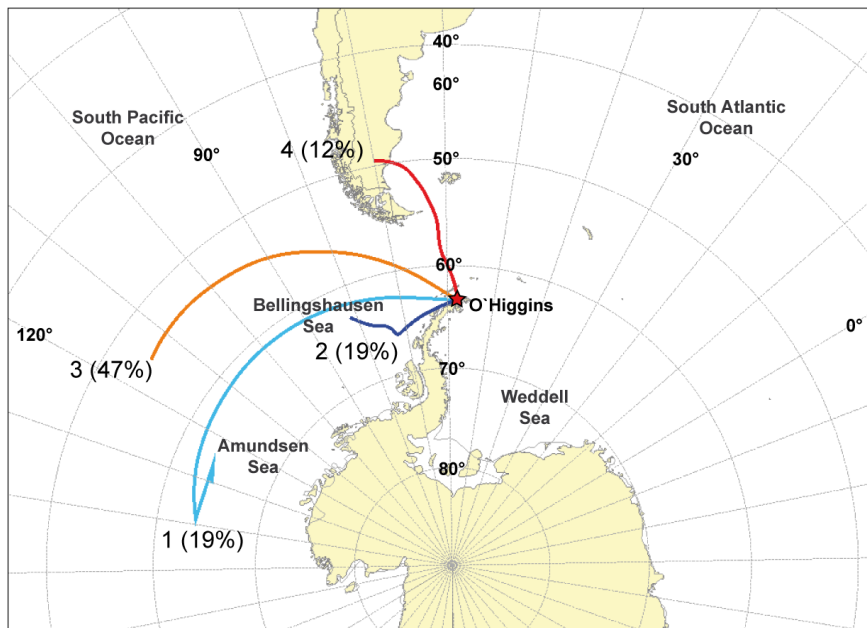


Figure 3.16: Backward trajectories clustering for precipitation events at OH station. Four main clusters are identified, the percentage of trajectories bundled to each cluster is stated in parenthesis (cf. Table 3.6). From a total of 139 trajectories, 4 events are not associated to any of the clusters.

3.7 Conclusions

Our results demonstrate that the combination of stable water isotope analyses with different meteorological data sets offer a valuable proxy for paleo-climate reconstruction in the north Antarctic Peninsula region. Undoubtedly, this task has been correctly recognized by previous studies as a complicated one (King and Comiso, 2003; Sime et al., 2009). Nonetheless, isotope analysis ($\delta^{18}\text{O}$ and δD) of precipitation samples collected in a daily schedule during 14 months (2008 to 2009) from Frei and O'Higgins stations at the northern Antarctic Peninsula, highly reflect the meteorological

variability of the region. The second order parameter d excess calculated for all samples, shows to be a good indicator of air temperature variability and single extreme meteorological events (elevated d excess values). Moreover, mean monthly $\delta^{18}\text{O}$ and d excess values highly correlate with the air temperature oscillations. We calculated temperature gradients of $0.41\text{‰ }^{\circ}\text{C}^{-1}$ ($r = 0.8$) and $0.59\text{‰ }^{\circ}\text{C}^{-1}$ ($r = 0.7$) for $\delta^{18}\text{O}$ and d excess, respectively. Several firn cores extracted from the ice caps adjacent to both stations were examined in order to study the implication of the precipitation data for the firn/ice core interpretation. From visual inspection and isotope analyses it is evident that all cores retrieved below 600 m a.s.l. show evidence for percolation and refreezing due to summer melt. Moreover, from the high-resolution analyses (5 cm) several isotopic features can be recognized. The d excess slightly increases towards high altitudes probably reflecting a stronger influence of maritime conditions at coastal zones. The $\delta^{18}\text{O}$ from firn cores does not capture well the local seasonal temperature fluctuation, as consequence of the low seasonal temperature oscillation ($\sigma_{\text{air}} = 3.6^{\circ}\text{C}$) and local post depositional effects. On the other hand the d excess, since it does not depend on the local conditions exhibit a much better seasonality, thus allowing the dating of firn accumulated at this region. The synchronicity of d excess and air temperature implies a local moisture source for the precipitation arriving at this region. Low absolute d excess values indicate a moisture source with typical oceanic characteristics with an estimated mean relative humidity of 87%, according to the relationship calculated by Uemura et al. (2008). A backward trajectory analysis (3 days backward) of all registered precipitation events show that the air masses follow two main paths before snow and/or rain falls: one from the South Pacific (50° - 60°S) and a second one from the Bellingshausen-Amundsen Sea (south of 60°S); the first occurring preferentially in summer-autumn and the second in winter-spring. Correspondingly the northern path shows more positive $\delta^{18}\text{O}$ and lower d excess values, confirming that both parameters are sensitive to changes in the moisture source region. Hence, stable isotope time series of the firn cores were compared to different meteorological variables such as: SST, h , T_{air} , and SIF. The d excess show a strong correlation to humidity and sea surface temperature of the surrounding ocean ($r = 0.7$ to 0.8 for both parameters); as well as a correlation to the sea ice cover is observed ($r = 0.5$ to 0.7), explained by the influence of sea ice directly on the air temperature and ocean-atmosphere interaction. Finally, the core retrieved at the Laclavere Plateau (1030 m a.s.l.), which was explored for the first time ever in 2010, represent very promising conditions for future glaciological investigations: restricted melt evidence of firn and snow, a high accumulation rate which ensures that a high resolution archive is stored in the ice cover, as well as low MAAT of this area estimated to be around -10°C . In this paper we show the potential of the stable water isotope for the interpretation and reconstruction of the climate variability of this region.

4 Seasonal to decadal climate variability in the northern Antarctic Peninsula region from 50 years of meteorological records and ice-core time series

Francisco Fernandoy, Hanno Meyer, Elizabeth Thomas, Jefferson Simões and Marcos Tonelli

(In preparation for submission)

4.1 Abstract

As a hotspot of the recent global warming, the Antarctic Peninsula is a key region to study short-term climate variability. We base our study on the analysis of stable water isotope composition from several ice and firn cores and the meteorological records from station with records longer than 40 years. We found a correlation between the meteorological variability at the northern Antarctic Peninsula and the Southern Annular Mode (SAM). A marked change in correlation between SAM and air temperature is observed since the beginning of the 1980s, which is linked to the rapid warming trends in the region. The SAM-air temperature correlation is especially strong during autumn and winter at the west side of the northern Antarctic Peninsula and in summer and autumn at the east side, which coincides with the seasonal air temperature trends during the instrumental period. A new firn core retrieved from the west/east ice divide of the Antarctic Peninsula (Laclavere Plateau) exhibits a good correlation to SAM variability in summer-autumn, pointing out that precipitation events are highly dependent on SAM. Thus, a key region to explore the recent shift of the SAM. Time-series analyses suggest that the interaction between the atmospheric mode and regional climate occurs with defined patterns. However, this last assumption needs further confirmation due to the high variability and shortness of the records. Hence we suggest the extraction of a new medium-depth ice core to be used as a long-term climatic archive for the last 100 to 150 years in this area.

4.2 Introduction

The regional climate records variability during the instrumental period in Antarctica (the last 50 years) shows an increasing trends of air and ocean surface temperatures (Levitus et al., 2005; Chapman and Walsh, 2007). However, a strong climatological contrast between the West and East parts of the continent is evident. While West Antarctica shows a significant increase of mean annual air temperature (T_{air}) of $+0.17^{\circ}\text{C decade}^{-1}$ (Adams et al., 2009), in East Antarctica no significant warming trend has been observed. However, East Antarctica displays a strong spatial and seasonal

variability, where some coastal areas show significant warming (about $+0.2^{\circ}\text{C decade}^{-1}$) and others significant cooling (about $-0.2^{\circ}\text{C decade}^{-1}$) in both the interior and coastal zones (Kwok and Comiso, 2002; Schneider et al., 2006; Chapman and Walsh, 2007). The overall continental temperature trend has been estimated to be at around $+0.08^{\circ}\text{C decade}^{-1}$ since around 1960 to the present (Chapman and Walsh, 2007; Steig et al., 2009). The recent warming observed in West Antarctica has a main focus at the Antarctic Peninsula (AP), where the positive temperature trend reaches $+0.3^{\circ}\text{C decade}^{-1}$ as a mean (Chapman and Walsh, 2007), with a maximum of $0.56^{\circ}\text{C decade}^{-1}$ at the Station Vernadsky (formerly Faraday, West Antarctic Peninsula - WAP) and $+0.41^{\circ}\text{C}^{-1}$ at Esperanza (East Antarctic Peninsula - EAP) (Turner et al., 2005). The strong warming at the WAP has a regional significance and extends southward as demonstrated by ice-core data (Thomas et al., 2009), but diminishes to the north with a trend of only $+0.2^{\circ}\text{C decade}^{-1}$ at the South Orkney Islands (Mayewski et al., 2009; Zazulie et al., 2010). The recent warm phase probably started in the middle of the 19th century or earlier. At this time the temperature was in average 0.2°C cooler than today (Schneider et al., 2006; Turner et al. 2009). The geographical setting of the AP makes this region especially sensitive to climate change. The relatively narrow (~ 100 to 300 km wide) but long spine of the AP, extends from the Drake Passage (Bellinghausen Sea/South Pacific Ocean Sector) in the north ($\sim 62^{\circ}\text{S}$) to the West Antarctic plateau to the south (around 1250 km of extension). The climate regime at the WAP is strongly maritime, since the AP acts as a natural barrier for the dominant westerly winds (Schwerdtfeger, 1975; Peel, 1995). At the EAP a more continental regime is observed, where the temperatures are to 5°C to 10°C lower than at the same latitude on the west side (Schwerdtfeger, 1975; Peel et al., 1988). The strengthening of the circumpolar westerlies during the last decades generated the intensification of the surface winds fields that now pass over the topographical barrier of the AP mountain chain. These relatively warm air-masses now reach the east coast of the Peninsula. This also combined with a Foehn wind effect (van den Broeke, 2005), leading to an increase of T_{air} especially during summer (Turner et al., 2005).

The exact background mechanism causing the recent (and also past Holocene) warming events is still not completely understood, mostly due to the lack of well-dated and high-resolution data (Turner et al., 2009). Most likely the warming phenomenon is linked to the intensification of the circumpolar westerlies (Mayewski et al., 2009). Westerly winds are a marked feature of the southern hemisphere atmospheric circulation. Westerlies and a constant low pressure front over coastal Antarctica are driven by the Earth's rotation and ascent of air masses in the contact region of the middle and south latitude atmospheric circulation cells, Ferrel and Polar cell, respectively (Ainley et al., 2009). The atmospheric mass exchange responsible for the intensification of the westerlies is

known as the Southern Annular Mode (SAM). SAM is a circumpolar pattern, defined as a synchronous anomaly of the air pressure at sea level between the middle and high latitude regions, (40° and 65° latitude south), respectively (Marshall, 2003). Following Marshall's (2003) SAM index definition, the shift to a positive phase of the SAM has been pointed out as the main driver of the seasonal to inter-decadal climate variability over Antarctica (Gillett et al., 2006; Marshall, 2007).

During the Holocene, changes in the strength of the circumpolar westerlies were attributed to the Earth's orbital parameters, i.e.: solar activity (energy output), concentration of greenhouse gases and active volcanism (Mayewski et al., 2005; Mayewski et al., 2009). At the AP, a Mid-Holocene major climate warm period occurred at 4.5-2.8 ka BP, which could probably explained by the constant increase of insolation since the early Holocene and a poleward displacement of the circumpolar westerlies (Bentley et al., 2009). All major Holocene climatic events were synchronus or preceded by changes of the atmospheric circulation (circumpolar westerlies). In contrast the recent warming event has been abrupt without any major atmospheric circulation changes. Moreover, the natural variability alone cannot explain the present climatic scenario without a non-natural (anthropogenic) input (Marshall et al., 2006; Gillett et al., 2008; Mayewski et al., 2009).

The relationship between SAM and *T_{air}* has been intensively investigated (e.g.: van den Broeke, 1998; Gordon et al., 2007; Marshall et al., 2011). It is generally accepted that enhanced polarity of the air-pressure anomaly between sub-tropical and polar latitudes controls the intensity of the westerly winds (Marshall, 2003). The correlation between SAM and *T_{air}* has been found to be positive for the AP and restricted to coastal areas of West Antarctica, however negative for East Antarctica (Marshall et al., 2011). The polarward displacement of circumpolar westerlies initiated that more heat is transported to southern latitudes and now reaching the West Antarctic Coast and especially the WAP (Adams et al., 2009). The SAM is responsible for up to 35% of the climate variability of the Southern Hemisphere (Marshall, 2007). The positive SAM phase change in the last decades has produced a warming exceeding 1°C over the AP during autumn, and cooling of the same magnitude over East Antarctica (Marshall, 2007). In response to higher *T_{air}*, the surface of the adjacent ocean (Bellinghousen-Amundsen Sea) has showed signs of abrupt warming (Meredith and King, 2005) that produced a strong retreat of sea ice in this region, which acts as a positive feedback mechanism leading to further warming (Weatherly et al., 1991; Meredith and King, 2005).

The El Niño Southern Oscillation (ENSO) is an oceanic-atmospheric tropical oscillation generated in the equatorial pacific. This oscillation influences the global climate system through atmospheric teleconnections (Fogt and Bromwich, 2006). However, at southern latitudes ENSO is mostly subordinated to the intensity and phase of SAM and detectable only as an intermittent signal (Fogt et

al., 2010). ENSO events are most noticeable when they occur during weak SAM phases or when La Niña (El Niño) events coincide with positive (negative) SAM phases (Fogt et al., 2010). Moreover, the Ross Sea sector (West Antarctica) seems to have more direct connection to ENSO events. The influence of ENSO on the sea surface temperature (SST) in this region occurs through the interaction and teleconnection with the Amundsen Sea Low (ASL). ENSO positive events displace the ASL to the east, directing the flow of katabatic winds into the Ross Sea area, thus reducing the oceanic warming effect in this region. However, the eastern region of the Ross Sea area is not affected by the katabatic flows, therefore showing a positive correlation to ENSO events (Bertler et al., 2004; Bertler et al., 2006). The displacement of the ASL in east direction forces the transport of moisture, producing an increase of the precipitation at the southern AP.

In this paper, we mainly focus on the influence of SAM and ENSO on the most northern region of the Antarctica Peninsula. We use the meteorological records from three different stations (>40 years) and new isotopic information from recent precipitation and firn-cores collected in this region. The statistical analysis has been performed on a seasonal to decadal scale to identify possible correlation and cyclicity within climatic records, as well as the influence of these atmospheric modes on local meteorology at the northern AP.

4.3 Study region:

The area under investigation is located at the northern Antarctic Peninsula. This region is of high scientific interest due to the remarkable recent climatic event, considered to be one of the hotspots of global warming (Vaughan et al., 2003). Additionally, the northern AP including the South Shetland Islands concentrate more scientific stations than any other region of Antarctica, giving the advantage of a relative good spatial coverage of meteorological records. Nonetheless, in general these records date back less than 50 years. For this reason other climate archives such as ice cores are required to understand the recent climate variability in a broader context.

The meteorological records used in this investigation comprise the stations Bellingshausen (BELL) (62.2°S, 58.96°W) at the King George Island (KGI, South Shetland Islands), and the stations O'Higgins (OH) (63.32° S, 57.9° W) and Esperanza (ESP) (63.4°S, 56.98°W) located at the Antarctic Peninsula (Figure 4.1). All three stations are located at <50 m a.s.l., and have over-wintering crews operating the whole-year.

The OH and ESP stations are located at the west (WAP) and east (EAP) coast of the Antarctic Peninsula, respectively, at distance of 50 km in a straight line, but divided by the mountain range of the AP. To the east of OH, the mountain chain reaches up to 1030 m a.s.l. at the Laclavere Plateau,

but with several depressions that allow the circulation of air masses between EAP and WAP. The mountain range loses height to the north, and meets the ocean in the Antarctic Sound at the Bransfield Strait. The glaciology of this region has not been extensively explored until today. During 2008 and 2010, several firn cores were extracted including a first time at the northern WAP ice divide presented in this paper. The firn cores were retrieved in key locations completing an altitudinal profile from OH to the Laclavere Plateau (1030 m a.s.l.) at the WAP. The stable water isotope information obtained from these cores is included in the discussion part of this paper. A detailed composition of these sample has been submitted elsewhere (Fernandoy et al., in review).

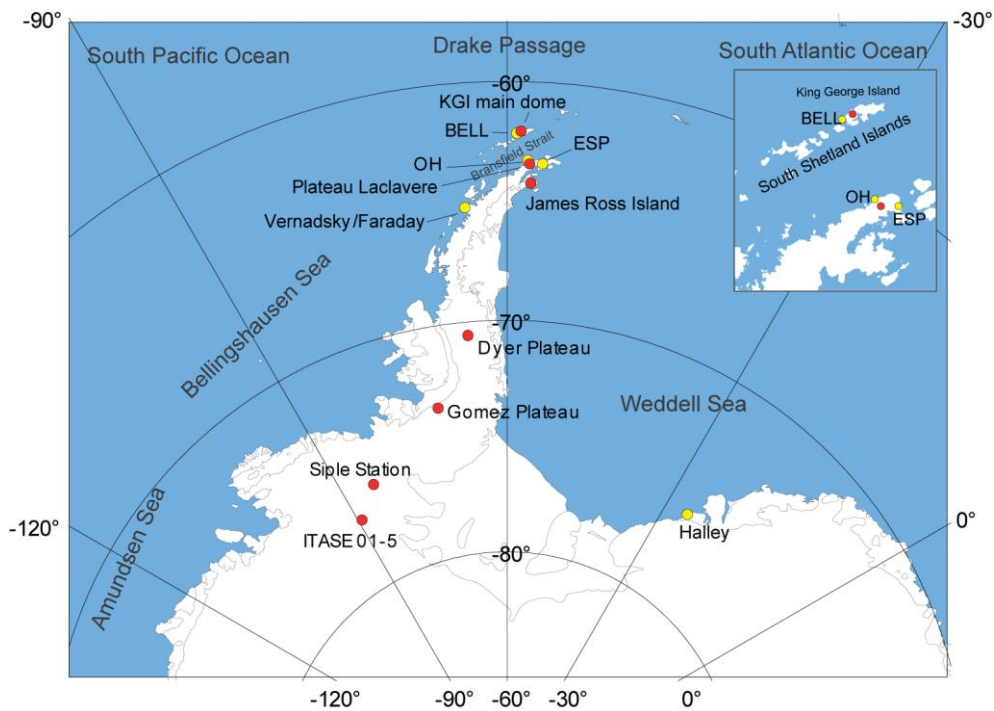


Figure 4.1: Locations referenced in the text, including shallow and middle-depth ice (firn) cores (red dots) and the permanent scientific station (yellow dot). The detail map (upper right corner) shows the exact location of the three stations: BELL (KGI), OH and ESP (WAP) investigated here.

The second study site is located on KGI, the largest of the Shetland Islands with a total area of 1250 km² and almost completely covered by ice (around 90%). The highest point of the island reaches around 700 m a.s.l. at the main glacier dome (Figure 4.1). This island has been subject of glaciological investigations during the last 15 years (e.g.: Wen et al., 1998; Simões et al., 2004a; Blindow et al., 2010; Rückamp et al., 2010), therefore making this locality of special interest to understand the recent climate variability of the region, since geophysical characteristics of the ice sheet are well documented. However, relatively warm summer temperatures (above the melting

point) may initiate substantial surface melt processes. Therefore the interpretation of isotope records of firn cores from KGI needs special consideration of melting and refreezing processes. Additionally, the accumulation rates described in this region are extremely high (around $2500 \text{ kg m}^{-2} \text{ a}^{-1}$), implying that the time span contained in firn cores is very restricted (but offers high temporal resolution).

Finally we compare the recent variability of the northern AP to a longer record using stable water isotope data from the Gomez Plateau ice core (Thomas et al., 2008; Thomas et al., 2009). This core was retrieved at 1400 m a.s.l. the south-western AP (73.59°S , 70.36°E) by a team of the British Antarctic Survey in 2007.

4.4 Data and methods:

4.4.1 Meteorological data

The meteorological data (*T_{air}*) were extracted from the Reference Antarctic Database for Environmental Research (READER) of SCAR (available at: <http://www.antarctica.ac.uk/met/READER/>) (Turner, 2004). Surface temperature data is available as monthly means calculated from 6-hour observations. Monthly mean values were officially included in the READER data set only when more of 90% of the observations were available and no gap larger than two consecutive days existed (otherwise these are only counted as preliminary data or not accurate).

Our study focuses on the surface *T_{air}* records from three stations located at the northern most region of the AP: BELL, OH and ESP (Figure 4.1). All three stations have meteorological time series longer than 40 years. The longest record belongs to ESP, beginning in 1945, but with important data gaps until 1960. Therefore, we use only the ESP data since 1960. OH data exists since 1963. However, several months have less than 90% of daily data and were excluded of the statistical analysis. In only few exceptions (about 10), these months had to be incorporated to the READER data calculations in order to not produce bias in the annual means. BELL has the shortest record (beginning in March, 1968), but with an excellent continuity of the time series, without any months missing. In this paper all three datasets are inter-compared showing a strong coherence for the complete common 42 years period of the time series (1968-2010).

4.4.2 SAM and ENSO indices

The SAM, is a zonal air pressure difference between 40° and 65° latitude south (Marshall, 2003). The Marshall's (2003) SAM index consists of the empirical difference of air pressure at mean

sea level of 12 land stations. The index is basically based on the definition of the Antarctic Oscillation index of Gong and Shaowu (1999) and is available as monthly means since 1957 to the present (available at: <http://www.nerc-bas.ac.uk/icd/gjma/sam.html>).

We used the sea surface temperature anomaly of the ENSO 3.4 region (N3.4 index) as defined by Trenberth (1997), and Trenberth and Stepaniak (2001), which is available from the NCAR Climate analysis section data catalog (http://www.cgd.ucar.edu/cas/catalog/climind/TNI_N34/index.html). The N3.4 index is defined as the sea surface temperature anomaly in the equatorial Pacific region (5°N-5°S, 170°-120°W). The sea surface anomaly index reconstruction is available as monthly means since 1871 to 2007. According to Fogt et al. (2010), the sea surface anomaly at the N3.4 region is correlated to the southern latitudes through the South Pacific teleconnection, especially in conjunction with SAM events.

4.4.3 Stable-water- isotope time series

Stable water isotopes from firn and ice cores expands the climatic information from to areas where no instrumental data are available. Different data sets of stable water isotopes ($\delta^{18}\text{O}$ and δD) were used to investigate the relationship of T_{air} during precipitation moment with the major atmospheric modes (ENSO-SAM). We incorporate two shallow firn cores to the analysis extracted in 2009 and 2010 from the dome of KGI (FP-1), and a firn core retrieved from the Laclavere Plateau (OH-6) at the AP, a key location dividing WAP and EAP (Figure 4.1). Near to the location the core FP-1 (KGI) a Brazilian team extracted a 45 m firn core from the main dome in the austral summer of 1995/96 (Simões et al., 2004a; Simões et al., 2004b). This core shows strong signs of melt and percolation, but still contains interpretable geochemical signals, which were included to our analysis. In complement to the isotope information retrieved from firn cores, a collection of precipitation samples is available since 2008 for both OH and BELL stations. Unlike firn/ice cores, daily precipitation samples are not affected by post-depositional processes as undergone by the cores, therefore they could reveal a more accurate picture of the atmospheric conditions and precipitation events, but clearly in a restricted regional and temporal coverage. For a more detailed description of the firn core and precipitation samples see Fernandoy et al. (2011). In order to understand the recent climate variability on a larger than seasonal or inter-annual time scale, we include a longer stable water isotope record of a recently retrieved ice core from the Gomez Plateau at the southwest AP (Figure 4. 1). This location is well suited for comparison with the north region of the AP, since it exhibits a robust coherence with T_{air} variations at the WAP (King and Comiso, 2003; Sime et al., 2009). Moreover, the isotopic composition of this ice core is correlated statistically significant to the

meteorological record of the stations to the north (e.g.: Thomas et al., 2008; Thomas and Bracegirdle, 2009; Thomas et al., 2009).

4.4.4 Statistical treatment

The statistical analysis of the data was carried out using classic statistical techniques including Pearson's product-moment correlation, seasonal decomposition, and spectral and cross-spectral analysis of the time series.

All data sets were first analyzed producing correlation matrices to reveal possible linear dependency of the different data sets. The correlations were tested for significance by Student t-test and informed as statistically significant at p-level (alpha) <0.05. In some specific cases the significance level is considered at p<0.1 (these exceptions are explicitly highlighted). Due to shortness of the time series, most of the correlation matrices are carried out using a pairwise deletion of missing data. This lead to an improvement of the statistical significance (more valid points), but the comparison between various data sets is performed with different time spans (e.g.: meteorological record of BELL runs for 42 years, while OH runs 47 years).

For the spectral and cross-spectral analysis all data sets were detrended (linear regression model) and in some cases (*T air* monthly mean) seasonally adjusted, to avoid the over representation of the 1-year period since it will overwhelm all other possible cycles. The seasonal adjustment was performed using the Census method I in its additive model. Spectral analyses were carried out following the methodology described by Schulz and Mudelsee (2002), using the DOS-based software REDFIT (available at: <http://www.geo.uni-bremen.de/geomod/staff/mschulz/>). This methodology is especially suitable for data with high variability, since it tests the time series against a red-noise (first-order autoregressive AR-1) background and allows the analysis of unevenly-distributed data without interpolations. Significance levels were fixed at 95% and 99% percent (false-alarm level). Thereafter, time series were checked by a cross-spectral analysis to investigate how the series interact. The analysis was carried out using the SPECTRUM methodology as defined by Schulz and Stattegger (1997). The squared coherency values (C_{xy}^2) of the cross-spectrum analysis were tested at a significance level of 95% and 99% (false-alarm level). The single time series were band-pass filtered using an harmonic-filtering algorithm (Schulz's software ENVELOPE) (see also: Mudelsee and Schulz, 1997).

4.5 Results:

4.5.1 Air temperature (T_{air}) trends:

The recent climate variability of the AP has been extensively described and discussed (e.g.: Adams et al., (2009) and references therein). Most of the authors coincide that the recent temperatures increase is centered at the latitude of the Vernadsky station at the AP, and that the magnitude of the trend slowly decreases to the north. The meteorological records from the northern AP stations fully reflect this tendency. However, despite of the short distance separating OH and ESP stations (about 50 km in a direct line), they show a significant difference of mean temperature (1.3°C) and temperature range (Table 4.1). In spite of the longer distance between of OH and BELL (around 140 km) located at the WAP and KGI respectively, the meteorological records are similar with a difference of the MAAT (1.4°C) explained by the latitudinal difference. Both stations present in average warmer temperatures with respect to ESP, a restricted seasonality (lower standard deviation) and temperature range, which reflects the oceanic control on the local meteorology (Domack et al., 2003a). The ESP station, located at the EAP, presents colder winter temperatures (-5.1°C MAAT) with respect to OH (-3.8°C) and BELL (-2.3°C), and a wider temperature range (Table 4.1), reflecting more continental conditions. The WAP is clearly influenced by the westerly winds of the circumpolar through, while the pass to the east of the relatively humid and warm current is blocked by the mountain range of the AP. The east side is then dominated by colder and drier continental winds, which are transported to the north by atmospheric low center located east of the Weddell Sea (Schwerdtfeger, 1975; Domack et al., 2003a; King and Comiso, 2003).

Station	n (years)	Mean	Min.	Max.	Range	Std. Dev.
BELL	42	-2.34	-4.01	-0.73	3.28	0.80
OH	44	-3.77	-5.43	-2.28	3.15	0.76
ESP	49	-5.09	-7.69	-3.01	4.68	1.18

Table 4.1: Basic statistics of the meteorological record of the stations BELL, OH and ESP from the northern AP beginning in 1968, 1963 and 1960, respectively, to 2009. All three stations are located <50 m a.s.l.

Moreover, the temporal coherence of the three stations: O'Higgins (OH), Bellingshausen (BELL) and Esperanza (ESP) is high, pointing out that the positive trend of the T_{air} is a regional feature. Figure 4.2 shows the monthly temperature record of these stations beginning in 1960, 1963 and 1968 for ESP, OH and BELL, respectively. All three stations show a similar T_{air} increase of around $+0.2^{\circ}\text{C decade}^{-1}$ during the last 50 years (Table 4.2). These trends are also in good agreement with

longer records from the region, as registered at Orcadas station (Zazulie et al., 2010). However, there is a clear difference of the seasonal temperature variations between OH/BELL and ESP stations. The differences of the two climate regimes (West-East AP) observed from annual temperature records are also reflected on the seasonal temperatures scale. From Figure 4.2, it can be observed that the three different meteorological records correlate relatively well. However, the maxima in summer are displaced in several of the years from one station with respect to the others. This can be validated with the correlation coefficients of the annual and monthly values combined to seasonal means according to: summer (December, February, January – DJF), autumn (March, April, May – MAM), winter (June, July, August – JJA) and spring (September, October, November –SON) (Table 4.3). The annual coefficients shows that the best correlation is found between OH - BELL, and OH – ESP, the lowest correlation (but still statistically significant) is found between BELL – ESP.

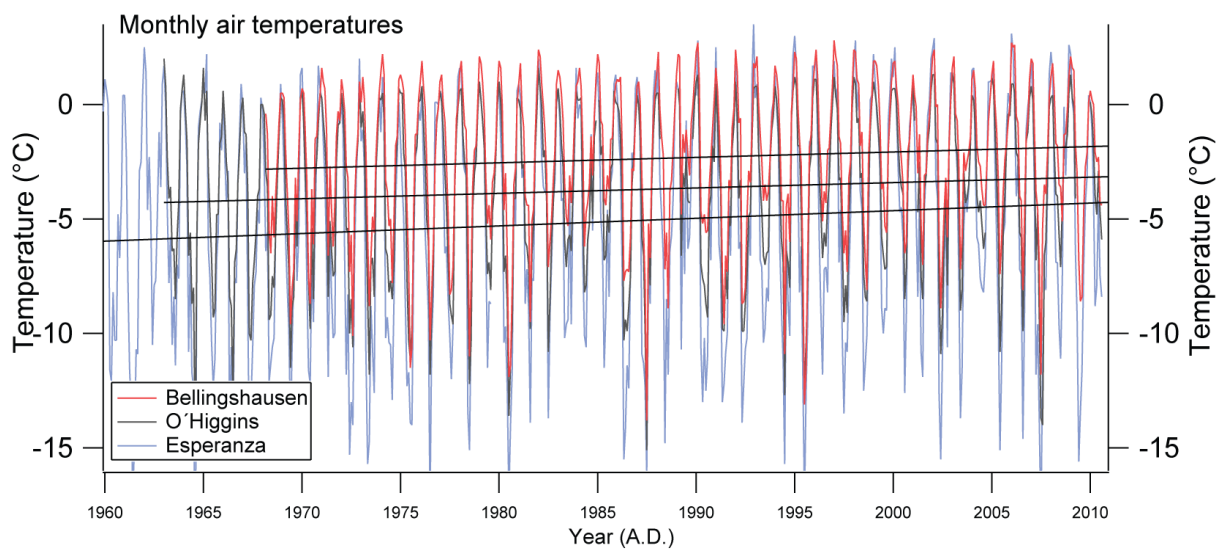


Figure 4.2: Air temperatures (monthly means) of the stations located at the northern Antarctic Peninsula: Bellingshausen (red line), O’Higgins (dark grey) and Esperanza (light blue line). The linear trend of T_{air} (black line) runs practically parallel to the three time series, the values of the linear trends are described in the table 4.2.

The difference between BELL and ESP reflects the influence of local events occurring to the north of BELL in the Drake Passage sector and that can be identified in the OH records as well (King, 1994). This confirms that the north WAP and EAP are (at least to some grade) under the influence of different climate regimes.

Station	Temperature trends ($^{\circ}\text{C a}^{-1}$)					Period
	Annual	Summer	Autumn	Winter	Spring	
BELL	+0.026 $p < 0.05$	+0.007 $p > 0.05$	+0.033 $p < 0.05$	+0.043 $p < 0.05$	+0.009 $p > 0.05$	1968-2009
OH	+0.022 $p < 0.05$	+0.007 $p > 0.05$	+0.037 $p < 0.05$	+0.045 $p < 0.05$	+0.009 $p > 0.05$	1963-2009
ESP	+0.032 $p < 0.05$	+0.039 $p < 0.05$	+0.042 $p < 0.05$	+0.025 $p > 0.05$	+0.025 $p < 0.05$	1960-2009

Table 4.2: Temperature trends (regression coefficients) of the three northern Antarctic Peninsula Stations: Bellingshausen (BELL), O’Higgins (OH) and Esperanza (ESP). The trends include the data records available from the READER project (SCAR). The periods included in the analysis begin in 1960 to avoid period with extensive lack of data. Additionally to the annual means the seasonal summer (DJF), autumn (MAM), winter (JJA) and spring (SON) are show as well. No statistically significant (p -level = 0.05) trend values are marked (light blue).

Correlations are particularly strong during autumn-winter and low in summer. For all seasons the lowest correlation is always between the ESP and BELL records. The highest correlation coefficients are found in autumn and winter. This can be explained by the homogeneity of the atmospheric circulation during autumn and winter, which are dominated by high atmospheric pressure (King and Comiso, 2003; Tymofeyev, 2009).

	Temperature correlation coefficients														
	Annual			Summer			Autumn			Winter			Spring		
	BELL	OH	ESP	BELL	OH	ESP	BELL	OH	ESP	BELL	OH	ESP	BELL	OH	ESP
BELL	1.00	0.94	0.87	1.00	0.43	0.37	1.00	0.95	0.87	1.00	0.94	0.89	1.00	0.90	0.81
OH		1.00	0.93		1.00	0.60		1.00	0.92		1.00	0.93		1.00	0.90
ESP			1.00			1.00		1.00			1.00			1.00	

Table 4.3: Correlation coefficients (r) matrix of T_{air} of annual and seasonal means with statistically significant at p -level = 0.05 or lower.

The seasonality also plays an important role for the recent temperature trends, since the processes controlling the climate variability of the region are modulated by the natural annual oscillations (King et al., 2003). Therefore, seasonal temperature trends are not homogeneous and show differences especially with respect to ESP (Table 4.2). The main factors controlling the climate variability are the the ocean circulation processes west to the AP, the sea-ice feedback mechanisms and the atmospheric circulation, which interact between them (Marshall, 2002; King et al., 2003; Simmonds, 2003; Adams et al., 2009).

From Table 4.2, it can be drawn that OH and BELL (WAP) present the highest and statistically significant trends during autumn and winter, while spring and summer have only moderate positive trends (statistically not significant). The strongest warming trends of the seasonal means for both OH and BELL stations are practically identical (about $0.4^{\circ}\text{C decade}^{-1}$ for autumn and winter), reflecting therefore the regional influence of the warming phenomenon on the WAP. On the other side the strongest (and most significant) trends for ESP occur during summer and autumn season (about $0.4^{\circ}\text{C decade}^{-1}$), with no significant trend during winter. This underlines the difference between both climate domains at WAP and the EAP is obvious.

The origin of the difference of the seasonal trends between EAP and WAP, has been previously investigated (e.g: Turner et al. 2009), and related to atmospheric and oceanic processes. The *T air* of WAP shows a noticeable response to the sea ice cover, since this region is directly exposed to low level westerly (intensified) winds, which originate at the ocean directly to the west (Bellingshausen-Amundsen Sea) (King, 1994; King et al., 2003; Marshall et al., 2006). On the other hand, it has been found that the *T air* summer conditions of the previous season can predispose the sea ice conditions of the next year/season (Weatherly et al., 1991). In turn, winter sea ice conditions will strongly regulate the *T air* of the following season (Weatherly et al., 1991; Jacobs and Comiso, 1997). Furthermore, surface water temperatures at the WAP coastal region have significantly increased during the last half century additionally reducing the rates of sea ice production (Meredith and King, 2005).

On the other side at EAP, the strongest trends were found during summer and autumn. We suggest that the increased intensity of the westerly have reached a threshold, especially during summer when the atmospheric pressures is lower, that allows warm air masses from the western ocean (Amundsen-Bellingshausen Sea) to overcome the natural barrier of the AP. The more frequent pass of warm air masses has also contributed to the enhancement of the Foehn winds effects. This effect produce then a further warming of the air masses (King and Comiso, 2003; van den Broeke, 2005; Marshall et al., 2006).

4.5.2 Meteorological variability and its relationship to SAM:

The SAM is the principal mode of the climate variability on the Antarctic Peninsula Region (Marshall, 2007; Marshall et al., 2011). During the last decades, and in parallel to the atmospheric warming, a strong shift to a positive anomaly has been observed from different SAM index reconstructions. The SAM index of Marshall (2003) shows a significant shift from negative to marked positive values during the last 50 years, with a trend ($+ 0.2 \text{ units decade}^{-1}$) similar to that of *T air*

(Figure 4.3). The SAM variability is highly correlated to annual temperature variations for at least the last half century in this region (Table 4.4.).

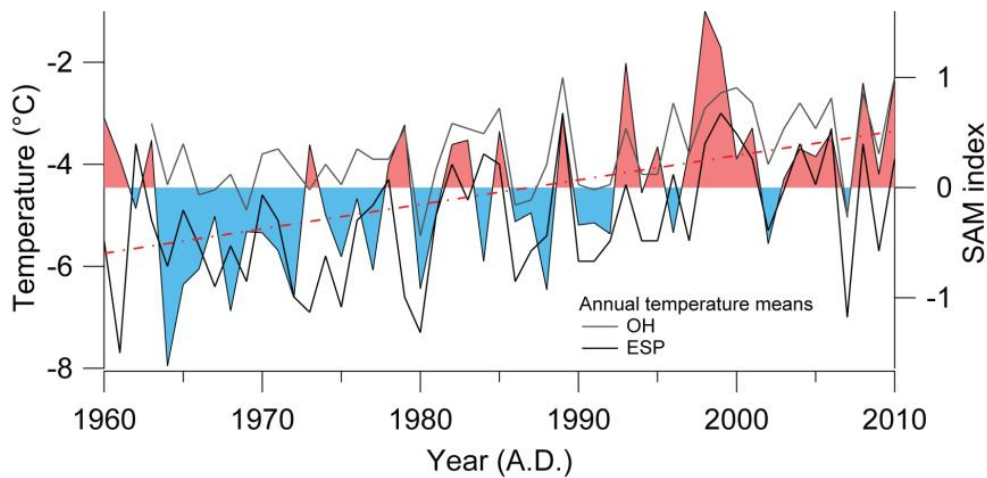


Figure 4.3: Annual mean (1960-2009) of T_{air} of OH (bold grey line) and ESP (bold black line) stations and the SAM index positive (red areas) and negative (blue areas) phases. The SAM index trend is also shown (dashed red line, $0.2 \text{ units decade}^{-1}$).

In Fig. 4.3 the annual T_{air} means for ESP and OH station are displayed against the SAM anomaly for 1960-2010. The highest correlation exist between SAM and annual mean temperatures of both WAP stations (OH and BELL), whereas the correlation between SAM and ESP is slightly lower. All significance levels are very high ($p < 0.01$), clearly documenting a strong relationship of the atmospheric mode and the variability of T_{air} . The coefficient of determination (r^2) for the time series suggest the SAM could explain up to 44% of the annual T_{air} variability at the WAP and 32% at the EAP. Marshall et al. (2006) found even higher values (of about 80%) using detrended time series.

	Annual mean Temperatures		
	BELL	OH	ESP
SAM	0.65	0.66	0.57
	n=43	n=48	n=48

Table 4.4: Correlation coefficients (r) of the annual temperature means and the SAM index. All correlations are significant at $p\text{-level} \ll 0.05$. Note that the valid observations are not the same for the three stations. The time interval of the correlation is 1960 to 2009 for OH and ESP and 1968 to 2009 for BELL.

From monthly means it is observed that the relationship between T_{air} and SAM is not homogeneous throughout the year. Moreover, seasonal T_{air} trends for the period 1960-2009 (Table

4.2) seem to be related to the seasonal *T air* / SAM correlation (Table 4.5). All correlations are found to be positive and again a similar pattern to the *T air* trends appears. The best *T air* / SAM correlations are observed during autumn (MAM) for BELL and OH, whereas for ESP during summer (DJF). Moreover, in many cases it can be observed that the seasonal SAM signal is significantly correlated to *T air* of the preceding season (e.g.: autumn SAM and winter *T air*). This implies that the variability of *T air* of one season will be pre-conditioned by the SAM phase of the preceding season and likely amplifying the *T air* trends.

The correlation matrix in Table 4.5 indicate that the positive *T air* trend is driven by the SAM. Marshall et al (2006) showed that the highest trend of SAM is found in autumn and summer, which is confirmed by the correlation matrix (Table 4.5). Both WAP station (BELL, OH) display strong correlation coefficients in autumn, but diverge especially in summer. In both cases the correlation coefficients for spring (SON) are lower but not significant at BELL with a significance level just above the $p = 0.05$ level. ESP show a larger correlation coefficient in summer than in spring, again confirming that the *T air* trend of this season is considerably related to the increase of the westerlies produced by the SAM strengthening.

SAM	BELL				OH				ESP			
	DJF	MAM	JJA	SON	DJF	MAM	JJA	SON	DJF	MAM	JJA	SON
	DJF	0.28 $p=.070$	0.31 $p=.044$	0.19 $p=.226$	-0.04 $p=.797$	0.51 $p=.000$	0.33 $p=.022$	0.22 $p=.125$	-0.05 $p=.755$	0.60 $p=.000$	0.34 $p=.016$	0.11 $p=.429$
MAM	0.19 $p=.223$	0.62 $p=.000$	0.44 $p=.003$	0.15 $p=.323$	0.32 $p=.029$	0.61 $p=.000$	0.47 $p=.001$	0.18 $p=.226$	0.34 $p=.016$	0.50 $p=.000$	0.35 $p=.011$	0.12 $p=.404$
JJA	-0.15 $p=.340$	0.22 $p=.154$	0.47 $p=.001$	0.14 $p=.363$	-0.28 $p=.054$	0.18 $p=.230$	0.44 $p=.002$	0.09 $p=.564$	-0.14 $p=.334$	0.14 $p=.343$	0.44 $p=.001$	0.02 $p=.880$
SON	-0.09 $p=.560$	0.17 $p=.276$	0.17 $p=.270$	0.29 $p=.058$	-0.06 $p=.674$	0.17 $p=.241$	0.22 $p=.125$	0.38 $p=.007$	-0.06 $p=.701$	0.08 $p=.584$	0.18 $p=.215$	0.39 $p=.006$

Table 4.5: Seasonal correlation coefficients (r) between SAM and air temperatures for the period 1960-2009 at the BELL (42 years), OH (47 years) and ESP (50 years) stations. Correlation coefficients (r) and significance levels (t-Test) are shown. All significant correlations are marked in red (p -level < 0.05).

In summary, BELL and OH behave in some extent different to ESP, as indicated by higher correlation coefficients in autumn. However, the difference of the summer season shows some

similarity of OH and ESP records, since highly correlated to SAM with low p-levels, instead correlation coefficients at BELL are poor.

4.5.3 Stable water isotopes of precipitation and firn cores and their relationship to SAM:

Between 2008 and the present, precipitation samples and several firn cores were collected from OH, Frei station (KGI), and surrounding areas. Frei is located at the same geographical position than BELL, therefore it will be referred to BELL. All samples were analyzed for stable water isotopes at the facilities of the Alfred Wegener Institute in Potsdam, Germany. The stable water isotope composition of precipitations not only reflects the climatic conditions during precipitation ($\delta^{18}\text{O}$ and δD), but also the conditions at the moisture source can be inferred (deuterium excess or *d*-excess) (Dansgaard, 1964; Gat, 1996). Nonetheless, the high variability of the meteorological conditions, as well as local features (e.g.: topography) would significantly affect the isotopic composition.

Important climatic information can be extracted from the isotopic composition of precipitation and firn of the northern AP region (See Fernandoy et al. (in review) also for more detail on the stable water isotope methodology). Unfortunately the collection of precipitation samples covers a short period only, and in some times the collection it has been interrupted due to logistical reasons. Fernandoy et al (in review), shows that the *d*-excess of the precipitation is in fact captures the *T air* variability. A statistically significant relationship has been observed between OH monthly mean $\delta^{18}\text{O}$ and *T air* ($r = 0.65$), as well as for *d*-excess and *T air* ($r=0.72$). However, no correlation has been found between OH precipitation ($\delta^{18}\text{O}$ and *d*-excess) and SAM in the period 2008-2009. Figure 4.4 shows the monthly mean *d*-excess of precipitation from OH and BELL. Unfortunately, this time-span is too short to display any clear relationship between *d* excess of precipitation and SAM, since most likely the correlation between *T air* is lagged by a few weeks or months with respect to SAM variability (see Table 4.5). Therefore, a longer time record is needed to draw a clearer picture of this relationship.

The stable isotope time-series can be expanded when relating to firn and ice cores. These have the advantage of represent a continuous record of the precipitation falling at a region. Moreover, it has been estimated that the precipitation is approximately constant at all seasons (Fernandoy et al., in review).

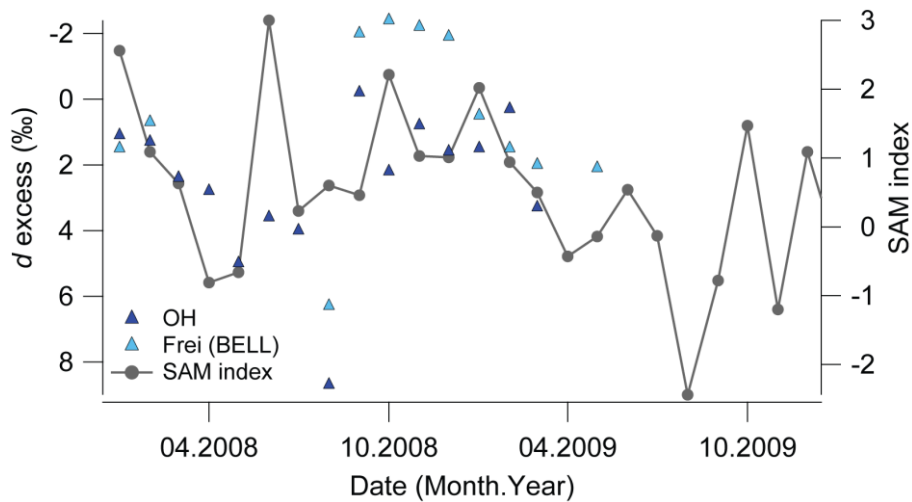


Figure 4.4: Stable water isotope composition (d -excess) of monthly mean precipitation samples collected during 2008 and 2009 from BELL (light blue triangles) and OH (dark blue triangles) as well as the SAM index (grey line). No significant correlation is inferred for this short time span between the time-series.

Here, we present the stable water isotope data of two shallow firn cores (up to 16 m depth) which were retrieved at two key localities from KGI and the AP. The core from KGI, (FP-1) was obtained at the main dome of the island (700 m a.s.l.) whereas the core from the AP (OH-6) derives from the Laclavere Plateau (1030 m a.s.l.) (Figure 4.1). As mentioned above, the latter location is of special interest since it divides WAP from the EAP. The high accumulation rates at both points (about $2500 \text{ kg m}^{-2} \text{ a}^{-1}$) (Fernandoy et al., in review), allow us to calculate a seasonal (monthly) estimate of the stable water isotope composition for a period between 2005 and the end of 2009, which may then be compared to the SAM variability (Figure 4.5). It should be taken into consideration that the firn core from KGI is affected by melt and percolation during summer, which may provoke a homogenization (or blurring) of the original isotope signal. In contrast, OH-6 does not show signs of melt and percolation and should contain a relatively unchanged atmospheric signal.

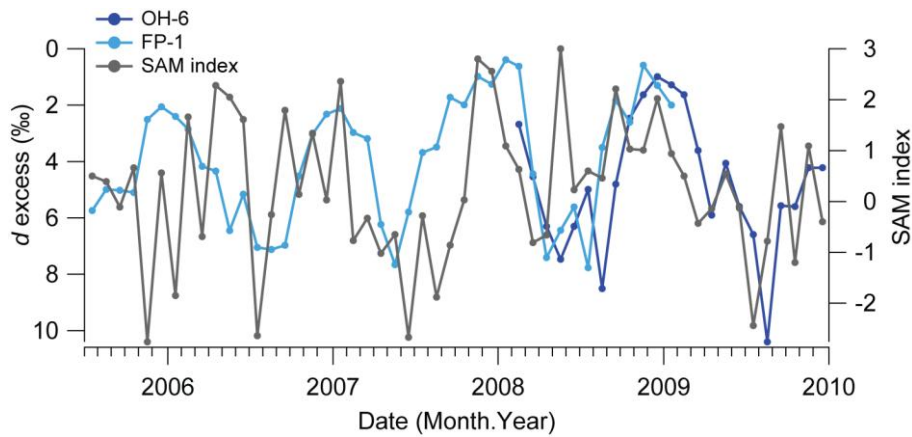


Figure 4.5: The d -excess of the cores OH-6 (AP, dark blue line) and FP-1 (KGI, light blue line). Additionally, the SAM index time series (grey line) are shown. Note that the d -excess axis (left) has been inverted for an easier visualization of the correlation with the SAM index.

The monthly mean d -excess has been found to be the best T_{air} indicator for this region (Fernandoy, in review). Therefore, monthly mean d -excess from both firn cores were grouped in summer-autumn and winter-spring months and compared to SAM index for a similar time interval. A significant correlation is found between d -excess and SAM during the summer-autumn period for both OH-6 ($r=-0.76$) and FP-1 ($r=-0.43$), respectively. These negative correlations coincide with the relationship observed between T_{air} and SAM (Table 4.6), therefore confirming the assumption that SAM plays a key role in the climate variability of the region. On the other hand no important correlation is observed for winter-spring. Moreover, it is important to note the difference between the correlation coefficients of OH-6 and FP-1. OH-6 (as by the T_{air} / SAM relationship) exhibit a strong correlation during summer, this correlation is however weaker for FP-1, probably as consequence of the homogenization of the isotope signal due to melt and percolation in the lower snow and firn layers.

Data from a firn core retrieved near the FP-1 location in summer 1995/96 by a Brazilian team (Simões et al., 2004a) is compared to T_{air} and SAM in Figure 4.6. The core reached 50 m depth, and shows evident signs of percolation and refreezing. Simões et al (2004a), described that the dating of the core was not conclusive and they estimated an accumulation rate of $590 \text{ kg m}^{-2} \text{ a}^{-1}$. However, according to new evidence (Fernandoy et al., in review), the accumulation rates of this area were found to be considerably higher (about $2400 \text{ kg m}^{-2} \text{ a}^{-1}$). Using this new estimate, the dating of the core was reviewed and re-dated (Figure 4.6). The d -excess was measured by Simões et al. (2004a) for the first 7 m only, where a clear yearly cycle is visible. For the rest of the core only δD is available. The δD profile shows a strong homogenization towards the bottom, nonetheless annual means

calculated with our new age model shows a clear similarity to the T_{air} at BELL and up to some extent to the SAM annual variability (Figure 4.6).

	summer-autumn	winter-spring
OH-6	-0.76 p=0.007 n=11	-0.22 p=.492 n=12
FP-1	-0.43 p=0.05 n=21	-0.01 p=.948 n=21

Table 4.6: Correlation coefficients (r) and significance levels (p) of linear regressions of the seasonal d -excess values of the firn cores FP-1 (KGI) and OH-6 (AP) with the SAM index. Note that time span of both cores differs: The core FP-1 covers the time period about August 2005 to February 2009 and OH-6 from about March 2008 to January 2010.

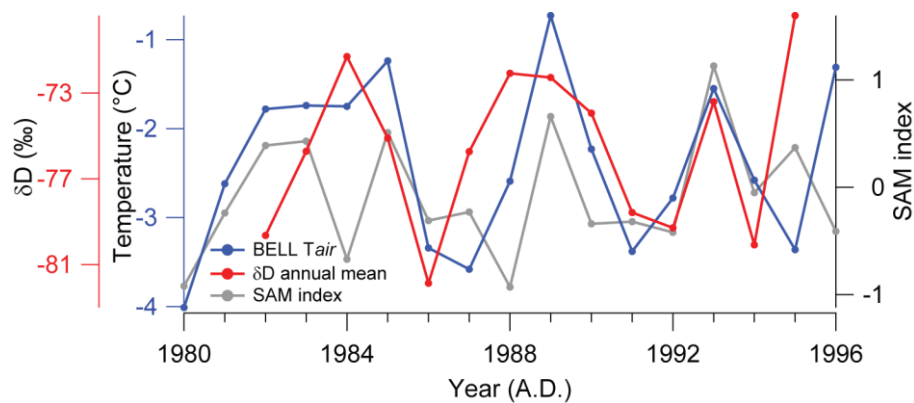


Figure 4.6: Annual means of T_{air} at BELL station (blue line), SAM index (grey line) and estimated δD annual means for the core of Simões et al. (2004a). A similarity is observed for all three curves, however the correlations are statistically not significant.

However, no statistically significant correlation was found between δD of this core and SAM index or BELL T_{air} . Unexpectedly the δD curve has a significant correlation ($p < 0.1$) with T_{air} at OH station ($r = 0.44$). This indicates that in spite of strong percolation and refreezing at KGI some of the climatic signal may still be stored in this core. A longer record, especially from the Laclavere Plateau, would be potentially a great archive to study the temporal evolution of the SAM influence on the climatology of this region.

4.6 Discussion

Several studies have confirmed the increasing air temperature trends during the last decades in the AP (e.g.: Vaughan et al., 2003; Turner et al., 2005; Chapman and Walsh, 2007). Our results make now clear that these trends are spatially and temporally highly coherent to the SAM variability in the northern AP region observed from meteorological data, as well as from the stable water isotope information from firn cores. However, the SAM variability has strongly changed in time, showing a noticeable transition to positive values in the middle to the end of the 1970s (see Figure 4.3). This change has been coincidentally identified from different temperature trends recorded at different stations of the AP, thus, marking a clear break towards a rapid increase of T_{air} the temperatures since then (Kejna, 2003). Moreover, an inversion of the sign of the correlation between T_{air} and SAM has been described at Halley Station (East Antarctica) after the 1980s (Marshall et al., 2011). In the same way, the reversal of the correlation between SAM and the meteorological data can be observed for BELL, OH, and ESP stations (Table 4.7). The reversal of the sign of relationship between T_{air} and SAM variability is most evident during the winter and spring season at all three stations.

For the period 1960-1980 a negative T_{air} / SAM correlation is observed in spring for the three stations (significant only at BELL), while for autumn to winter only a weak correlation can be assessed for BELL and OH. On the other hand, ESP is the only station which shows a significant (positive) correlation during summer, however the OH correlation in summer is high, but significant only at $p\text{-level} < 0.1$.

For the second period (1980-2009), the sign of the T_{air} / SAM relationship during the spring becomes positive and significant for all stations. Additionally a particularly striking increase of the correlation is present in autumn to winter for all three stations. An outstanding change seems to have taken place at the OH station record, since the correlation between T_{air} and SAM during the period 1960-1980 is in fact closer to ESP (located at the EAP) than to BELL (South Shetland Islands). Though, during the second period OH correlations become more similar to BELL, with exception of the summer, which remains significantly correlated to SAM.

a

Annual means correlation 1960-1980

SAM	Annual means correlation 1960-1980											
	BELL				OH				ESP			
	DJF	MAM	JJA	SON	DJF	MAM	JJA	SON	DJF	MAM	JJA	SON
DJF	0.17 p=.625	0.08 p=.804	0.49 p=.125	0.53 p=.092	0.68 p=.096	0.12 p=.793	0.47 p=.293	0.44 p=.321	0.44 p=.039	0.08 p=.722	0.23 p=.310	0.18 p=.412
MAM	0.29 p=.384	0.38 p=.253	0.35 p=.289	-0.24 p=.486	0.64 p=.122	0.11 p=.817	0.05 p=.920	0.24 p=.606	0.43 p=.047	0.04 p=.847	0.16 p=.470	-0.09 p=.678
JJA	0.26 p=.447	-0.08 p=.813	0.29 p=.380	0.11 p=.752	-0.59 p=.160	-0.18 p=.704	0.45 p=.311	-0.91 p=.005	-0.13 p=.560	-0.20 p=.367	0.39 p=.074	-0.27 p=.233
SON	0.08 p=.809	0.41 p=.209	-0.72 p=.012	-0.68 p=.022	0.32 p=.483	0.56 p=.194	0.06 p=.895	-0.31 p=.492	-0.08 p=.709	-0.07 p=.757	-0.25 p=.262	-0.19 p=.394

b

Annual means correlation 1980-2009

SAM	Annual means correlation 1980-2009											
	BELL				OH				ESP			
	DJF	MAM	JJA	SON	DJF	MAM	JJA	SON	DJF	MAM	JJA	SON
DJF	0.22 p=.245	0.34 p=.065	0.02 p=.920	-0.19 p=.306	0.51 p=.003	0.38 p=.036	0.02 p=.926	-0.21 p=.260	0.62 p=.000	0.38 p=.036	-0.11 p=.572	-0.27 p=.139
MAM	0.09 p=.634	0.69 p=.000	0.46 p=.009	0.27 p=.138	0.18 p=.332	0.76 p=.000	0.50 p=.004	0.28 p=.132	0.29 p=.118	0.68 p=.000	0.45 p=.011	0.27 p=.137
JJA	-0.32 p=.080	0.36 p=.044	0.56 p=.001	0.15 p=.414	-0.17 p=.370	0.27 p=.135	0.54 p=.002	0.29 p=.115	-0.12 p=.514	0.30 p=.098	0.50 p=.005	0.24 p=.187
SON	-0.20 p=.285	0.06 p=.744	0.32 p=.083	0.49 p=.006	-0.28 p=.122	-0.01 p=.962	0.32 p=.081	0.55 p=.001	-0.26 p=.162	-0.01 p=.943	0.32 p=.084	0.65 p=.000

Table 4.7: Correlation matrixes between T *air* and SAM index seasonal means for the time interval (a) 1960-1980 and (b) 1980-2009. All statistical significant values are shown in red, additionally all significance (p) values are shown for comparison. Seasons with a reversal of the T *air* / SAM relationship are highlighted with a red frame.

The evident break in the T *air* / SAM correlation in the early 1980s is most likely to linked with the rapidly increasing temperatures particularly in autumn and winter. On the other hand, it shows that the positive trend of air temperatures prior to 1980 cannot be attributed (or at least not completely) to the SAM. Therefore, spectral analysis were carried out for all monthly mean time series to test if any cyclic patterns in the meteorological data that could explain this break in the correlation coefficients and general trends, and if so, how cycles interact with the SAM (cross-spectral analysis). Additionally, the ENSO reconstruction (N3.4) (Trenberth and Stepaniak, 2001) was used in order to investigate possible cycles in a decadal to inter-decadal period. It is presumed that ENSO interacts in an sporadic manner with the Antarctic climatology especially in conjunction with SAM, reinforcing the influence of this latter mode over the AP climatology (Fogt et al., 2010).

For this analysis detrended and seasonal decomposed time series were used to avoid the annual seasonality signal will overwhelm all other possible patterns and the interference of linear

trends. Figure 4.7 show the spectrogram of all three meteorological records as well as SAM and ENSO index time series. From the spectral analysis, several conclusions can be drawn. In Figures 4.7a-c (meteorological record of BELL, OH and ESP, respectively), it can be observed that monthly means are not the ideal data set for this analysis, since the high variability is playing a role in the spectrograms obliterating true patterns. This can be observed from the numerous minor peaks emerging from background level. Nevertheless, the most important features are clearly visible. A peak at about 3.7 years from the OH and BELL, can be found at the ENSO spectral density as well, pointing out a possible relation in cyclical patterns with this period. In contrary this peak is not observed for ESP spectral density. Another important feature are the abundant peaks around the period of 0.4 years, in principle these peaks could be associated to the natural seasonality, but it should be recalled that the time series were first seasonally decomposed (Census I method). Instead, these periodicities are more likely to be related to SAM variability, which present a sharp peak around this period (quite above the false alarm level). Other low period peaks at around 0.2 years are present at all three stations, which again are coincident with SAM. A longer period peak is observed for ESP (around 7 years), however no other time-series shows a similar peak.

Nonetheless, it should be noted that SAM index and the stations data used here are available only for a restricted time interval (50 years or less). The shortness of the record impedes further investigation of the time series, in this way a spectral analysis of annual variability produces no significant results due to the margin of error associated (noise larger than signal). Finally the cross-spectrum's squared coherency of the meteorological data against SAM time-series (Figure 4.7f) and ENSO (Figure 4.7g), which can be interpreted as the grade of common variation in a specific period, reflect again the high level of noise present in the analyses of the monthly mean data. Some of the important peaks (most likely periods to present common variation) are shown for significance level (false alarm level) higher than 99%. Most periods with significant coherency, are found at the single spectrograms as well, however no clear common periodicity can be concluded most likely due to the high noise level present on the monthly time-series signal.

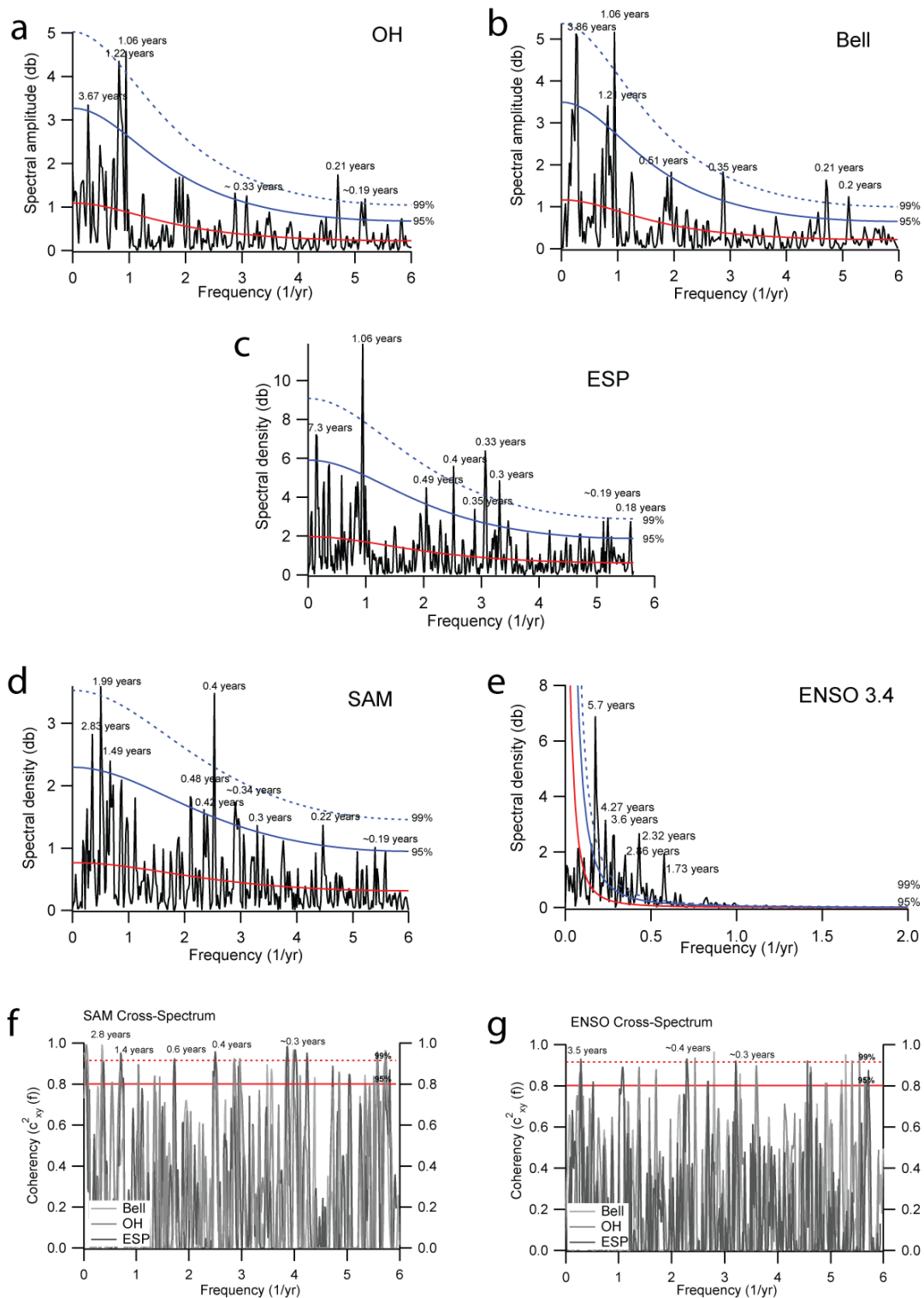


Figure 4.7: Spectral and cross-spectral analysis of the meteorological time-series. Figures (a) to (e) show the spectral density (y-axis in decibel scale) against frequency, the false alarm level (significance level) is shown at 95% (bold blue lines) and 99% (dashed blue lines), as well as the theoretic red-noise level (bold red line). At the bottom the squared coherency (c^2_{xy}) of the cross-spectrums BELL, OH and ESP against (f) SAM time series and (g) ENSO. The false alarm levels are shown at 95 % (red bold line) and 99% (dashed red line).

In order to further analyze how SAM is connected to the climatology of the region, the different time-series were bandpass-filtered in order to eliminate the noise present in the signal. The bandpass filter used is a modified version of the harmonic-filtering algorithm of Ferraz-Mello (1981), which was obtained using the free available software ENVELOPE (<http://www.geo.uni-bremen.de/geomod/staff/mschulz/>; the mathematical background and implementation of the software are available from this website).

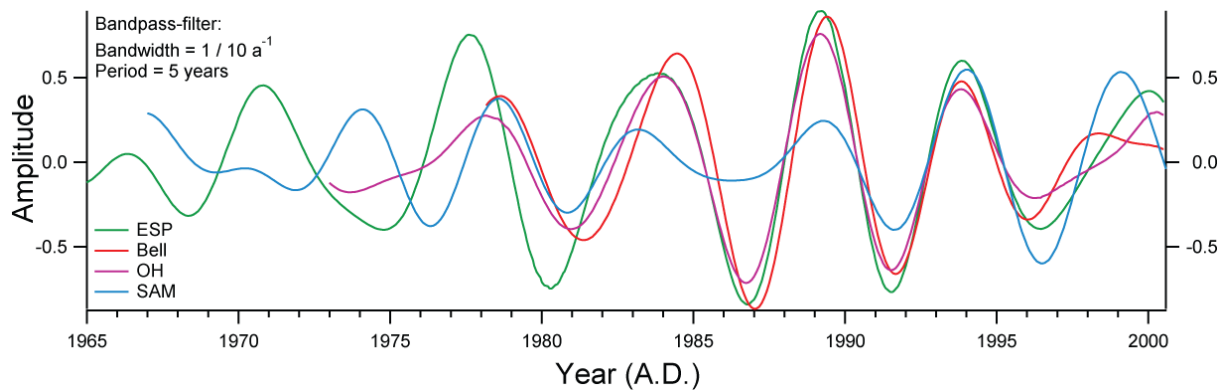


Figure 4.8: Bandpass filtered time-series of meteorological data (*T air*) from OH (purple line), BELL (red line) and ESP (green line), and SAM index (light blue line).

Figure 4.8 shows the filtered time-series for the complete record periods from OH, BELL and ESP in comparison to the SAM index. Using a filter period of 5 years the majority of the noise was cancelled. The figures shows how the amplitude and phase of the transformed time-series strongly change in time. Moreover, since the end of the 1970s it can be observed that SAM and *T air* oscillation became progressively in-phase. The *T air* oscillation reached a maximum amplitude at around 1989, which is coincidentally the warmest year in the registry for all three stations. Unfortunately these observations cannot be extended properly to the time before the 1960s due to the lack of longer records.

A well-suited alternative to meteorological time series in Antarctica are the climate records extracted from ice cores. The ice cores from the AP region are scarce, and some of the existing cores were retrieved at the EAP (e.g.: Dolleman Island and James Ross Island). Climate proxies from these cores most likely do not represent the WAP climate variability (Sime et al., 2009). Another core to investigate the recent climate variability of the WAP, further in the past than the last 50 years, is the core retrieved at the Gomez Plateau (73.59°S / 70.36°W) (Figure 4.1), which according to Thomas et al. (2009) and Sime et al. (2009) well reflects the regional climate variability of the WAP. The annual $\delta^{18}\text{O}$ means are significantly correlated to the meteorological record of the Vernadsky station

($r=0.44$, $p<0.05$) (Thomas et al., 2009). Moreover this correlation can be extended further to north, where the mean $\delta^{18}\text{O}$ record positively correlates to the OH meteorological record ($r = 0.34$, $p<0.05$). This correlation is slightly lower than the Gomez correlation with Verndasky, but it has to be kept in mind that Gomez is located more than 600 km south of Verndasky and more the 1200 km south of OH. The positive correlation between annual means of OH T_{air} and the $\delta^{18}\text{O}$ record from Gomez Plateau is explained by the circulation patterns at the AP. Thomas and Bracegirdle (2009), demonstrated that the westerly air currents at the north AP are deflected to the south by the mountain chain, these air flows reach the southern AP, where moisture transported from the southern ocean finally precipitates.

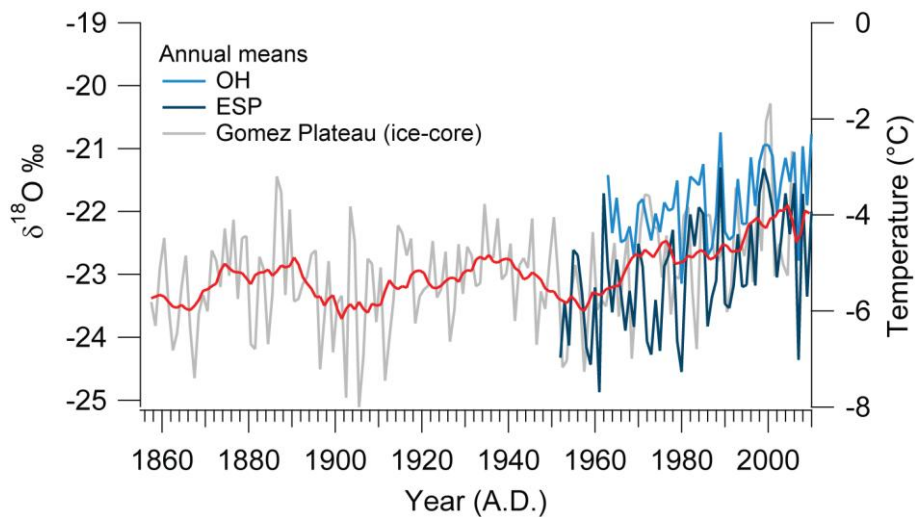


Figure 4.9: Comparison of the T_{air} time series from OH (light blue line) and ESP (dark blue line) stations to $\delta^{18}\text{O}$ time series from the Gomez Plateau ice core. The correlation of T_{air} and $\delta^{18}\text{O}$ is statistically significant only for OH ($r=0.34$). The rapid increase of $\delta^{18}\text{O}$ (and T_{air}) values since the 1960s is visible from the 11-year moving average smooth (red bold line).

The $\delta^{18}\text{O}$ time-series from the Gomez plateau ice core shows, that just before the instrumental period (around 1950) a small decrease of T_{air} precedes the beginning of the recent warming trends. The recent increase of T_{air} derived by Thomas et al. (2009) from the $\delta^{18}\text{O}$ values is around $0.5^\circ\text{C decade}^{-1}$, which is almost the double of the northern AP trend and therefore closer to the Vernadsky (Faraday) station trends. Nonetheless the spectral analysis (Figure 4.10) of the $\delta^{18}\text{O}$ time-series shows similar cycles as seen before for the northern AP station. From Figure 4.10a, it is observed that the cycles at around 3 and 5.1 years are the most significant ones. Both can be correlated most likely to SAM variability, as seen from the cross-spectral squared coherency for Gomez ice core and SAM (Figure 4.10c). Nonetheless, a similar 2.8 years period cross-correlation is

observed from the spectrum of $\delta^{18}\text{O}$ and ENSO (Figure 4.10b), pointing out a possible relationship of ENSO and SAM at this period. A larger 7-year period from the $\delta^{18}\text{O}$, is apparently driven by the SAM. The longer annual record, as compared to the meteorological data, leads to a substantial reduction of the noise in the time-series signal, improving the interpretation of the cycles in T air ($\delta^{18}\text{O}$) changes and of the cross-correlation with the atmospheric modes.

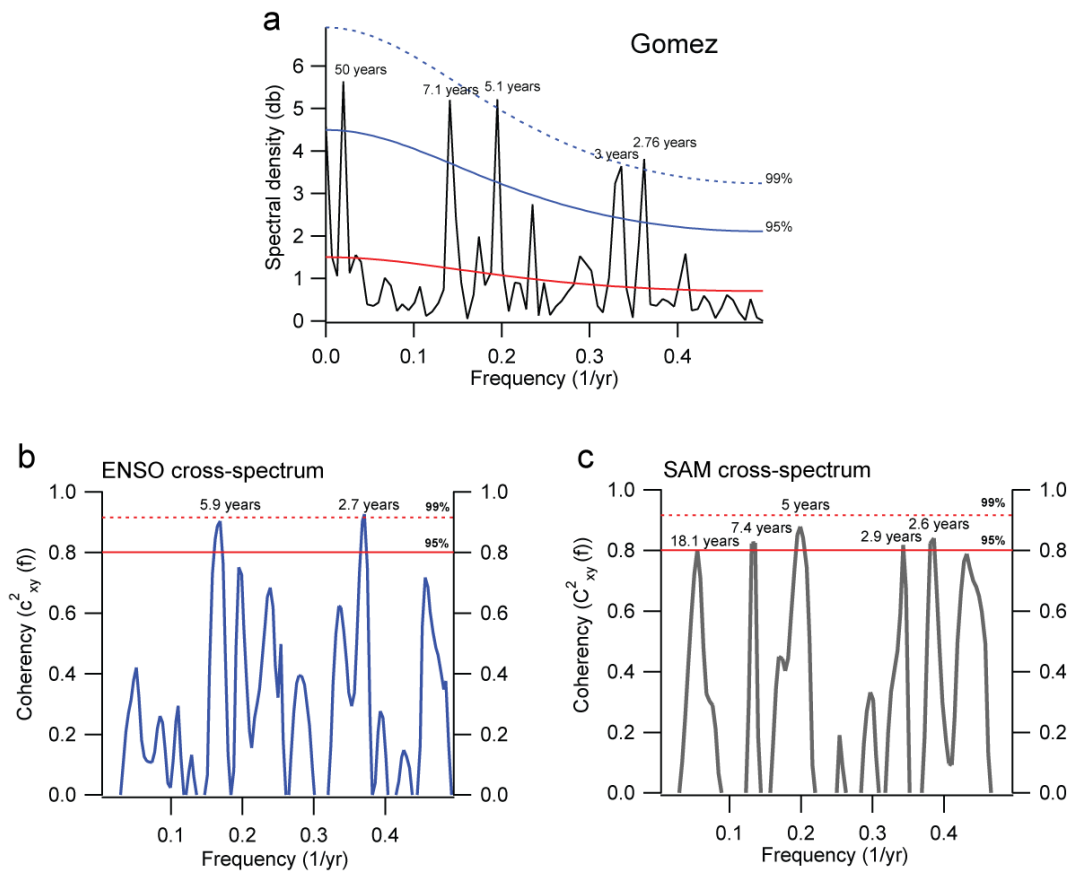


Figure 4.10: (a) Spectral density of the $\delta^{18}\text{O}$ time series calculated for annual means from 1858 to 2006, and cross-spectral squared coherency for (b) $\delta^{18}\text{O}$ and ENSO (1871 to 2006) and (c) $\delta^{18}\text{O}$ and SAM index (1957 – 2006) annual means.

4.7 Conclusions

In this paper, we demonstrate the spatial and temporal coherence of the recent climate variability at the northern Antarctic Peninsula. Using meteorological data from three different stations and stable water isotope data sets from firn and ice cores retrieved in the north (Simões et al., 2004a; Fernandoy et al., in review) and south Antarctic Peninsula (Thomas et al., 2009), a significant correlation between the atmospheric modes and air temperature trends has been found. All data sets show a positive correlation to the SAM index. Moreover a marked break was

detected in the early 1980s, when the correlation coefficients between T *air* and SAM rapidly increased and became statistically significant during practically all seasons. The stable water isotope composition of firn cores extracted recently in the area of investigation, show that precipitation events during summer and autumn have a more significant correlation to SAM, while in winter the correlation is weaker (and not significant). Thus, the shift of SAM to its positive phase during the last decades could have an effect on the precipitation regime of the region, especially during summer and autumn seasons. This scenario has been already described from the Gomez Plateau ice core for the southern Antarctic Peninsula (Thomas et al., 2008). Annual $\delta^{18}\text{O}$ means of this core retrieved in 2007 show a significant correlation to T *air* records from the northern Antarctic Peninsula. Time-series analysis (spectral and cross-spectral analyses) show that the mean annual $\delta^{18}\text{O}$ and meteorological annual means data display cyclic recurrent patterns (e.g.: 2.7, 5.1 and 7 years) that can be attributed to the influence especially of the SAM, but also an ENSO signal is possible. Since the early 1980s through the 2000s an in-phase SAM and T *air* correlation is observed. The coupled oscillation reaches a maximum amplitude in 1989, which is the warmest year of the registry for all three stations. Therefore, we assume that the shift of SAM drives most of the climate variability of the region.

The Antarctic Peninsula is characterized by two distinctive climatic regimes, the west coast with a milder and warmer climate (OH and BELL stations) dominated by the westerly wind flows, and the east coast (ESP station) with a colder and drier climate characterized by flow of continental air masses transported by the atmospheric depression east of the Weddell Sea. The intensification of the westerlies is now influences both regions, but with a seasonal component especially evident in the summer and autumn of the east and west coast, respectively. At the divide of both areas in the northern Antarctic Peninsula (Plateau Laclavere), a firn core has been extracted in 2010. Hence, this coring location is a key region to understand of the recent climatic evolution. The isotopic composition of this firn core is highly correlated to the SAM variability (but only on a short time period). A longer record from this area would allow to comprehend the how the shift of SAM has influenced the climatology of this region. This is at the moment not possible due to the lack of long climate records (e.g.: of ice cores) from the north Antarctic Peninsula.

5 Temporal and spatial variation of stable isotope ratios and accumulation rates in the hinterland of Neumayer Station, East Antarctica

Francisco Fernandoy, Hanno Meyer, Hans Oerter, Frank Wilhelms, Wolfgang Graf and Jakob Schwander

(Journal of Glaciology, Vol. 56, No. 198, p. 673-687)

5.1 Abstract

Four firn cores were retrieved in 2007 at two ridges in the surroundings of Ekströmisen, Dronning Maud Land, coastal East Antarctica to investigate the recent regional climate variability and the potential for future extraction of an intermediate-depth core. Stable water isotope analysis, tritium content and electrical conductivity were used to date the cores. For the period 1981-2006 a strong and significant correlation between the stable-isotope composition of firn cores in the hinterland and mean monthly air temperatures at Neumayer station has been observed ($r= 0.54$ up to 0.71). Therefore, no atmospheric warming or cooling trend is inferred from our stable-isotope data for the period 1962-2006. The stable isotope record of the ice/firn cores could expand well beyond the meteorological record of the region. No significant temporal variations of accumulation rates were detected. However, decreasing accumulation rates were found from coast to hinterland, as well as from east (Halvfarryggen) to west (Søråsen). The deuterium excess (d excess), exhibits similar differences (higher d excess at Søråsen, lower at Halvfarryggen), with a weak negative temporal trend on Halvfarryggen (0.04‰ a^{-1}), probably implying increasing oceanic input. We conclude that Halvfarryggen acts as natural barrier for moisture-carrying air masses circulating in the region from east to west.

5.2 Introduction

The Antarctic ice provides one of the best paleo-climate archives for the Holocene and large parts of the Pleistocene, as demonstrated by the ice cores of the European Project for Ice Coring in Antarctica (EPICA) at Dome C and in Dronning Maud Land (back to 800 kyr) (EPICA Community members, 2004, 2006; Jouzel et al., 2007). One of the four tasks formulated by the International Partnerships in Ice Core Sciences (IPICS) is to recover the oldest ice core record in Antarctica (up to 1.2 to 1.5 Ma). Complementary, in the Northern Hemisphere a new deep-core is being extracted from the Greenland ice-cap, aiming to recover for the first time a complete record of the last

interglacial period (Eem) from Greenland. Additionally, a bipolar network of intermediate-depth high temporal-resolution cores back in time beyond the last glacial maximum is promoted within the IPICS 40k array, as well as a world-wide IPICS 2k array initiative, thus including ice cores studies in high mountain regions at lower latitudes (Brook et al., 2006). This network will allow study of both the pre-industrial era and the most recent climate evolution, which is presently not properly covered by the existing meteorological and ice core network. The work presented here was planned as a pre-site survey for an ice core contributing to the IPICS 40k array. Due to higher than expected accumulation rates, we realised that an intermediate-depth ice core will most likely not cover 40 ka and, thus rather contribute to the IPICS 2k array.

In the last few years, it has been demonstrated that atmospheric warming in West Antarctica and some restricted coastal areas (IPCC, 2007; Steig et al., 2009) is most likely related to the release of industrial gases into the atmosphere (Gillett et al., 2008). Based on meteorological and satellite observations, Steig et al. (2009) concluded that West Antarctica showed increasing air temperatures of $0.17 \pm 0.06^\circ\text{C}$ per decade between 1957-2006, with a strong maritime influence. In contrast, East Antarctica exhibited just $0.10 \pm 0.07^\circ\text{C}$ temperature rise per decade and is dominated by more continental conditions. Other authors report that East Antarctica have been slightly cooling during the last half of a century (Thompson and Solomon, 2002; van den Broeke and van Lipzig, 2004). This difference between East and West Antarctica was linked by Marshall et al. (2006) and Marshall (2007) to the intensification of the Southern Annular Mode (SAM). Statistically significant warming trends have been observed only on the Antarctic Peninsula and in some restricted areas of the East Antarctic coast. In general, there is a broad agreement that the Antarctic continent is subject to moderate warming only on the west side. This warming is in the range of the Southern Hemisphere's temperature increase of around 0.08°C to 0.12°C per decade, which probably began in the late nineteenth century with increasing rates since the 1970s (Turner et al., 2005; Schneider et al., 2006; Chapman and Walsh, 2007; Monaghan et al., 2008; Steig et al., 2009).

As a response to rising air and ocean temperatures, the mass balance of the Antarctic ice sheet reacts with a bimodal behaviour. West Antarctica is suffering overall a clear negative mass balance of $-48 \pm 14 \text{ km}^3 \text{ a}^{-1}$ (Rignot and Thomas, 2002). Extreme consequences on the dynamics of mass balance were observed at the northern Antarctic Peninsula. The disintegration of ice shelves along the Antarctic Peninsula triggered an accelerated out-flow of inland glaciers (Scambos et al., 2000; De Angelis and Skvarca, 2003; Rignot et al., 2004). These events have been most probably linked to the increase of the sea-water temperature (Levitus et al., 2000; Robertson et al., 2002; Shepherd et al., 2004). The situation in East Antarctica has been widely discussed, mostly because of

the impossibility to make direct observations in such vast territory. Rignot and Thomas (2002) could not confirm the sign of the mass balance ($+22\pm 23 \text{ km}^3 \text{ a}^{-1}$). The ice sheet seemed to stay close to a steady-state mass balance, with only local loss of mass especially in coastal regions (Rignot, 2006), or even thickens (Davis et al., 2005). In contrast, new satellite observation techniques based on gravity measurements, definitively demonstrate that the loss of mass in coastal regions, is leading to a negative mass balance of East Antarctica (Chen et al., 2009). This evidence displays the importance of making direct observations in coastal zones, where a big data gap still exists.

Many of the authors cited above agree that the future evolution of the ice sheet will be highly dependent on the reactions of ice shelves to increasing temperatures of ocean waters and the atmosphere. For this reason, more dense and accurate observations of accumulation rates and mass balance, especially in coastal zones, are needed. One of the principal aims of this paper is to reconstruct the recent climate variability at a coastal site of East Antarctica. With this objective and in order to evaluate the potential of ice cores at the coastal Dronning Maud Land for paleo-climatic reconstruction, the regional variability of stable water isotopes has been examined.

In this paper, we present new evidence supporting relatively stable conditions at least for the past 50 years in the hinterland of the German Neumayer Station, located in Dronning Maud Land, coastal East Antarctica (Figure 5.1). We base our observations on detailed stable isotope measurements of four firn cores retrieved in the austral summer of 2007.

5.3 Study area and background information:

In January 2007, a German-Swiss team drilled four firn cores on two ice ridges to the east (Halvfarryggen) and to the west (Søråsen) of Ekströmisen (Figure 5.1). The campaign was a pre-site survey to find a suitable location for intermediate deep coring in a coastal high-accumulation site to be carried out in the frame of the IPICS 2k array project (Brook et al., 2006).

At Halvfarryggen, two firn cores named B38 (84 m deep) and FB0702 (42 m deep) were drilled. At Søråsen B39 (78 m deep) and FB0704 (36 m deep) were retrieved. Additionally, 6 m deep firn cores FB0701 and FB0703 were drilled at the same positions as FB0702 and B39, respectively. High resolution isotope measurements of the last two shallow firn cores are used to fill a small gap of measurements of core FB0702, and to prove the reliability of stable isotope records. The cores B04 and FB0202 (Schlosser and Oerter, 2002b), both drilled at the Neumayer station, were also incorporated in our study. The geographical coordinates of all drilling sites are given in Table 5.1.

The closest meteorological stations are located at the base Neumayer II (70°39'S, 8°15'W) which provides air-temperature data between 1992 and 2008, and the former base Georg-von-Neumayer (70°37'S, 8°22'W) which provides data between 1981 and 1992. Both stations are from here on referred together as Neumayer station. The Neumayer station is located at a distance of 80 km to 164 km from the four drilling sites. According to König-Langlo and Loose (2007), the climatological conditions at the Neumayer station are dominated by the circumpolar trough, with dominating easterly winds and characteristic katabatic winds during high-pressure events. Mean annual 2-m air temperature (MAAT) in the vicinity of Neumayer station shows a clear inter-annual variability, with an average temperature of -16.1°C for the period 1982-2006. However, no significant temporal trend has been observed during this time span. On a regular schedule various glaciological observations have been carried out in the vicinity of the bases. Accumulation studies based on firn-core and snow-pit analyses as well as *in-situ* observations (stake arrays) are in good agreement and give a rate of about 360 kg m⁻² a⁻¹ for the period 1950-2000 (Schlosser and Oerter, 2002b).

The origin of the precipitation at Ekströmisen was investigated by Schlosser et al. (2004; 2008) combining backward trajectory models and stable-isotope analyses of fresh-snow samples. Six main trajectory clusters were found to reach Neumayer station at the 850 hPa level (assumed condensation level at Neumayer): the most frequent backwards trajectories originate over the Weddell Sea, closely followed by a cluster coming from the east along or slightly north of the coast. Other trajectories originate to the south of Neumayer station, South Atlantic Ocean (low latitude), the Bellingshausen Sea and one between the Antarctic Peninsula and South America (Schlosser et al., 2004; Schlosser et al., 2008).

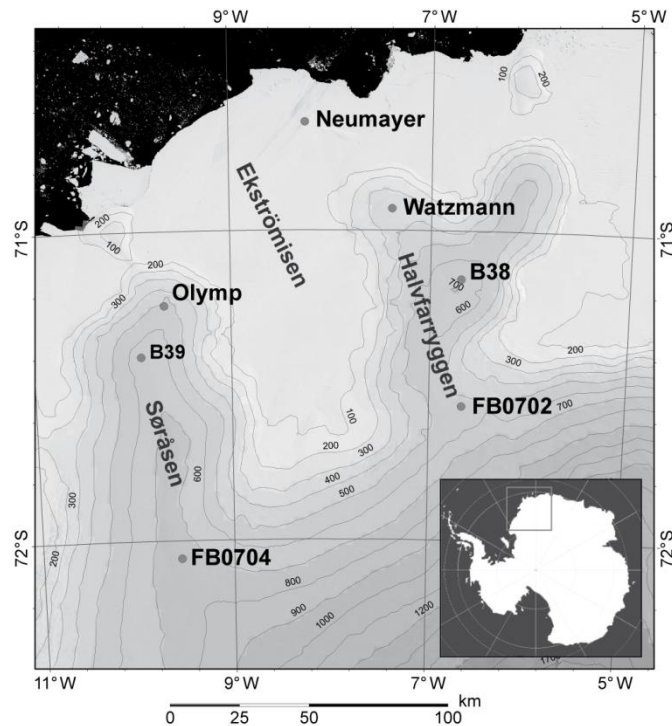


Figure 5.1: Geographical location of the drilling sites. B38 and FB0702 are located on Halvfarryggen (East ridge); B39 and FB0704 on Søråsen (West ridge). Neumayer is the overwintering base on the ice shelf Ekströmisen. Olymp and Watzmann are geophysical observatories. The shallow firn cores FB0701 and FB0703 were drilled at the same coordinates as FB0702 and B39, respectively. Contour intervals are 100 m. Elevations are given with respect to WGS84. The insert map shows the location of the area under investigation (light gray) in Dronning Maud Land. The length scale is related to 71°S. The underlying image is from Landsat Image Mosaic of Antarctica (LIMA) of the US Geological Service and the British Antarctic Survey (<http://lima.usgs.gov>), the Digital Elevation Model is from Wesche et al. (2009).

5.4 Methods

All firn cores were processed in the cold laboratory facilities of the Alfred Wegener Institute for Polar and Marine Research (AWI) in Bremerhaven. At first, the four cores were analysed using dielectric profiling (DEP) and γ -absorption (Wilhelms, 2000; Wilhelms, 2005) at 5 mm resolution, to determine electrical conductivity and density, respectively. Samples for water stable-isotope analysis were taken with a depth resolution of 1 m (B38 and B39) and 0.5 m (FB0702 and FB0704) for both $\delta^{18}\text{O}$ and δD , and with a higher resolution of 7 cm (B38 and B39) and 5 cm (FB0702 and FB0704) for $\delta^{18}\text{O}$ only (Figure 5.2). Stable-isotope measurements were performed with Finnigan-MAT Delta S mass spectrometers using the gas equilibration technique as described in Meyer et al. (2000) at the Alfred Wegener Institute. The accuracy of this method is better than $\pm 0.1\text{‰}$ for $\delta^{18}\text{O}$ and $\pm 0.8\text{‰}$ for δD . $\delta^{18}\text{O}$ and δD values are given as deviation from the Vienna Standard Mean Ocean Water (VSMOW) in permil. Tritium (^3H) concentrations were measured along selected parts of the cores B38 and B39 at a laboratory of the Helmholtz-Zentrum München to assist the dating.

From stable-isotope measurements, different basic parameters were calculated to characterize the recent local and regional hydrological conditions in the study area. The Global Meteoric Water Line (GMWL) is derived from the correlation between $\delta^{18}\text{O}$ and δD , at global scale, given by the relation: $\delta\text{D} = 8 \delta^{18}\text{O} + 10\text{‰}$ (Craig, 1961). At a regional scale this relation is expressed as the Local Meteoric Water Line (LMWL), which is influenced by local climatic and geographic conditions, as well as by input from secondary moisture sources, re-evaporation and/or sublimation (Merlivat and Jouzel, 1979; Clark and Fritz, 1997; Sharp, 2007). The second order parameter deuterium excess: $d = \delta\text{D} - 8 \delta^{18}\text{O}$ (Dansgaard, 1964) is known to reflect conditions in the moisture source region. The d excess depends on the Sea Surface Temperature (SST), the wind speed and mainly on the relative humidity (from now on called “ h ”) at the source (Clark and Fritz, 1997; Sharp, 2007). Unlike $\delta^{18}\text{O}$ and δD , the d excess generally does not vary during condensation of vapour masses (Merlivat and Jouzel, 1979; Sharp, 2007). Depletion of $\delta^{18}\text{O}$ and δD will follow approximately a Rayleigh distillation model during condensation and precipitation of moisture (Jouzel and Merlivat, 1984). Therefore, the evolution of the $\delta^{18}\text{O}$ and the δD content is directly related to air temperature, height, and distance from the source. The combination of both isotope systems allows us to study not only the precipitation process and its climatic implications, but also the origin and evolution of moisture masses.

5.5 Results

5.5.1 Dating of the firn cores:

The four firn cores were dated using annual layer counting of seasonal variations of $\delta^{18}\text{O}$, assisted by DEP profiles and the tritium measurements. The seasonal cycles of $\delta^{18}\text{O}$ are generally easy to distinguish (Figure 5.2). According to annual layer counting, the oldest layers were deposited in 1935 (in core B39), 1959 (FB0702), 1960 (B38) and 1962 (FB0704). This dating was confirmed by the distribution in depth of the tritium content in the cores B38 and B39. (Figure 5.3, for details of the used method see Oerter et al. (1999)).

The seasonal variations of the electrical conductivity (DEP) were used to check the layer counting (Figure 5.4). However, no dominant peaks with volcanic-related events were found. Even the well-known acid depositions from the eruptions of Mt. Pinatubo in 1991 (deposition in 1992) or Mt. Agung in 1963 (deposition in 1964), as mentioned by Traufetter et al. (2004) and Hofstede et al. (2004), could not be observed in our DEP profiles. However, a maximum in the DEP profiles of the coastal cores B38 and B39 was found and likely related to the year 1975. This peak could be linked to

the occurrence of the Weddell Polynya phenomenon. The Polynya was a large sea-ice free region in the Weddell Sea during the winters of 1974 to 1976 (Carsey, 1980). One of the most recent explanations for this peculiarity is the dynamic interaction of oceanic currents and the sub-marine topography in front of the Dronning Maud Land coast (Holland, 2001). The air-sea interaction contributed to an increase of the sea surface salinity (Moore et al., 2002). Therefore, this local moisture source could influence the di-electrical profiles of the cores in this period of time. In the hinterland cores FB0702 and FB0704, a similar maximum is observed slightly later (1976 or 1977). A second DEP peak (1997-1998) is coincident with another polynya event in the Weddell Sea (Ackley et al., 2001), but this last peak is not clearly visible at the cores B38 and B39 (Figure 5.4). As consequence, the uncertainty of the dating was estimated to be less than ± 2 years for all cores. For B38 and B39, a dating uncertainty of ± 1 year is likely. In general, these examples show the difficulty in using DEP peaks for dating purposes in coastal areas with high snow accumulation rates. This is also due to the fact that DEP profiles are affected by high-content of sea salt components (Bertler et al., 2005), which may blur volcanic signals.

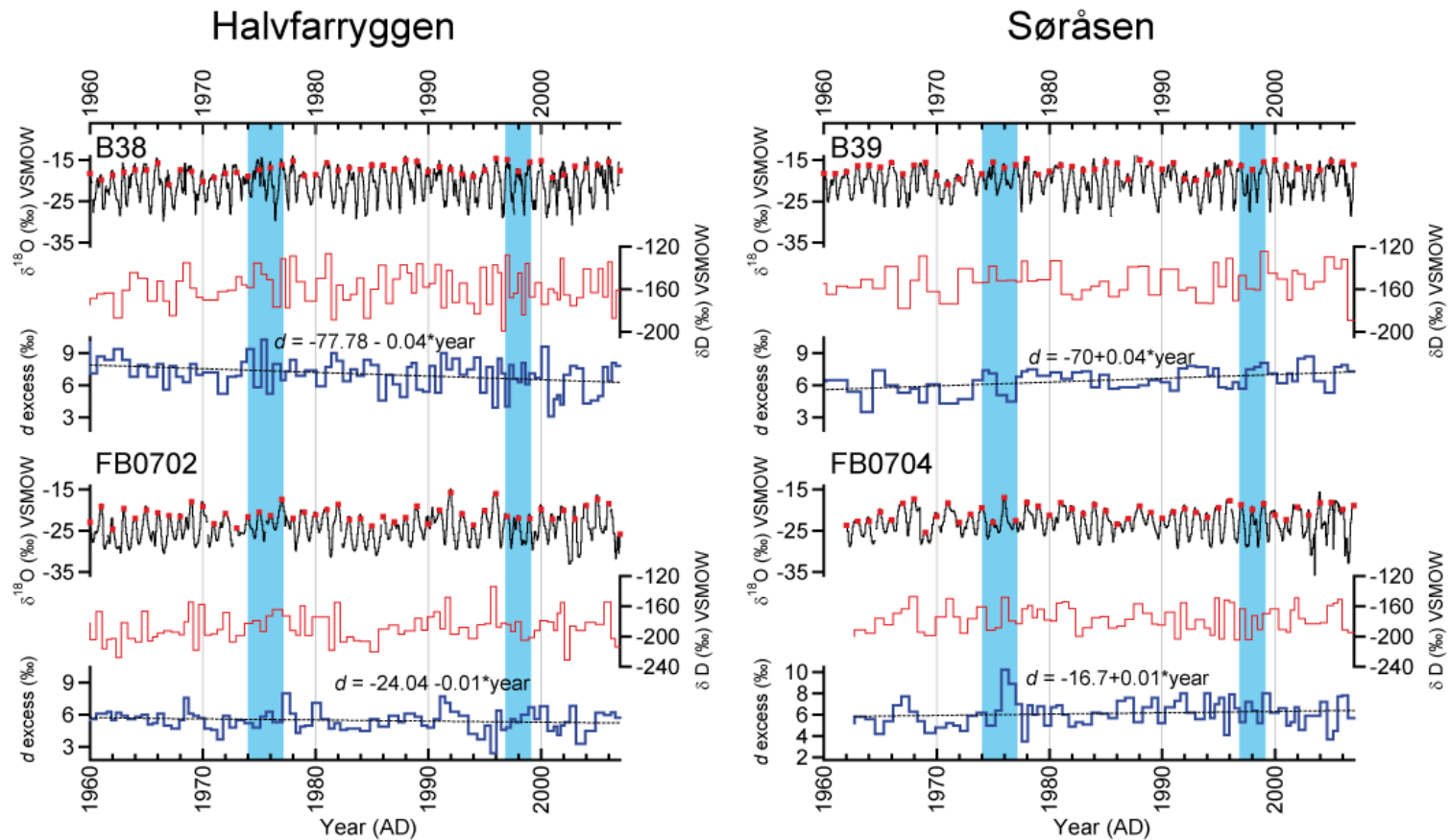


Figure 5.2: Time series (1960-2007) of stable water isotopes from the cores B38 and FB0702 (Halvfarryggen) as well as B39, and FB0704 (Søråsen). Black lines show $\delta^{18}\text{O}$ data with high depth resolution (5-7 cm). The seasonal cycles are clearly visible for all cores and could be used for the dating. Red dots indicate the austral summers defined as annual boundaries. The red lines show δD data on a lower depth resolution (1 m and 0.5 m). At the bottom of each diagram (blue lines) d excess data at 1 m (B38 and B39) and 0.5 m (FB0702 and FB0704) resolution is shown. Dashed black lines represent linear regressions of d excess time series. A negative temporal trend for Halvfarryggen (B38 and FB0702) and a positive temporal trend for Søråsen (B39 and FB0704) were found. Only trends in B38 and B39 are statistically significant (p level < 0.01). Light blue bars represent the periods of prominent polynya events in the Weddell Sea region (1974-1976 and 1997-1998)

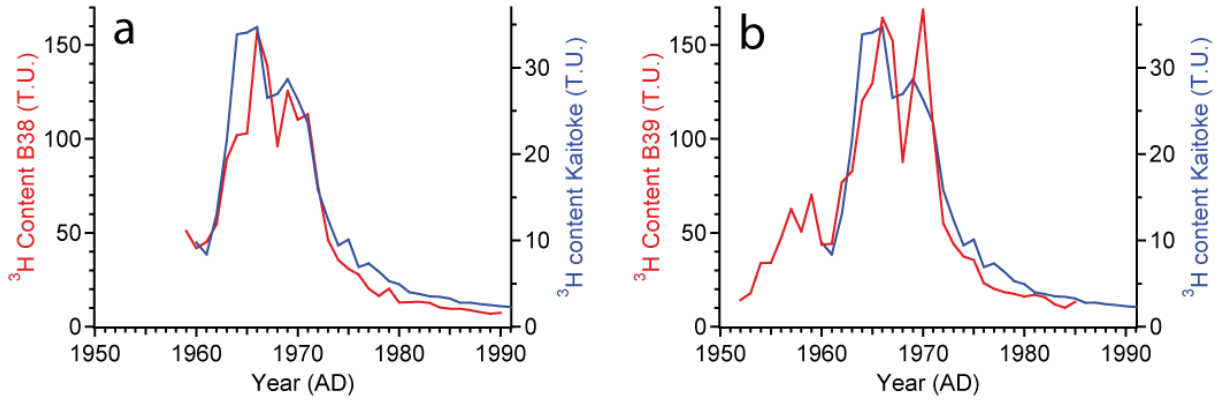


Figure 5.3: Both figures show the fit of the tritium profile (red curve) of firn cores B38 (a) and B39 (b), to the tritium profile of precipitation (blue curve) at Kaitoke (New Zealand). Tritium data of precipitation from IAEA/WMO (2006).

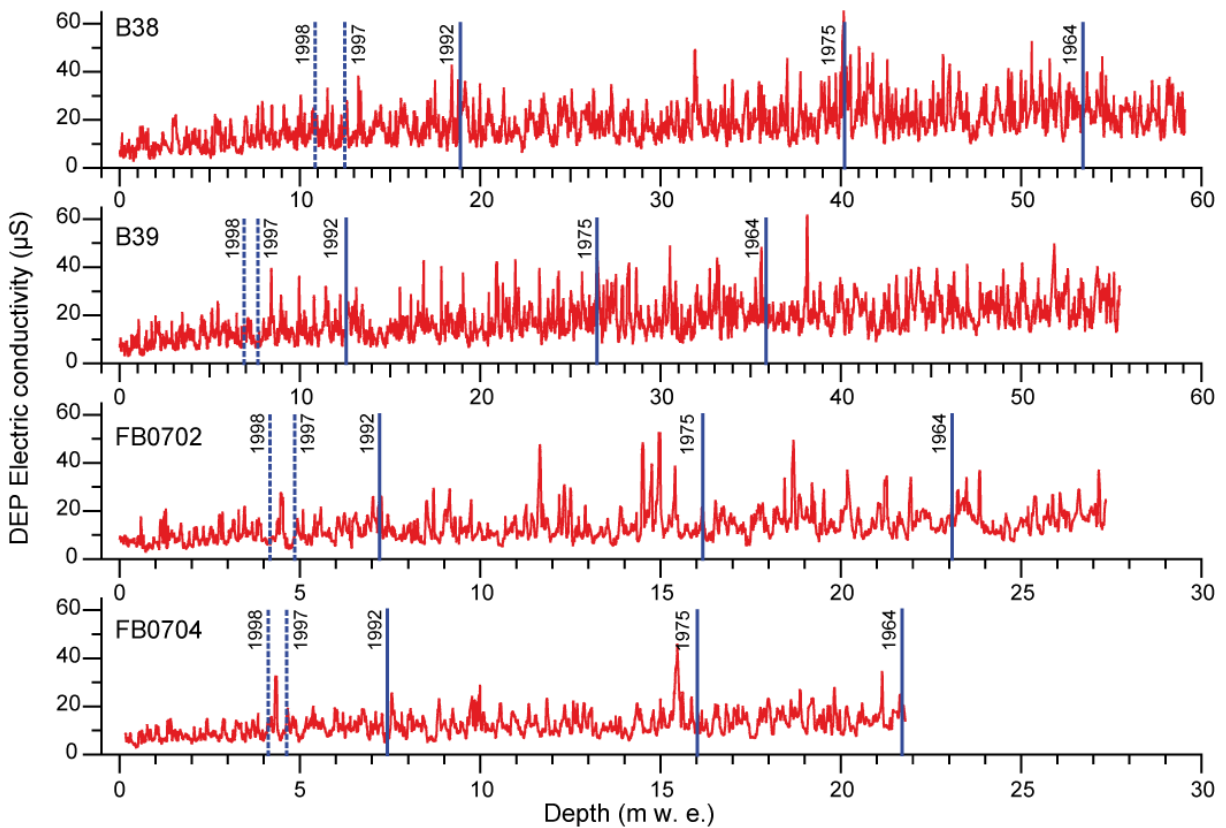


Figure 5.4: DEP records for the cores B38, B39, FB0702, and FB0704, plotted against the depth in meters of water equivalent. The years 1964 and 1992 for the known volcanic events of Mt. Agung and Mt. Pinatubo are marked as vertical blue bold lines, none of them can be clearly recognized in these DEP profiles. The third blue line marks the year 1975, in the corresponding depth of B38, elevated electric conductivity is observed. Dashed blue lines show a peak visible only in both inland cores, observed between 1997 and 1998. DEP measurements were carried out at 5 mm resolution.

5.5.2 Accumulation:

The accumulation map compiled by Rotschky et al. (2007) gives an accumulation rate of $170 \text{ kg m}^{-2} \text{ a}^{-1}$ for the area of Halvfarryggen, which originate from one shallow core (covering the time period 1964-1995) at the site of the geophysical observatory Watzmann (Figure 5.1). However, our results show much higher accumulation rates for the time span 1962 to 2006 for this area, with large spatial variation (Table 5.1). On the summit of Halvfarryggen (B38) an extraordinary high accumulation rate of $1257 \text{ kg m}^{-2} \text{ a}^{-1}$ was determined. Further to the south (FB0702) the accumulation rate decreases to $547 \text{ kg m}^{-2} \text{ a}^{-1}$. On the north of the western ridge of Søråsen (B39) an accumulation rate of $818 \text{ kg m}^{-2} \text{ a}^{-1}$ has been determined, which decreases further to the south (FB0704) to $489 \text{ kg m}^{-2} \text{ a}^{-1}$ (Figure 5.5). From these values a negative gradient in accumulation rates is likely to be observed, not only from north to south, but also from east to west. Though, the shallow firn cores FB0201 and FB0203 (table 5.1) (Masson-Delmotte et al., 2008), drilled in the vicinity of the geophysical observatories Watzmann (Halvfarryggen) and Olymp (Søråsen) respectively, are both closer located to the coast, they show high accumulation rates of 1123 and $1105 \text{ kg m}^{-2} \text{ a}^{-1}$ respectively. These data seem not to fit the regional pattern, however, as both cores are located on the slope of their respective ridges and could therefore to some extent be influenced by snow drift. This finding underlines the problem of mapping the surface mass balance in coastal areas with complicated topography, based on sporadic observations and with little geophysical (e.g. GPR) back ground information. Accumulation rates patterns can vary greatly over relatively short distances (See Eisen et al. (2008) for a detailed discussion on this matter).

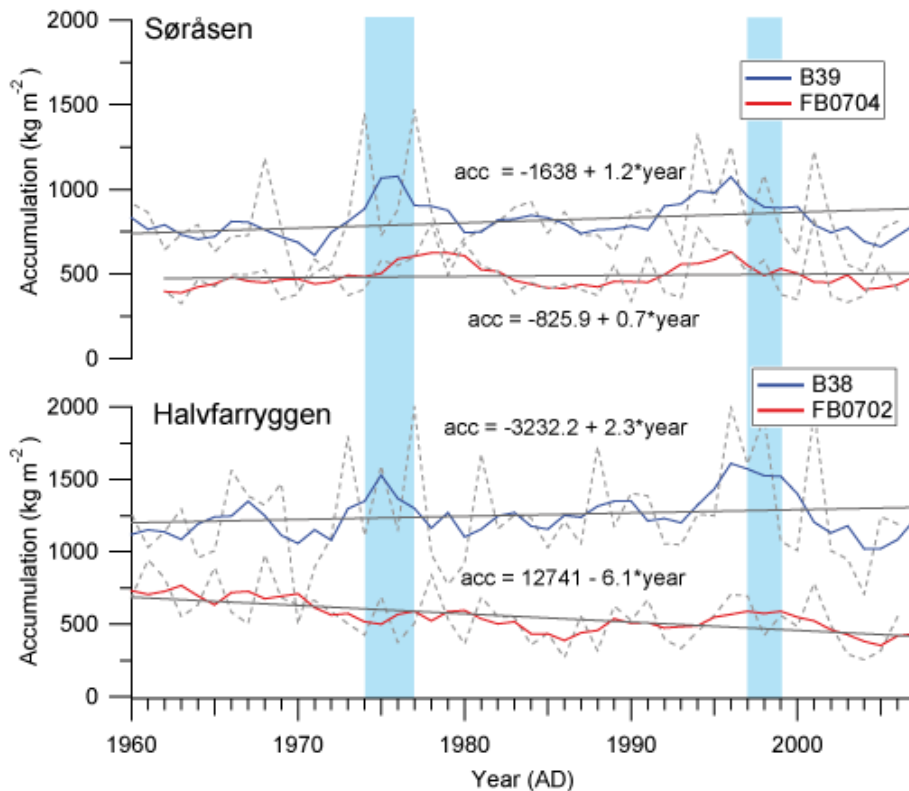


Figure 5.5: Mean annual accumulation (acc) rates for the cores B39, FB0704, B38 and FB0702 for the period 1960-2006. Annual accumulation rates (light grey dashed lines) were smoothed with a 5-year running mean function (red and blue bold lines). The cores closer to the coast (B38 and B39) are shown by blue lines and the inland cores (FB0702 and FB0704) by red lines. Years of Weddell Sea polynya events are represented by the semi-transparent light blue bars (1974-1976 and 1997-1998).

Two prominent high-accumulation peaks are distinguishable in both northernmost cores (B38 and B39), the first between 1974-1977 and later 1996-1998. This feature is especially visible in the smoothed data (Figure 5.5.). The first high accumulation event occurred during the period of the Weddell polynya and coincides with a high peak of DEP. During the Weddell polynya years, a local increase of precipitation amount was detected (Moore et al., 2002). Elevated SST above the region free of sea-ice causes more evaporation and cloud coverage, with a restricted moisture source producing locally increased precipitation rates. This feature is not observed in our inland cores, pointing to the local extent of the Weddell polynya effect. The second peak could be also related to a more recent polynya event, as shown by elevated conductivity profiles as well. However, this second high accumulation peak begins at least one year before the polynya.

All firn cores except FB0702 show no significant temporal accumulation trends. FB0702 shows a decreasing accumulation rate of $6.1 \text{ kg m}^{-2} \text{ a}^{-1}$ (p -level < 0.01). The topographical situation of core FB0702 from the eastern ridge could favour a local intensification of wind speed. Cold air

masses originating on the higher plateau of Dronning Maud Land flow in down-slope direction and are slightly deflected in western direction due to the Coriolis effects and the dominant regional wind regime (van den Broeke et al., 2002; van den Broeke and van Lipzig, 2003). The wind reaching the east of Halvfarryggen, is then channelled between the north summit of Halvfarryggen and the descending slope from the plateau of Dronning Maud Land. A similar phenomenon has been observed in other locations in Antarctica (van den Broeke et al., 2002; van den Broeke and van Lipzig, 2003). Snow drift is commonly reported from meteorological observations at Neumayer station. During these events the wind speed can reach up to 30 m s^{-1} at surface level, mainly connected to easterly storms. Katabatic winds proceeding from the south are reported as well (König-Langlo and Loose, 2007). Intensified snow drift and/or erosion could therefore explain the decreasing accumulation rates in FB0702. This effect is not observed at FB0704 location, and therefore it is likely interpreted as a restricted local feature.

5.5.3 $\delta^{18}\text{O}$ and δD

The firn cores B38 (690 m a.s.l.) and B39 (655 m a.s.l.) are located 81 km to the south-east and 110 km to the south-west of Neumayer station, respectively. The respective mean annual $\delta^{18}\text{O}$ values (accumulation weighted) are -20.58 ‰ for B38 and -19.96‰ for B39 for 1960 to 2007. These values are close to the annual average $\delta^{18}\text{O}$ for fresh snow collected at the Neumayer station between 1981 until 2006 ($\delta^{18}\text{O}=-20.49\text{‰}$) (Figure 5.6). This is a substantial observation, which implies that despite the elevation difference of approximately 600 m between Neumayer station and the drill sites, no significant altitude effect is visible in the stable-isotope data.

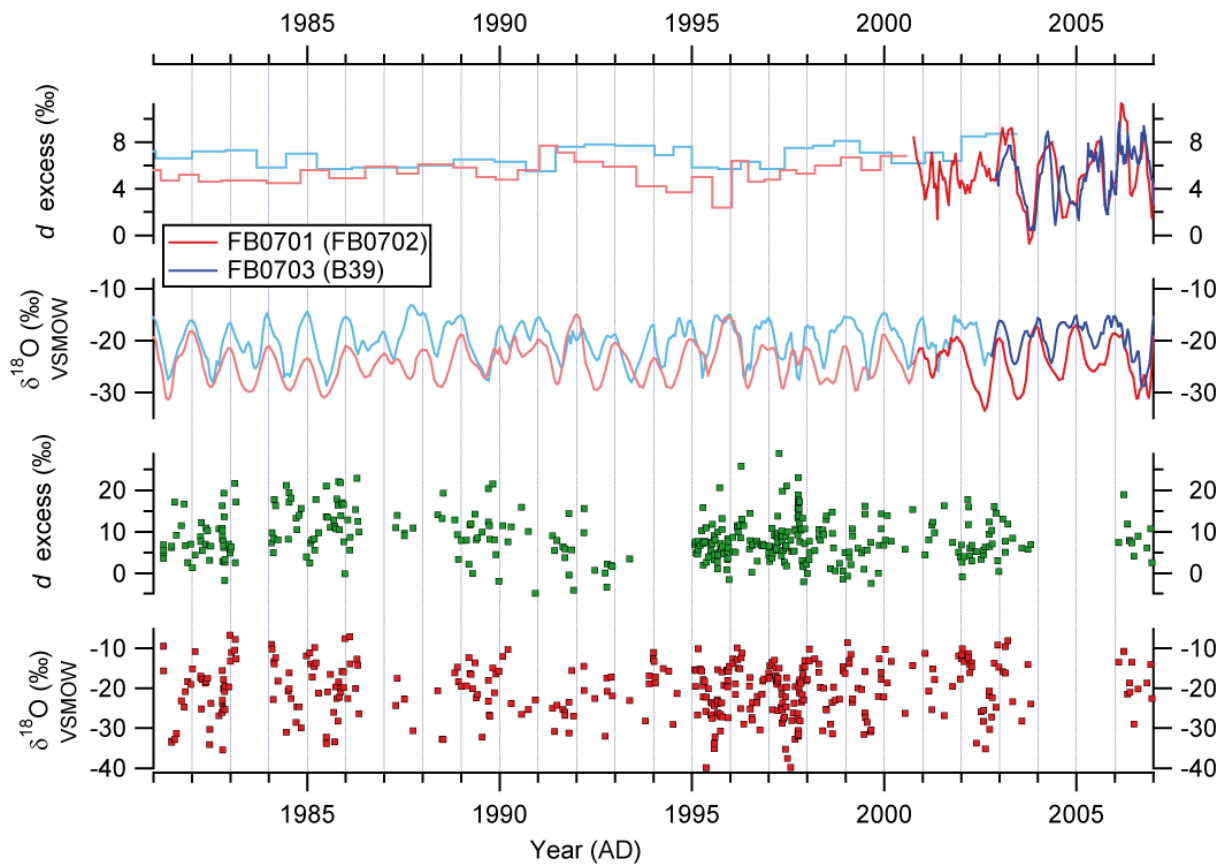


Figure 5.6: $\delta^{18}\text{O}$ and d excess data of fresh-snow samples (bottom) collected at Neumayer station in the period 1981-2006, and of the shallow firn cores FB0701 and FB0703 (top). The cores FB0701 (red bold line) and FB0703 (blue bold line) cover the time span 2000-2007 and 2003-2007, respectively. B39 and FB0702 are shown only for comparison in light color lines (blue and red, respectively), these cores were drilled at the same position as FB0701 and FB0703, expanding the isotope record to the past. At the bottom (red and green squares), it can be observed that the sampling of fresh snow is not homogeneous in time and some time-intervals are only weakly or not covered at all.

The other two cores, located towards the interior of the continent, have more negative $\delta^{18}\text{O}$ values: -24.23‰ for FB0702 (539 m a.s.l.) and -22.74‰ for FB0704 (760 m a.s.l.) (Table 5.1). The

discrepancy of mean $\delta^{18}\text{O}$ values between these two cores cannot be explained by altitude or by continental effects. Potentially, an important input of snow from higher elevations coming from the south of Halvfarryggen and transported by wind is the most likely explanation. Nonetheless, no direct observation of this process (wind drift and/or erosion) has been made and these inferences are based only on our isotope data. For that reason, other phenomena can not be discarded at this stage.

A gap in δD measurements of the core B39 (uppermost 6 m) was filled with the isotope data from the core FB0703, which was drilled at the same geographical coordinates of B39. FB0701, drilled near FB0702, was used to compare and verify the accuracy of the measurements. No important differences were detected (differences in $\delta^{18}\text{O}$ are on average 0.1‰ and 0.3‰ for δD). The $\delta^{18}\text{O}$ and d excess values of both cores are plotted in figure 5.6.

The co-isotope $\delta^{18}\text{O}$ vs. δD plot (Figure 5.7), shows a good correspondence for the slopes of the firn cores and fresh snow. For all four firn cores, slopes are similar to the slope of the Global Meteoric Water Line (GMWL) (Craig, 1961). This implies a strong oceanic influence and likely no secondary re-evaporation occurring at this area.

However, core B38 has a slightly lower slope of 7.6 and negative intercept ($\delta\text{D} = -0.4\text{‰}$). In this case, if $\delta^{18}\text{O}$ values greater than -18‰ are removed (related to warm summer temperatures), then the slope would increase to 7.7 and the intercept becomes positive ($\delta\text{D} = 2\text{‰}$) probably demonstrating that conditions in the moisture source (or a shift of the source) occurred during the summer season.

The meteoric water line for fresh snow from Neumayer station is very close to the GMWL, revealing that relative humidity (h) at the moisture source of the snow precipitating at the coastal zone is slightly higher than the global average (85%) (Clark and Fritz, 1997), whereas the four hinterland core's water lines are displaced below the GMWL (lower intercepts). This displacement seems more likely to be related to post-depositional processes than to primary evaporation or moisture source conditions. That can be demonstrated observing the stable-isotope composition of shallow firn cores retrieved earlier in the vicinity of the Neumayer station (e.g. B04 and FB0202 (Schlosser and Oerter, 2002b)) (Figure 5.1, Table 5.1). All intercepts of these cores, except for FB0202, are displaced to lower intercepts with respect to fresh snow. Consequently, the low intercepts are typical for coastal firn cores in the Ekströmisén region. The core FB0202, retrieved close to Neumayer Station, shows similar intercept and slope in the co-isotope relation as the snow samples, but has a short timespan (19 years) only. In contrast, the core B04, also retrieved near to the station, has a longer timespan (91 years) and a noticeable displacement with respect to snow values. This may suggest that post-depositional processes (diffusion and/or redistribution within the

snow column) are acting slowly and preferentially over the deuterium isotope, since no important change in the slopes is detected.

The mean meteoric water line calculated for whole Antarctica ($\delta D = 7.75 \cdot \delta^{18}O - 4.93$) by Masson-Delmotte et al. (2008) agrees with the slope of our LMWL, but differs in the intercept, which is typical for coastal zones.

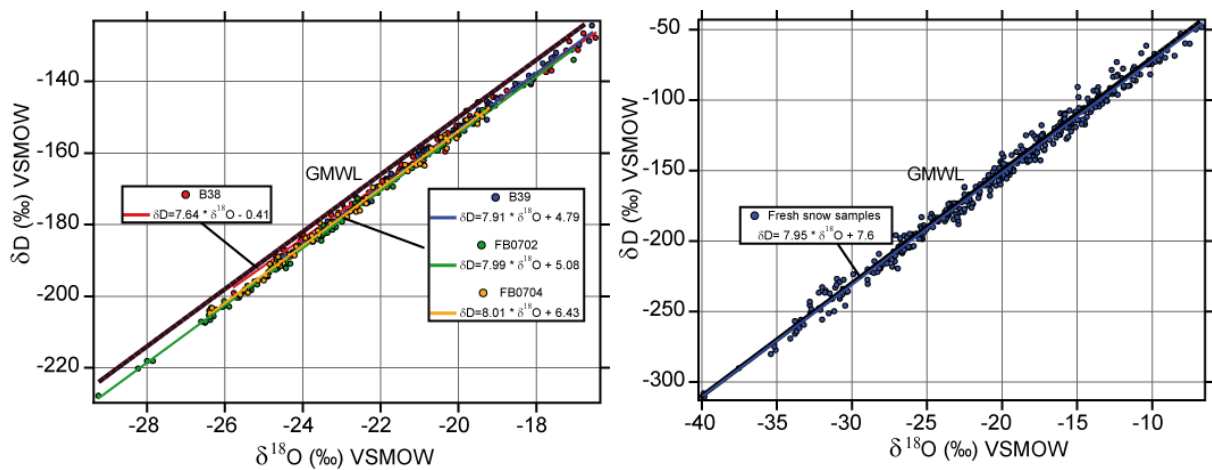


Figure 5.7: Plots showing the relationship between $\delta^{18}O$ and δD (1 m and 0.5 m means) for the four ice cores (diagram left) and fresh snow samples from the Neumayer station (1981-2006) (right diagram). Linear regressions of the co-isotope relationship of firn cores and snow samples were performed to be compared with the GMWL. Slopes in general agree well with the value 8 of the GMWL, except for the core B38 (see explanation in text).

	B38	FB0702⁺	B39⁺⁺	FB0704	B04[*]	FB0202	FB0201^{**}	FB0203^{**}				
Coord.	71.16°S/6.70°W	71.57°S/6.67°W	71.41°S/9.9°W	72.06°S/9.56°W	70.62°S/8.37°W	70.65°S/8.25°W	71.21°S/6.79°W	71.46°S/9.86°W				
Altitude	690 m a.s.l.	539 m a.s.l.	655 m a.s.l.	760 m a.s.l.	35 m a.s.l.	42 m a.s.l.	600 m a.s.l.	630 m a.s.l.				
Depth	84 m	43 m	78.5 m	36 m	50.6 m	13 m	16 m	14 m				
Age	1960-2007	1959-2007	1935-2007	1962-2007	1892-1981	1980-2001	1995-2001	1996-2001				
Acc. (kg m² a⁻¹)												
Mean	1257	547	818	489	352	329	1123	1105				
sdev	347	168	238	128	91	109	214	214				
Min	501	257	405	326	172	146	752	703				
Max	2003	979	1467	835	572	627	1398	1278				
δ¹⁸O ‰	(1m resolution)	(7cm resolution)	(0.5m resolution)	(5cm resolution)	(1m resolution)	(7cm resolution)	(0.5m resolution)	(5cm resolution)	(5cm resolution)	(4cm resolution)	(4.5cm resolution)	(6.5cm resolution)
Mean	-20.62	-20.63	-24.25	-24.23	-19.82	-19.86	-22.76	-22.78	-20.79	-20.26	-20.36	-20.12
sdev	2.16	1.12	2.29	1.45	-1.63	1.31	2.04	1.30	2.63	3.13	3.48	3.79
Min	-25.77	-22.59	-29.54	-27.32	-22.90	-22.78	-26.40	-25.12	-27.50	-27.97	-30.34	-31.09
Max	-16.48	-18.59	-17.04	-20.75	-16.57	-17.46	-19.23	-19.87	-12.20	-12.71	-12.72	-14.07
n (samples)	78	1180	77	768	54	821	70	715	1081	385	486	379
δD ‰	(1 m resolution)	(0.5 m resolution)	(1 m resolution)	(0.5 m resolution)	(5 cm resolution)	(4 cm resolution)						
Mean	-158.0	-188.6	-152.1	-175.9	-158.7	-156.6	-	-	-	-	-	-
sdev	16.6	18.3	13.0	16.4	21.8	25.5	-	-	-	-	-	-
Min	-199.1	-231.0	-177.9	-204.6	-212.5	-218.5	-	-	-	-	-	-
Max	-126.6	-134.0	-124.4	-147.5	-93.3	-94.4	-	-	-	-	-	-
n (samples)	78	77	54	70	924	385	-	-	-	-	-	-
d excess ‰	(1 m resolution)	(0.5 m resolution)	(1 m resolution)	(0.5 m resolution)	(5 cm resolution)	(4 cm resolution)						
Mean	6.9	5.4	6.5	6.1	6.0	5.5	-	-	-	-	-	-
sdev	1.5	1.0	1.1	1.3	3.3	1.7	-	-	-	-	-	-
Min	3.1	2.4	3.5	3.5	-6.1	-0.7	-	-	-	-	-	-
Max	10.3	8.0	8.7	10.2	16.3	10.6	-	-	-	-	-	-
n (samples)	78	77	54	70	910	385	-	-	-	-	-	-
Co-isotope relation												
δD vs δ¹⁸O Slope	7.64	7.99	7.91	8.01	8.04	8.07	-	-	-	-	-	-
δD vs δ¹⁸O Intercept	-0.41	5.08	4.79	6.43	6.79	8.13	-	-	-	-	-	-

+ Same location of FB701, ++ Same location of FB0703, * Schlosser and others (2002a), ** Masson-Delmotte and others (2008)

Table 5.1: Data set of the cores B38, B39, FB0702 and FB0704 analysed in this paper, summarizing geographical characterization (coordinates and altitudes refer to WGS84), dating, accumulation rates and isotope composition for the common time span 1962-2006. Measurements of δ¹⁸O were performed at high resolution (5 and 7 cm) for all cores. Additionally δD (and δ¹⁸O) were measured at 1 and 0.5 m resolution. The local meteoric water lines (LMWL), shown at the bottom, were calculated using a linear regression function of the correlation between δ¹⁸O and δD.

		Fresh Snow				
GvN			$\delta^{18}\text{O} \text{‰}$	$\delta\text{D} \text{‰}$	$d \text{ excess} \text{‰}$	LMWL
Coord.	70.62°S/8.37°W					
Altitude	35 m a.s.l.	Mean	-20.54	-156.3	8.6	$\delta\text{D} \text{ v/s } \delta^{18}\text{O}$ Slope
Sampling	1981-1992	sdev	6.64	53.3	5.4	7.95
Neumayer II		Min	-39.88	-310.6	-4.8	
Coord.	70.65°S/8.25°W	Max	-6.70	-48.3	28.9	$\delta\text{D} \text{ v/s } \delta^{18}\text{O}$ Intercept
Altitude	42 m a.s.l.	n (samples)	396	383	383	7.60
Sampling	1992-2006					

Table 5.2: Summary of stable water isotope data of fresh-snow samples collected at the Neumayer station from 1981 to 2006. At the right column, slopes and intercepts of the calculated LMWL are presented. Coordinates and altitudes refer to WGS84.

5.5.4 Deuterium excess:

The secondary parameter deuterium excess ($d = \delta\text{D} - 8 * \delta^{18}\text{O}$) of precipitation is directly linked to the relative humidity (h), sea surface temperature (SST) and wind speed conditions at the moisture source (Dansgaard, 1964; Clark and Fritz, 1997). Therefore, it can be used as a tool to distinguish between different source regions or changes of evaporation conditions in a stationary moisture source. Mean d excess values for the firn cores vary from 5.4‰ (FB0702) to 6.9‰ (B38) (Table 5.1; Figure 5.8), thus are well below the mean value of 8.6‰ for fresh-snow samples at Neumayer station (Table 5.2). These differences of d excess values between fresh snow and firn cores could either reflect the influence of different moisture sources (different h and/or SST to those of the fresh snow) or post-depositional phenomena (sublimation and/or diffusion) in the snow cover of coastal Dronning Maud Land. Earlier cores drilled in the vicinity of the Neumayer station (Table 5.1) differ in mean d excess values with respect to snow as well. The firn core FB0202 (1981-2001) covers almost the same time period as the fresh-snow samples (1981-2006). For the core, a lower average d excess value (5.5‰) was measured than for fresh snow (8.6‰). This d excess is close to those of the firn cores from Halvfarryggen and Søråsen, implying that the dissimilarity in d excess between fresh snow and firn cores is not produced by primary conditions of the snow, such as evaporation or condensation conditions. Vapour diffusion in the snow column has been reported by Schlosser and Oerter (2002a) at Ekströmisen, producing a smoothing of the isotope signal due to isotopic redistribution by diffusion in the snow column. The high resolution isotope measurements of the cores FB0701 and FB0703 (retrieved at the same geographical position as FB0702 and B39,

respectively) show a clear decrease in d excess with depth (-0.19‰ m^{-1} and -0.34‰ m^{-1} , respectively). These trends are attenuated in the related longer cores in Halvfarryggen (FB0702, -0.009‰ m^{-1}) or even positive at Søråsen (B39, 0.019‰ m^{-1}), reinforcing the assumption of post-depositional processes in the upper firn layers. Removal and isotopic modification by sublimation can not be discarded as a cause of the d excess variation. Based on an extensive data base, Masson-Delmotte et al. (2008), pointed out that mass loss caused by sublimation in low elevation areas of Antarctica (< 2400 m a.s.l.) could lead to a decrease of the d excess. Ablation leads to longer exposure of the snow to the atmosphere, facilitating the isotopic re-mobilization and fractionation. However, sublimation is likely not to be preponderant in the snow column, since no great differences in the co-isotope slope are detected, as expected for strong sublimation (Satake and Kawada, 1997; Zhou et al., 2008).

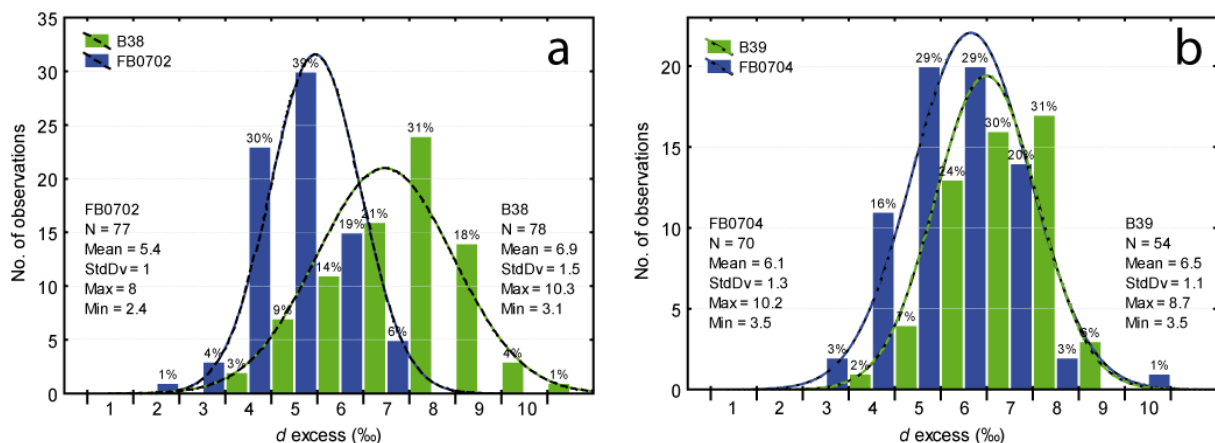


Figure 5.8: Histograms showing the statistical d excess distribution for the four firn cores. a) Cores from Halvfarryggen are presented, where FB0702 shows slightly lower d excess values. b) The firn cores from Søråsen are shown. All cores were fitted to a normal distribution function (dashed line).

Histograms presented in 5.8, demonstrate a common pattern of the distribution of d excess for cores B39 and FB0704 from Søråsen and B38 from Halvfarryggen (mean $d=6.5\text{‰}$, 6.1‰ and 6.9‰ , respectively). On the other hand FB0702 (Halvfarryggen) shows a slightly lower d excess (mean $d=5.4\text{‰}$). This likely reflects an additional moisture influence in the core FB0702, which is in agreement with the interpretation of its δ values.

5.6 Discussion

5.6.1 $\delta^{18}\text{O}$ -Temperature relationship:

To investigate the relationship between stable-isotope composition and air temperatures, we compare monthly averages of air temperatures at Neumayer station (1981-2007) with the $\delta^{18}\text{O}$ annual cycles from firn cores (B38, B39, FB0702, and FB0704) in order to explain the variance of the water isotope composition (5. 9). High-resolution $\delta^{18}\text{O}$ values were re-sampled to a monthly scale. We used a linear interpolation function of the seasonal isotope curves, assuming evenly-distributed snow fall events during the whole year. In spite of the distance of the drilling sites from the stations, the air temperature oscillations explain up to 50% (coefficient of determination, r^2) of the $\delta^{18}\text{O}$ variations (Figure 5. 10a-d); this relationship decreases to its lowest values (30%) within core B39.

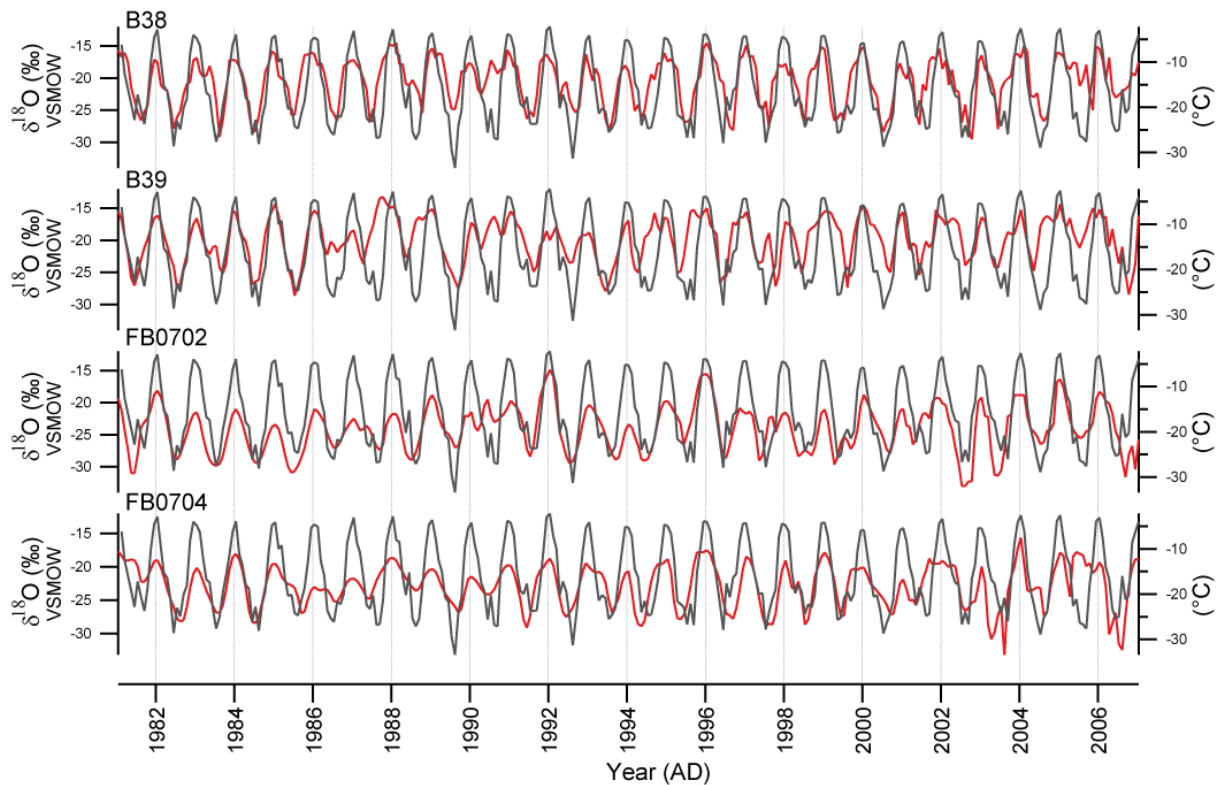


Figure 5.9: Comparison of mean monthly air temperatures composite at Neumayer station (grey lines) and the high-resolution $\delta^{18}\text{O}$ seasonal cycles (red lines).

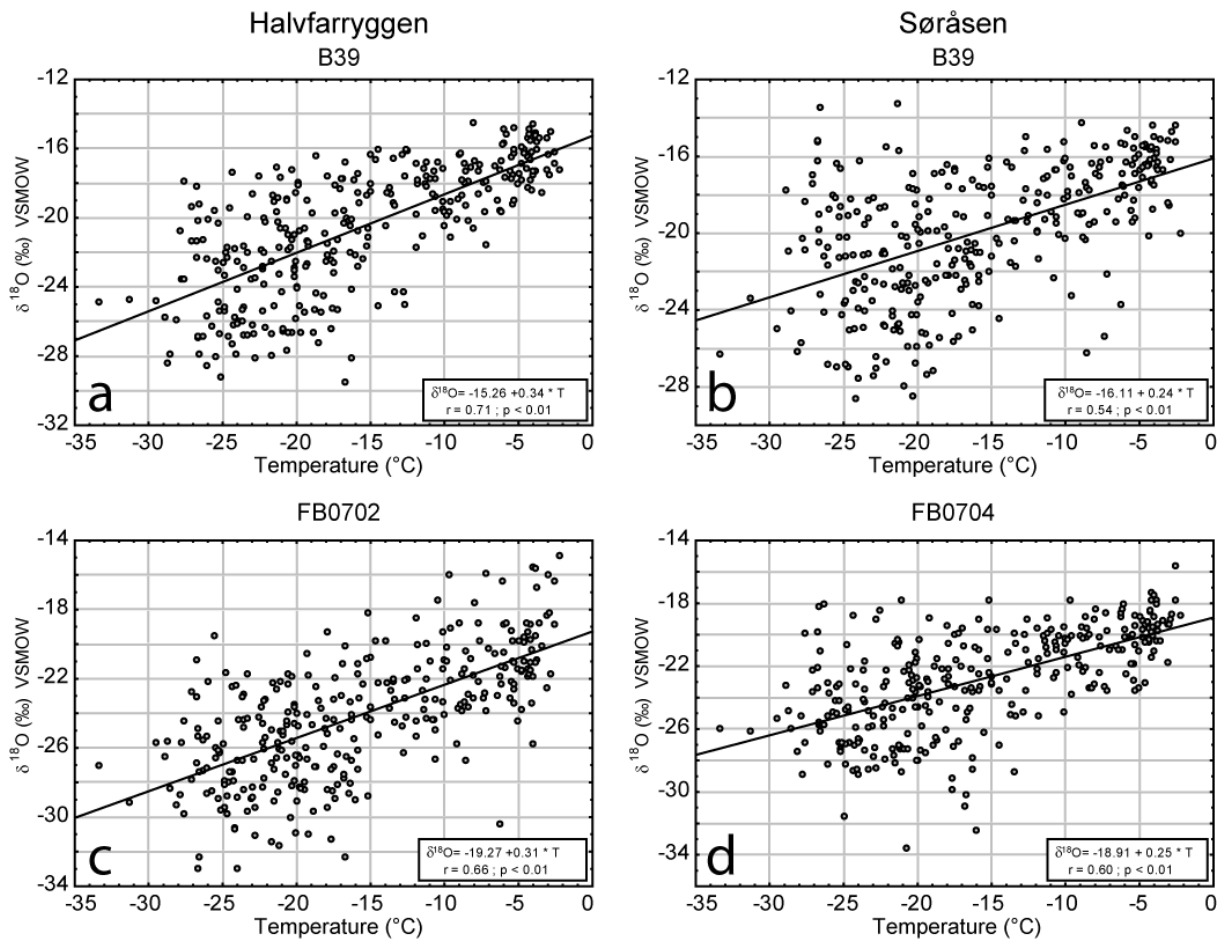


Figure 5.10: Correlation of re-sampled mean $\delta^{18}\text{O}$ values (12 per year) from the firn cores B38 (a), B39 (b), FB0702 (c) and FB0704 (d) to monthly mean air temperature at Neumayer station. Correlation coefficients and statistic significance levels are displayed for all linear regressions.

For fresh snow samples collected at Neumayer station (Figure 5.11), as well as for all four firn cores (Figure 5.10), a positive correlation between isotope composition and air temperature is evident. Air temperatures at 2 m level explain 47% of the $\delta^{18}\text{O}$ variation (r^2). We conclude that both archives (firn cores and fresh snow) are good indicators of the regional climatological conditions and especially linked to variations of air temperatures.

A gradient of the $\delta^{18}\text{O}$ -Temperature relationship is noticeable between both ridges with values of about 0.34 to 0.31‰ °C⁻¹ for Halvfarryggen and about 0.25‰ °C⁻¹ for Søråsen. In order to investigate whether or not this gradient is caused by post-depositional processes, we compared the isotope/temperature slopes for both $\delta^{18}\text{O}$ and δD on the shallow firn cores FB0701 (same position as FB0702) and FB0703 (same location as B39), following the same procedure as described earlier for the longer cores. The snow/firn contained in the shorter cores was exposed for a shorter time to local environmental conditions, therefore it should be affected to a lesser degree by possible post-depositional effects. Nevertheless, for both cores the slopes are similar to those at the same

position, i.e. $0.36\text{‰ }^{\circ}\text{C}^{-1}$ for FB0701 (Halvfarryggen) and $0.18\text{‰ }^{\circ}\text{C}^{-1}$ for FB0703 (Søråsen) for ^{18}O . The deuterium/temperature slopes are practically identical (multiplied by factor 8) to the oxygen slopes: $2.94\text{‰ }^{\circ}\text{C}^{-1}$ for FB0701 and $1.35\text{‰ }^{\circ}\text{C}^{-1}$ for FB0703. This re-confirms that the difference between both ridges is most likely a depositional phenomenon, dependent on the original stable isotope composition of precipitation.

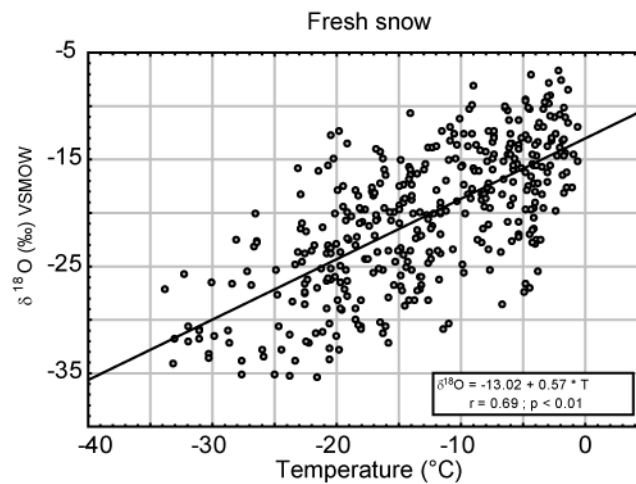


Figure 5.11: Correlation of $\delta^{18}\text{O}$ values from fresh-snow samples against air temperature (T). Snow samples were collected at the Neumayer station during the years 1981 to 2006.

Helsen et al. (2005) investigated the relationship between stable isotopes and local temperature at the neighbouring area of Riiser-Larsenisen, using an altitude profile from sea level to 2892 m a.s.l. (Kohnen Station). They reported important differences between coastal and the high elevation areas. At coastal zones, the snow fall events are well distributed during the whole year. Contrary, snow fall events at higher areas, occur preferentially in winter associated with cyclonic activity. Additionally, the difference between 2-m air temperatures and condensation temperatures increases with the elevation of the area, due to dominant air-temperature inversion at higher regions. Thus, leading to an important seasonal and thermal bias in the interpretation of $\delta^{18}\text{O}$ as a direct indicator of 2-m air temperature variations. A similar difference of the temperature-isotope gradients was identified by Oerter et al. (1999), comparing shallow firn cores and 10 m borehole temperatures. They concluded that the isotope-temperature relationship at Ekstrømsisen ($1.20\text{‰ }^{\circ}\text{C}^{-1}$ for $\delta^{18}\text{O}$) decreases with increasing height towards the Amundsenisen Plateau ($0.69\text{‰ }^{\circ}\text{C}^{-1}$). Correct interpretation of the temperature-isotope relationship should take into account these factors. Low altitude zones like Halvfarryggen and Søråsen are therefore better suited for an easier and simpler interpretation of the climatic signal contained in the isotope composition at a seasonal to sub-seasonal scale.

5.6.2 Temporal stable isotope trends:

As previously demonstrated, the isotopic composition of the firn cores from both ridges (Halvfarryggen and Søråsen) reflects relatively well the meteorological conditions of the southern hinterland of Ekstrømissen. However, the correlation between the different stable isotope data sets for our study region has not yet been explored.

Aiming to find possible regional signals during the common time interval from 1962 to 2006, a $\delta^{18}\text{O}$ anomaly index ($\Delta^{18}\text{O}$) was calculated to compare the firn cores on a common temporal scale. This index also allows removal of the isotopic effects (altitudinal and continental) and accumulation gradients from each individual data set (different cores), since the index refers to the average value for each core and not to absolute $\delta^{18}\text{O}$ values. The anomaly index was calculated by subtracting the accumulation weighted $\delta^{18}\text{O}$ average (1962-2006) from annual mean values (5.12a). A correlation matrix of $\Delta^{18}\text{O}$ (Table 5.3) shows a good correlation of this anomaly index between cores B38-B39 ($r=0.43$). This correlation decreases further inland towards cores FB0702 and FB0704 ($r=0.31$). However, a high inter-annual variability was detected ($\sigma=1.12\text{‰}$ up to 1.46‰ in B38 and FB0702, respectively). Thereafter, annual oxygen isotope values were smoothed using a 5-year running average function leading to further improvement of the correlation between the cores.

In figure 5.12a, positive (red colours) and negative (blue colours) phases of the smoothed $\Delta^{18}\text{O}$ index are displayed. The correlation matrix of the smoothed data demonstrate a statistically significant temporal correlation (at level $p<0.05$) between B38, B39, FB0702 and FB0704 for the period 1962 to 2006. However, B39 does not correlate with FB0704. The strongest correlation is observed between the northern cores B38 and B39 as well as the hinterland cores FB0702 and FB0704 ($r=0.57$ for both pairs). Consequently, common “positive” (warm) or “negative” (cold) phases are evident for the firn cores (figure 5.12a). A common positive $\Delta^{18}\text{O}$ index is likely found between 1975 and 1980 (prior to the meteorological records). However, the maximum peaks during this phase are not coincident in time, and vary from around 1976 for B38, 1978 for B39 and FB0702, and 1979 for FB0704. This positive phase is followed by a less apparent negative phase, also showing a lag on the minimum peaks. Additionally, the $\Delta^{18}\text{O}$ index of all cores show a rather positive phase around 2005 and a negative phase around 1965.

Temporal trends were calculated for all firn-cores using linear regressions from smoothed $\Delta^{18}\text{O}$ time series (Figure 5.12b). Using this parameter, no statistically significant trend (at $p\text{-level} < 0.05$) in the common time span was found for the cores B38, FB0702 and FB0704. In contrast, the core B39 shows a slight positive trend (Figure 5.9b).

Borehole temperature profiles (Figure 5.13) made one day after the drilling, also show a slight decreasing temperature with depth, thus reinforcing our observations and are coincident with our isotope data. Unfortunately, a precise estimation of temperature trends is not possible, due to possibly remaining heat in the holes after the drilling. Temperatures decrease in an order of 0.006 to $0.013^{\circ}\text{C m}^{-1}$. The profile of FB0704 is not shown, because the temperature at this borehole was measured less than 24 hours after the drilling.

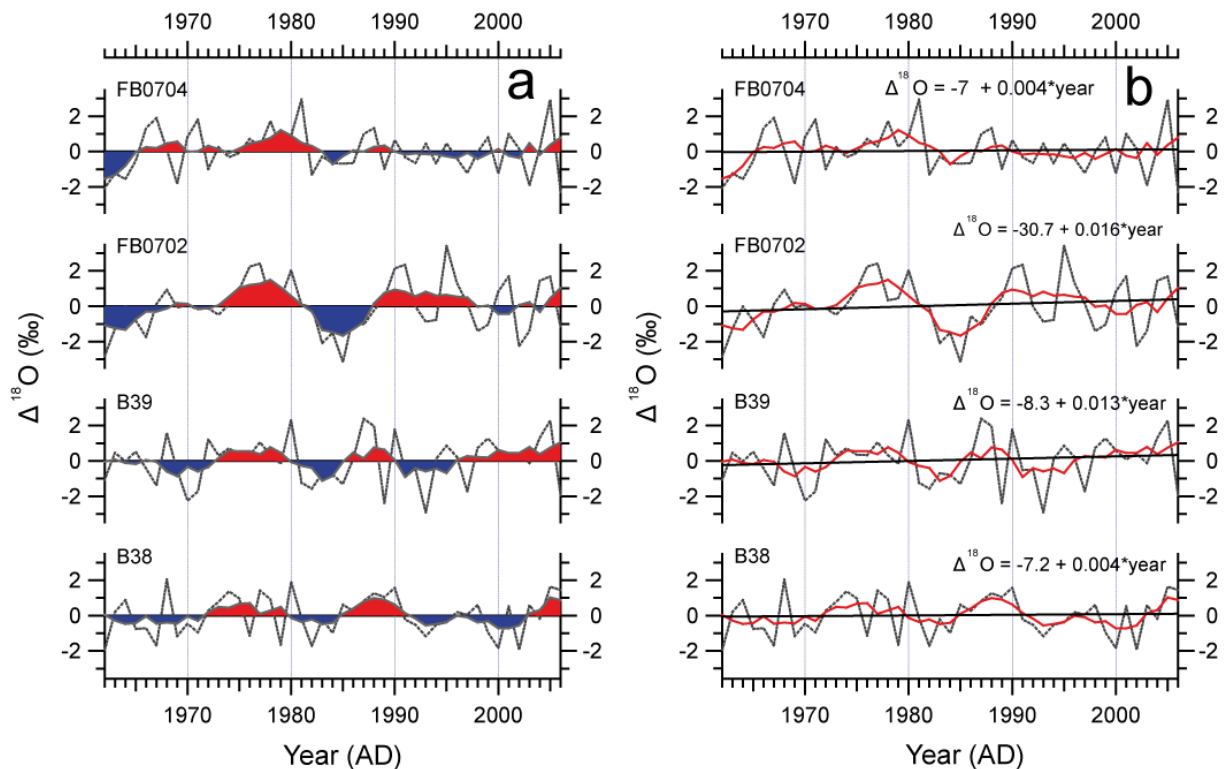


Figure 5.12: a) The $\delta^{18}\text{O}$ anomaly index is shown (bold grey line), the values were obtained by subtracting the accumulation weighted annual $\delta^{18}\text{O}$ average from single annual $\delta^{18}\text{O}$ values. Positive (red areas) and negative (blue areas) smoothed index values are displayed to illustrate the correlation in time between the isotope data of the cores. Middle black line is showing the mean accumulation weighted $\delta^{18}\text{O}$ average (zero line). b) Linear regressions calculated for the anomaly indices of figure 5.12a. 5-Year running mean smoothed index ($\Delta^{18}\text{O}$) is shown as a bold red line. For every core linear regression lines are shown. No statistic significant trends (p level < 0.05) were found, except for the core B39, which shows a positive tendency of $0.013\text{‰}^{18}\text{O a}^{-1}$ ($r = 0.32$).

	Mean acc. Weighted $\delta^{18}\text{O}$ values				Smoothed mean $\delta^{18}\text{O}$ values				Year
	B38	B39	FB0702	FB0704	B38	B39	FB0702	FB0704	
B38	1.00	0.43	-	-	1.00	0.57	0.36	0.34	-
B39		1.00	0.34	-		1.00	0.30	-	0.32
FB0702			1.00	0.31			1.00	0.57	-
FB0704				1.00				1.00	-

Table 5.3: Correlation matrix illustrating statistically significant correlation coefficients (r) between the $\delta^{18}\text{O}$ values of cores B38, B39, FB0702, and FB0704. An increase of correlation coefficients is observed in the smoothed data. Strong correlation between the pairs B38-B39 and FB0702-FB0704 is obtained in both cases (smoothed and not smoothed). At the right column: significant temporal trend was found for the core B39 (time interval 1962-2006). All statistically significant values are at a p-level < 0.05.

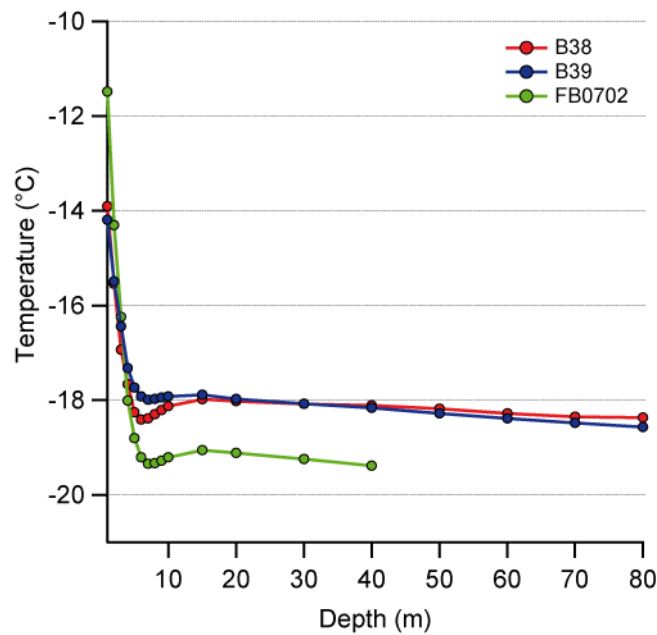


Figure 5.13: Borehole temperature profiles for cores B38, B39 and FB0702. All profiles show a slightly decreasing temperature with depth. Temperatures were measured every meter the first 10 meters, every 5 meter between 10 and 20 meter depth and every 10 meter between 20 meter depth and the bottom of the hole. The profile of core FB0704 has been excluded, because of signs of remaining heat influence.

5.6.3 Temporal and spatial variation of the d excess:

The temporal variation of d excess could reflect changes of the atmospheric circulation system in this region. This possibility was examined as for $\delta^{18}\text{O}$, using linear regressions as shown in Figure 5.1 (bottom). Since the d excess values were calculated from low-resolution measurements it is not possible to calculate an exact annual mean value. In general, both coastal cores (B38 and B39) present statistically significant temporal variations in the secondary parameter d excess. However, the trends for both ridges are of opposite sign. Halvfarryggen exhibits -0.04‰ a^{-1} variation of d excess and Søråsen $+0.04\text{‰ a}^{-1}$; both slopes are moderate. For the inland cores FB0702 and FB0704, no statistically significant temporal trends were found, only minor trends (0.01‰ a^{-1}) concordant in sign with those of the coastal region were observed. However, the influence of post-depositional effects on the d excess trends (e.g.: diffusion), cannot be completely neglected. However, this effect is restricted only to the first meters of firn, as determined by Schlosser and Oerter (2008). Diffusion ceases to be important when the critical density of 550 kg m^{-3} is reached. In our cores this density is reached between 8 and 10 m depth for the north- and southward cores, respectively. If trends for both cores are calculated outside the diffusion zone, they are still present and preserve their sign. The trend for B38 is then statistically significant at p-level <0.1 . This observation could reveal a local variation of moisture transported to both ridges, although post-depositional effects cannot be excluded.

During the polynya periods 1974-1976 and 1997-1998, the d excess profiles display slightly higher values ($d = 8\text{-}10\text{‰}$) than the mean d excess of the cores. This could point to the addition of moisture from a local source region (with lower humidity and/or higher SST than the main moisture source (Uemura et al., 2008). According to Moore et al. (2002), the SST had been significantly higher in polynya years, which would support the hypothesis of local moisture addition.

The reconstruction of moisture sources of accumulated precipitation within the recovered firn cores is difficult. In general, lower d excess values have been related to higher h and lower SST at the moisture source (Dansgaard, 1964; Clark and Fritz, 1997). Thus, it can be interpreted that the dominating moisture source of precipitation at Halvfarryggen and Søråsen should have a higher humidity and/or lower SST than the global average, since the global meteoric water line is defined with a d excess value of 10‰ .

Schlosser et al. (2008) reconstructed the source of snow precipitated at Neumayer station (between 1981 and 2000) based on combined backward trajectory computation and stable isotope analysis. They found that the two most common atmospheric circulation paths arriving at Ekströmsisen, originate either from the Weddell Sea or from the coastal east. In both source regions, d excess values are around 9‰ . Other frequent paths with different d excess were also identified,

but only oceanic moisture sources from relatively low latitudes (north of 62°S) are able to produce a low d excess between 6 and 7‰ in this area. Uemura et al. (2008) demonstrated a great variability of d excess in the coastal zone of East Antarctica, analyzing water vapour collected directly above the sea surface. The d excess values were found to fluctuate between -5‰ and +18‰, as a consequence of moisture mixing from continental and oceanic sources. Based on similar variations in our study area (5. 8), a mixture of air masses from different moisture sources is indicated from our data, with a common signal for the whole region. The relatively coarse resolution of our measurements, as well as post-depositional effects, should be taken into account. Masson-Delmotte et al. (2008) studied the geographical distribution of d excess around Antarctica, demonstrating that at low altitude coastal areas (<2000 m a.s.l.) the variation of d excess is mainly linked to regional conditions (moisture source). They demonstrated in general, relatively low d excess values for the coastal Antarctica (around 5‰ average) and higher values for the whole data set (7.8‰). Our data correspond well to Antarctic mean d excess values, but are situated above the observed coastal average.

5.7 Conclusions

Four firn cores were retrieved in January 2007 at Halvfarryggen and Søråsen, in the coastal area of Dronning Maud Land, East Antarctica, to study the recent climate variability in this region by stable-isotope methods. These studies provide time series back in time to at least to 1960.

Different proxies indicate that the four coastal Dronning Maud Land cores do not reflect only regional conditions, but also local features, as for example demonstrated by the influence of the Weddell Sea polynya events (see DEP, d excess and accumulation profiles).

Our studies demonstrate a statistically representative dependency of the water isotope composition at coastal Dronning Maud Land precipitation and air temperatures registered at the Neumayer station. The correlation between the isotopic composition of fresh snow samples at Neumayer station and air temperature is high ($r=0.69$), but no statistically significant temporal trend was found. This corresponds well with the findings of the data from firn cores and air temperatures. The best correlation between the isotopic composition of firn cores and air temperature at Neumayer station was found with respect to monthly means ($r=0.54$ to 0.71 in B39 and B38, respectively). A gradient in the relationship $\delta^{18}\text{O}$ and air temperature between the ridges of Søråsen and Halvfarryggen is evident. On Halvfarryggen (East ridge) the variation of air temperatures explains the seasonal isotopic composition of firn from between 43% (FB0702) up to 50% (B38) with an isotope/temperature gradient of $0.33\text{‰}/\text{°C}$. The relationship between $\delta^{18}\text{O}$ and air temperature decreases to 29% (B39) and 35% (FB0704) and a lower gradient of $0.25\text{‰}/\text{°C}$ at Søråsen (West ridge) is observed. Independent of spatial variations, no important temporal trends of $\delta^{18}\text{O}$ are found for

the firn cores as well as for fresh snow. Only B39 (Søråsen) shows a slight (and statistically significant) increase of $+0.013\text{‰ a}^{-1}$, corresponding to an increase of air temperatures of around 0.6°C between 1962 and 2006. At Halvfarryggen (B38 and FB0704) no significant temperature trend is visible for this time period. As a consequence no general warming (or cooling) trend can be inferred for the last half century. This conclusion agrees with MAAT data from Neumayer station for the period 1981 and 2006, where annual temperatures show no trend with an average of -16.1°C (König-Langlo and Loose, 2007).

The strong correlation of $\delta^{18}\text{O}$ variations between the firn cores in the hinterland of Neumayer station, allow us to conclude that condensation conditions of the precipitation are similar for the whole coastal region. The isotope fractionation process changes approximately at 700 m a.s.l., above which isotope altitude effects are detected (visible only in core FB0704). Similar conclusions were made by Helsen et al. (2005), who identified the beginning of altitudinal fractionation processes at coastal Dronning Maud Land during up-lift and cooling of moist masses when confronting the Antarctic continent. The $\delta^{18}\text{O}$ values of their snow pits at 1160 m a.s.l. (-30.4‰) are clearly depleted with respect to the coastal values (-21.4‰ to -23.3‰).

Spatial differences between the ridges are observed with regard to their respective accumulation rates (as for $\delta^{18}\text{O}$ values), especially at the firn cores closer to the coast. The accumulation rates of $1257\text{ kg m}^{-2}\text{ a}^{-1}$ on Halvfarryggen (B38) are higher than those of $818\text{ kg m}^{-2}\text{ a}^{-1}$ on Søråsen (B39). Towards the hinterland, a decrease in accumulation rates to about $500\text{ kg m}^{-2}\text{ a}^{-1}$ is observed for both inland cores (FB0702 and FB0704). However, FB0702 is most probably influenced by snow drift from higher altitudes and/or erosion, as demonstrated by its relatively low $\delta^{18}\text{O}$ values.

The spatial variations of accumulation rates, d excess values and the isotope/temperature relationship are likely to be linked to the wind regime and transport of moisture masses. The easterly wind, as dominant regional wind regime carries mixed oceanic moisture influenced by humidity of continental origin. The oceanic input over Halvfarryggen seems to have increased in the past half century, evidenced by the negative temporal trend of d excess for both cores of this ridge (however, statistically not significant for FB0702). An opposite tendency (positive sign) is found for Søråsen. No obvious explanation is possible for these trends, since both ridges are under the influence of the same regional climatic situation. Trends of d excess could either represent variations of the regional wind regime or be a product of post-depositional effects acting over the snow column. Relatively moist air masses are first confronted to Halvfarryggen (East ridge), then this ridge probably acts like a natural barrier blocking the passage of moisture to the west, thus producing a so called “shadowing effect”.

The summits of both Halvfarryggen and Søråsen are sites with high accumulation rates, and thus might be suitable locations for deep drilling, due to the appropriate geographical and ice conditions (ice thickness, MAAT, geographical location). Since the ice cover could reach 800 m of thickness or more in this area (Steinhage et al., 1999), the future drill site could reveal a high-resolution climate record of the atmospheric temperature evolution for at least the past 1.9 ka.

6 Synthesis:

6.1 Characteristics of the recent climate variability of Antarctica

The climate variability of the Antarctic Continent is known to be a complex and inter-reliant process. The natural variability of the Antarctic climate depends on many factors interacting on seasonal to millennial time scales. Variation of long time-scale variables (millennial to centennial scale), like orbital parameters and the concentration of greenhouse gases, produced the major glacial cycles in the past (Jouzel et al., 2007; Kawamura et al., 2007).

During the Holocene, several main phases of climate change have been observed in Antarctica from different climate proxies, where the Antarctic climate variations precede the changes on the northern hemisphere on a centennial time-scale, a phenomenon known as bipolar seesaw (EPICA community members, 2006; Abram et al., 2009; Stenni et al., 2010a). The most important climatic events are the strengthening of the circumpolar westerlies at around 6 ka BP and its later abrupt weakening at about 5 ka BP. A new major intensification of the westerlies occurred at 1.2 to 1 ka BP, characterized by a regional-scale decrease of atmospheric temperatures since then (Mayewski et al., 2009). In a regional context, the Antarctic Peninsula (AP) and coastal West Antarctica behave in anti-phase with respect to the rest of the continent, since in periods of intensified westerlies East Antarctica shows cooling trends, while in West Antarctica warming trends are observed (Bentley et al., 2009). Different records from the AP give evidence of three major warm phases during the Holocene: (1) an Early-Holocene climate optimum (11-9.5 ka BP), (2) a Mid-Holocene warm period (4.5-2.8 ka BP) and (3) the Recent Rapid Regional Warming (Vaughan et al., 2003; Abram et al., 2009; Bentley et al., 2009). In contrast to the dramatic recent atmospheric warming of the AP, East Antarctica's strongest warming is observed in the late Holocene (2.6 to 0.9 ka BP), with a general cooling since this time and relatively constant temperatures for at least the last 200 years (Abram et al., 2009; Mayewski et al., 2009). However, marine sediment records from the West Antarctic Peninsula (WAP) give evidence that the recent atmospheric warming has not reached the levels of the Mid-Holocene in this region (Domack et al., 2003b; Bentley et al., 2009). There is no definite indication of an equivalent of the Medieval Warm Period event across Antarctica, and only some sporadic evidence supports a Little Ice Age equivalent (Abram et al., 2009; Bentley et al., 2009). It is of major importance to know these Holocene climate variations in order to correctly estimate the recent climate variability of coastal Antarctica.

To understand the recent climate variability and forcing modes at the northern Antarctic Peninsula (West Antarctica) and coastal Dronning Maud Land (DML, East Antarctica) (Figure 6.1), a detailed characterization of the relationship between the stable water isotopes of firn and recent

precipitation to different meteorological parameters has been carried out. The isotopic composition of firn and precipitation both contain climatic information, which combined allow us to expand the meteorological record geographically and temporally beyond the instrumental period. The instrumental records in Antarctica are restricted and mostly confined to coastal locations, where the influence of local topography is most evident. The study of both firn and precipitation, give us the opportunity not only to study the climatic conditions at the precipitation site, but also to investigate the source of the moisture masses (mostly the Southern Ocean) including their characteristics and temporal evolution.

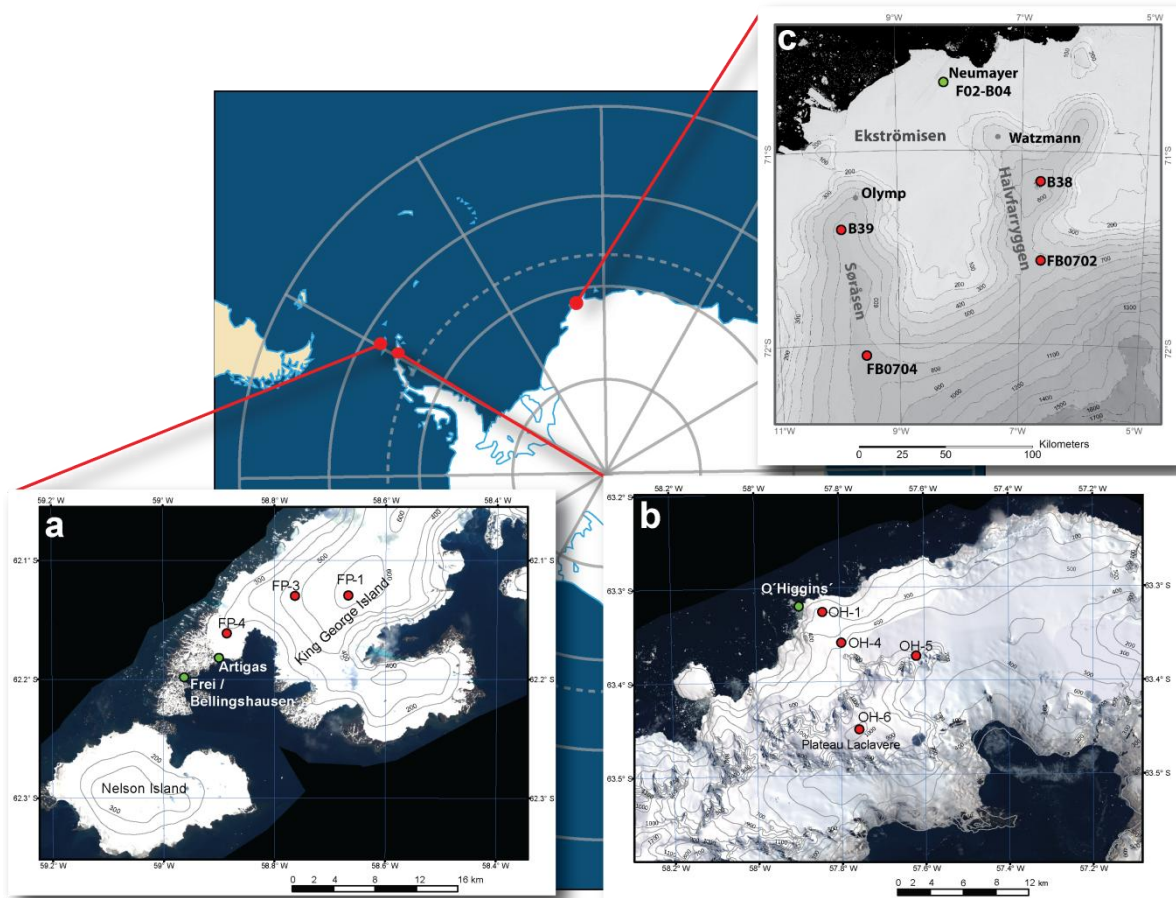


Figure 6.1.: Areas of investigation from (a) King George Island, South Shetland Island, (b) northern Antarctic Peninsula and (c) coastal DML. The locations where firn cores were retrieved (red dots) and permanent stations (green dots) are shown.

Two key locations were investigated in West Antarctica: (1) King George Island (62.03°S, 58.35°W) (South Shetland Island) and (2) the northern AP near the Chilean station O'Higgins (63.32°S, 57.9°W). The northern Antarctic Peninsula is characterized by westerly winds and relatively warm temperatures, which could reach maxima above 0°C in summer with a mean annual air temperature (MAAT) of -2.3°C and -3.7°C at King George Island and O'Higgins, respectively (Table 5.1). The seasonal fluctuation of air temperature is limited, but highly variable.

In East Antarctica, the coastal region of DML was studied and compared to the AP. Our study area comprises the surroundings of the Ekströmsen ice-shelf and the hinterland of this area towards Halvfarrygen and Søråsen (Fig 5.1 c). The closest meteorological stations are located at the base Neumayer III (70°40'S, 8°16'W), or its predecessors Neumayer II (70°39'S, 8°15'W), and Georg-von-Neumayer base (70°37'S, 8°22'W), which provide meteorological data since 1981 to present. Mean annual 2-m air temperature (MAAT) in the vicinity of the Neumayer station shows a clear inter-annual variability, with an average temperature of -16.1°C (Table 5.1).

6.2 Stable water isotope composition of recent precipitation and implications for the climate variability

From the stable water isotope analysis ($\delta^{18}\text{O}$ and δD) of recent precipitation from both locations: Fildes Peninsula (FP), King George Island and O'Higgins station (OH) at the Antarctic Peninsula (collected between 2008 and 2009), a strong oceanic signal is observed. The local meteoric water lines (LMWL) of precipitation from OH and FP indicate a little evolved precipitation, that condensate from moisture evaporated in the nearby Southern Ocean. This is confirmed by the computation of atmospheric 3-days backward trajectories during precipitation days. Almost 50% of all precipitation events at OH and FP originate from air masses transported from the South Pacific Ocean. These air masses are characterized by relatively high $\delta^{18}\text{O}$ values (mean $\delta^{18}\text{O} = -8.7\text{‰}$) and low d excess (mean d excess = 1.6‰). Another 40% of the air-parcels derived from the south-east in the Amundsen-Bellingshausen Sea. These precipitation events are characterized by more negative $\delta^{18}\text{O}$ values (mean $\delta^{18}\text{O} = -10.2\text{‰}$), which implies colder conditions, and slightly higher d excess (3.2 to 5.0‰). The Pacific Ocean-originated precipitation events occur preferentially during rather warmer days with lower atmospheric pressure. In contrary the Amundsen-Bellingshausen Sea events occur during colder days with higher atmospheric pressure. In general precipitation events at the northern AP occur in average during days about 0.5°C warmer than the MAAT. No seasonal bias in the number of precipitation events is found. However the path of air masses arriving at the region clearly varies according to the seasons. Summer and autumn precipitation events originate to >50% from the South Pacific, while winter and spring are rather dominated by more local moisture pathways from the Bellingshausen Sea sector.

The Coastal DML is under the influence of a much colder climate regime with dominant easterly winds. Therefore, the $\delta^{18}\text{O}$ and δD of precipitation collected at the Neumayer station (1981 to 2006) is noticeably more depleted with a mean $\delta^{18}\text{O}$ of -20.5‰ ($\delta\text{D} = -156.3\text{‰}$) in comparison to the AP (Table 5.1). Precipitation events at coastal DML occur in days 3.7°C warmer than the MAAT, which is clearly more biased than at the AP.

	Fildes Peninsula	O'Higgins	Neumayer
MAAT (°C)	-4.0 / -2.3 / -0.7	-5.4 / -3.7 / -2.3	-17.8 / -16.0 / -14.3
$\delta^{18}\text{O}$ ‰	-15.7 / -7.9 / -1.8	-19.4 / -9.2 / -3.8	-39.9 / -20.54 / -6.7
δD ‰	-126.5 / -62.3 / -10.7	-150.6 / -70.5 / -21.8	-310.6 / -156.3 / -48.3
d excess ‰ (vs. VSMOW)	-5.0 / 0.6 / 6.9	-6.6 / 2.7 / 22.3 (min. / mean / max.)	-4.8 / 8.6 / 28.9
Slope / Intercept	7.9 / 0.2	7.84 / 1.2	8.0 / 7.6
Moisture source	South Pacific / Amundsen-Bellingshausen Sea		Weddell Sea / coastal and continental east

Table 5.1: Summary of the MAAT and stable water isotope composition (min/mean/max) of recent precipitation collected at the Antarctic Peninsula (FP and OH stations) and DML (Neumayer station). Main moisture sources derived from the isotope composition of precipitation and atmospheric circulation models are shown.

The d excess of precipitation samples (mean d excess = 8.6‰) suggests a moisture source with lower relative humidity (h) and/or higher sea surface temperature (SST) than the AP. In contrast, the general lower d excess values at the AP represent conditions closer to humidity saturation at the water-air interface at the evaporation moment (Gat, 1996) and/or lower SST. The dominant moisture source of coastal DML is found in the Weddell Sea, closely followed by other sources at the eastern coast and from the continent. Another minor contribution derives from the South Atlantic sector and continental south (Schlosser et al., 2008). The origin of the precipitation at coastal DML is therefore a complex mixture of moisture masses, whereas at the AP region spatially rather constant.

The slopes of the LMWLs from DML and the AP are similar and in all cases close to 8. This implies that the in-cloud condensation occurs at equilibrium conditions. Moreover secondary fractionation (e.g.: during evaporation or sublimation) is not recognizable or does not play an important role in the coastal precipitation. The intercept of the LMWL are consistent with this conclusions, since these depend on the evaporation conditions. All three LMWLs are situated below the Global Meteoric Water Line (GMWL), which has been related to conditions of h of 85% (global average) (Rozanski et al., 1993). However, an empirical correlation between h and d excess observed from direct measurements of vapor over the ocean, is approximately defined by the expression $d = -0.61h + 55.7$ (Uemura et al., 2008), which slightly differs from the global mean. Following this equation, the evaporation at the main moisture source of the AP should occur under h conditions of about 88 to 90%, whereas conditions for DML should be of about 80% in general.

6.3 Stable water isotope variability of firn cores

The isotope composition of firn cores retrieved from the AP and DML (Figure 6.1) match greatly the observations made from the precipitation samples (compare Table 5.2). All firn cores reflect a maritime input. However, the AP cores have a relatively lower $\delta^{18}\text{O}$ (δD) variability compared to DML. The co-isotope relationship ($\delta^{18}\text{O}$ vs δD) for all cores is quite similar (slope around or 8) to the GMWL. Therefore it can be concluded that precipitation in the hinterland of both Antarctic regions is occurring under similar conditions to that of the coastal precipitation, without other important input of secondary moisture (e.g.: continental moisture) or without post-depositional effects (e.g: sublimation). An altitude effect of the isotope fractionation is detectable at a similar altitude for both regions: above 600 m a.s.l. at AP and above 700 m a.s.l. DML, when moisture masses are confronted to AP (Plateau Laclavere) and DML mountain ridges (Halvfarryggen and Søråsen), respectively.

However, post-depositional effects are clearly visible for the firn cores under 600 m a.s.l. from the AP and a strong homogenization of the isotope signal is observed in firn. This process is stronger at lower altitudes in the coast region (e.g.: cores OH-1, FP-4) and weaker further inland (e.g.: cores FP-1 and OH-6). Additionally, due to the small seasonal oscillations of air temperatures (about $\sigma = 3.5^\circ\text{C}$, monthly means), no clear annual variation of $\delta^{18}\text{O}$ (δD) is recognized from these cores. Thus, the recognition of annual accumulation layers at AP is difficult below 600 m a.s.l. and therefore the dating of these cores. However, at the AP the d excess was found to be a good indicator of air temperature change. The d excess variability depends mostly on the climatic conditions at the moisture source during the evaporation moment, and not directly from local conditions at the condensation location (Dansgaard, 1964; Gat, 1996).

As mentioned before, the moisture source of the region is principally located in the nearby southern ocean (South Pacific sector and Amundsen-Bellingshausen Sea), whose surface conditions are strongly controlled by the local sea-ice extension (Weatherly et al., 1991). Accordingly, a strong contrast during summer and winter exists, which is clearly recognized in the d excess of the firn cores retrieved in the region allowing the dating of the cores. New density profiles of the core OH-6 (Antarctic Peninsula) give a first accumulation rate of the northern AP. Accordingly, the calculated accumulation rate for the year 2009 at the Laclavere Plateau is around $2347 \text{ kg m}^{-2} \text{ a}^{-1}$ (Figure 6.2) . We therefore believe that the first approximation of AP accumulation rates made for core FP-1 (KGI, of about 2000 to $2500 \text{ kg m}^{-2} \text{ a}^{-1}$) is correct (Fernandoy et al., in review). This is the first calculated accumulation rate for this region from ground-based data. These values are in fact higher as previous estimation (e.g.: Turner et al., 2002), but in-line with the other measurements at KGI (Wen et al., 1998).

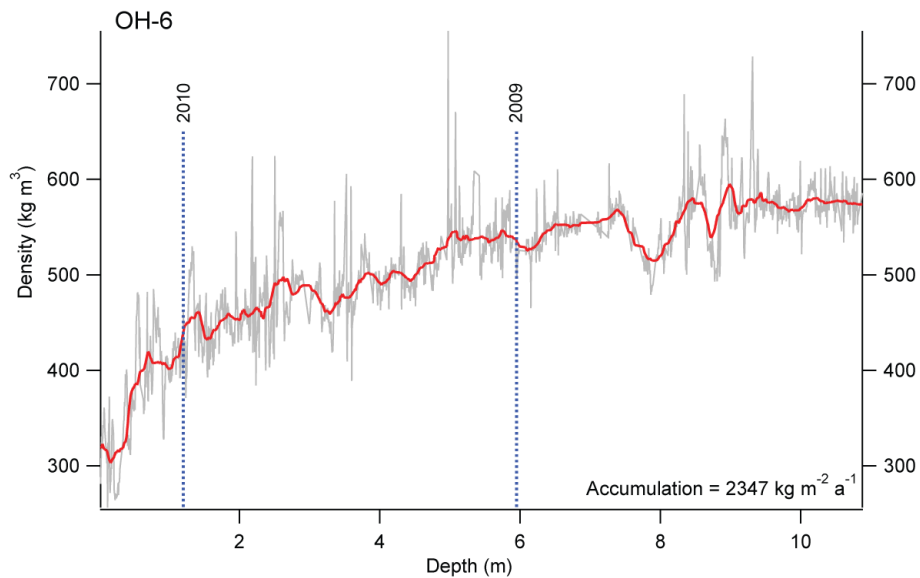


Figure 6.2: Density profile of the firn core OH-6 (northern Antarctic Peninsula). The snow-firn transition is observed at a depth of 8.4 m, which correspond to the accumulation of 2008.

The DML region is colder than the AP, and the seasonal temperature oscillation as measured at Neumayer station clearly noticeable ($\sigma=8^{\circ}\text{C}$, monthly means). Hence, in contrast to the AP, the annual temperature oscillations as registered at Neumayer are also visible in the $\delta^{18}\text{O}$ (δD) signal from all firn cores from this region. However, a clear spatial variability is observed between the coast and the hinterland. The correlation of mean annual $\delta^{18}\text{O}$ between cores toward the coast (B38 and B39), as well between the cores further inland (FB0702 and FB0704) is high ($r=0.6$). However the correlation is reduced if coastward and inland cores from the same ridge are compared ($r=0.4$) and absent between coastal Halvfarryggen (B38) and inland Søråsen (FB074) locations. This effect is most likely produced by an orographic uplift effect of the moisture masses that produced increasing adiabatic cooling towards the hinterlands. This also explains the high and extremely variable accumulation rates at this region, ranging from $360 \text{ kg m}^{-2} \text{ a}^{-1}$ near the coast up to $1250 \text{ kg m}^{-2} \text{ a}^{-1}$ on the summit of Halvfarryggen. Moreover, a shadowing effect is observed between Søråsen and Halvfarryggen, which explains the missing correlation between the $\delta^{18}\text{O}$ values as shown in Fernandoy et al. (2010). It has been observed that the accumulation rates of the regions are dependent on surrounding open sea conditions. In this way two high accumulation periods (1974-76 and 1997-98), were related to the occurrence of noticeable polynya events in the Weddell Sea region. In summary, both regions reflect local sea-ice conditions being responsible for changes in the d excess on seasonal (AP) and inter-annual (DML) scale. However, the interpretation of sea-ice conditions from DML is complicated, due to the variable origin of the moisture masses, which in many cases are characterised by similar d excess values (Schlosser et al., 2008).

	King George Island			Antarctic Peninsula			
	FP-1	FP-3	FP-4	OH-1	OH-4	OH-5	OH-6
Age	2005-2009	2007-2009	?	2006-2008	2007-2009	2008?-2009	2008-2010
$\delta^{18}\text{O}$ ‰	-18.2 / -9.2 / -5.2	-13.7 / -9.7 / -6.8	-8.5 / -7.8 / -6.6	-11.3 / -9.7 / -8.7	-14.1 / -10.4 / -7.0	-14.2 / -10.2 / -7.2	-19.8 / -12.0 / -6.5
δD ‰	-142.8 / -70.2 / -40.3	-105.8 / -73.7 / -43.9	-65.8 / -61.4 / -50.1	-88.9 / -75.3 / -67.4	-108.2 / -78.9 / -54.0	-111.2 / -78.1 / -52.1	-154.9 / -91.4 / -53.2
d excess ‰	-3.3 / 3.8 / 13.7	-2.3 / 3.8 / 11.0	0.2 / 1.2 / 2.6	0.0 / 2.2 / 5.0	-0.6 / 3.9 / 8.2	-0.6 / 3.9 / 8.2	-2.6 / 4.4 / 15.0
(vs. VSMOW)		(min. / mean / max.)			(min. / mean / max.)		
Slope / Intercept	7.8 / 1.7	7.7 / 0.4	-	7.6 / -1.4	8.0 / 3.5	8.0 / 4.0	8.0 / 4.0
Climate record	Air temperature, sea ice, moisture source, SAM variability			Air temperature, sea ice, moisture source, SAM variability			
	Dronning Maud Land						
	B38	FB0702	B39	FB0704	B04*	FB0202	
Age	1960-2007	1959-2007	1935-2007	1962-2007	1892-1981	1980-2001	
$\delta^{18}\text{O}$ ‰	-25.8 / -20.6 / -16.5	-29.5 / -24.3 / -17.04	-22.9 / -19.82 / -16.6	-26.4 / -22.7 / -19.2	-27.5 / -20.8 / -12.2	-28.0 / -20.3 / -12.7	
δD ‰	-199.1 / -158.0 / -126.6	-231.0 / -188.6 / -134.0	-177.9 / -152.1 / -124.4	-204.6 / -175.9 / -147.5	-212.5 / -158.7 / -93.3	-218.5 / -156.6 / -94.4	
d excess ‰	3.1 / 6.9 / 10.3	2.4 / 5.4 / 8.0	3.5 / 6.5 / 8.7	3.5 / 6.1 / 10.2	-6.1 / 6.0 / 16.3	-0.7 / 5.5 / 10.6	
(vs. VSMOW)			(min. / mean / max.)				
Slope / Intercept	7.6 / -0.4	8 / 5.1	7.9 / 4.8	8.0 / 6.4	8.0 / 6.8	8.0 / 8.1	
Climate record	Air temperature, moisture source, atmospheric circulation						
	* Schlosser and Oeter (2002a)						

Table 5.2: Overview of the estimated ages and stable water isotope composition (min/mean/max) of all firn cores of the study area at KGI an AP (top) and DML (bottom). Additionally the climate information derived from these cores is shown.

6.4 Isotope composition of firn cores and its relationship to the climate forcing modes

The very high accumulation rates at AP and DML allow us to study the isotopic composition on a sub-seasonal scale. Monthly resampling of the isotope profile (especially of d excess) from the AP firn cores, shows a good correlation to the air temperature ($r=0.6$ for d excess), and also to sea-ice concentration ($r=0.7$ for d excess). This demonstrates the potential of the d excess variability of firn (ice) cores of the region as proxy for the reconstruction of both air temperature and sea ice extent. Moreover, seasonal means (DJF, MAM, JJA and SON) show a good correlation to the Southern Annular Mode (SAM) (Marshall, 2003), which is the major mode of climate variability of the Antarctic Peninsula region (Marshall, 2007). The correlation of SAM and stable water isotope composition depends on the season with the best correlation in DJF-MAM (OH-6: $r=-0.76$, FP-1: $r=-0.4$ for d excess) and no significant correlation for JJA-SON. This correlation is also detected in meteorological records from the nearest stations O'Higgins, Bellingshausen and Esperanza. The strong positive correlation seems to have appeared in the early 1980s, when a marked brake of temperature trends is detected for the records of all three meteorological stations. Time-series analyses of the meteorological data show that at the beginning of 1980s, a change in both the amplitude and phase of SAM and air temperatures oscillations occurred. The oscillations seem to be in-phase for at least the following 20 years and especially in the 1990s. This coincides with the highest temperature records of the northern Antarctic Peninsula. This phenomenon is most likely caused by the change to a positive phase of SAM especially during summer and autumn (Marshall et al., 2006), which produces an strengthening of the westerly winds. A longer isotope record ($\delta^{18}\text{O}$) extracted from an ice core retrieved in Gomez Plateau, southern Antarctic (Thomas et al., 2009), shows that the warming trend already began in the early 20th century or sooner, but has accelerated in the last 50 years. Time-series analyses of $\delta^{18}\text{O}$ annual means from this core exhibit a clear connection to SAM on a seasonal to decadal time scale. Moreover a second climate forcing mode: El Niño Southern Oscillation (ENSO) (Trenberth, 1997) influences the region but only in an intermittent way. ENSO is most noticeable towards southern latitudes of AP (Bertler et al., 2006), but seems to be overwhelmed by the SAM to the north. Nonetheless, ENSO is visible in the climatology of the AP during in-phase SAM positive (negative) events and "La Niña" (El Niño) ENSO (Fogt et al., 2010).

At coastal DML no clear tendency is seen in the meteorological data from the Neumayer station, however, the instrumental record only begins in 1981. To the west slightly negative, but statistically not significant trends ($-0.11^\circ\text{C decade}^{-1}$) have been informed from the meteorological record of Halley station (Turner et al., 2005), whereas to the east (hinterland of Novolazarevskya

station) slightly positive air temperature trends ($+0.1^{\circ}\text{C decade}^{-1}$) for the last century have been calculated from an ice core $\delta^{18}\text{O}$ record (Naik et al., 2010). In both cases, a connection of the records with SAM has been found.

At Ekströmisen and hinterland, a statistically significant correlation has been found between air temperatures (monthly means) and monthly $\delta^{18}\text{O}$ resampled values for all firn cores ($r=0.54$ up to 0.71) (Fernandoy et al., 2010). Therefore, longer time series of air temperature can be reconstructed based on the isotope variations of firn. The longest record corresponds to the cores FB0202 and B04 (Schlosser and Oerter, 2002a), which were retrieved at the Ekströmisen ice shelf (70.65°S , 8.25°W and 70.62°S , 8.37°W , respectively) separated by a short distance and together covering the time interval between 1892 and 2002. For this period a slightly positive temperature trend ($+0.1^{\circ}\text{C decade}^{-1}$) has been calculated, which is similar to the trend found further east (Naik et al., 2010). However, for the period 1960-2002 no significant temperature trend for the coast (Ekströmisen) and the hinterland (firn core locations B38, B39, FB0702 and FB0704) have been detected. Therefore, the long-term temperature trend cannot be related to the recent warming phenomenon at least in this region, where relatively stable climatic conditions predominate for the last half century.

Nonetheless, a high seasonal to inter-annual climate variability exists in the region. Seasonal means of the air temperature record show a positive correlation with seasonal ENSO and SAM records for summer ($r=0.4$) and negative correlation for autumn ($r=-0.6$) during 1981 to 2002. Even though the meteorological record is very restricted in time, and no reliable interpretation of climate variability and forcing modes relationship at this region can be made.

It has been shown that the correlation of stable water isotope contents between the firn cores at DML is relatively good, thus, allowing us to test the climate variability for the region on a broad regional and temporal scale. Correlations between seasonal $\delta^{18}\text{O}$ means, SAM and ENSO show that the relationship is not constant and changing on a decadal time scale (Table 5.3). Similarly to the correlation between air temperature from the Neaumayer station and SAM, the estimated $\delta^{18}\text{O}$ (δD) summer (DJF) mean of the combined cores FB0202/B04 positively correlates to SAM ($r=0.5$), while the cores B38 and B39 are negatively linked to ENSO ($r=-0.4$ and -0.6 , respectively) for the period 1980-2002. However this correlation is weaker for summer seasons in the period 1970 to 2002 and not significant between 1960 and 2002, confirming the high interannual variability of the region. The winter season show a negative correlation ($r=-0.3$) of $\delta^{18}\text{O}$ (FB0202/B04) with SAM for the period 1950 to 2002, but the correlation becomes low and not significant in the period 1980-2002. All other seasonal correlations do not present coherent periods of correlation with SAM, and ENSO is only present on sporadic periods and not spatially uniform. Exceptionally,

		1960-2002						1970-2002								
		FB0202/B04			B38	B39	FB0702	FB0704	FB0202/B04			B38	B39	FB0702	FB0704	
		$\delta^{18}\text{O}$	δD	d excess	$\delta^{18}\text{O}$	$\delta^{18}\text{O}$	$\delta^{18}\text{O}$	$\delta^{18}\text{O}$	$\delta^{18}\text{O}$	δD	d excess	$\delta^{18}\text{O}$	$\delta^{18}\text{O}$	$\delta^{18}\text{O}$	$\delta^{18}\text{O}$	
SAM		0.22	0.19	-0.22	0.04	0.07	-0.05	0.21	SAM	0.41	0.34	-0.42	0.03	0.12	0.00	0.41
		p=.15	p=.23	p=.17	p=.81	p=.64	p=.76	p=.18		p=.02	p=.06	p=.02	p=.86	p=.51	p=.99	p=.02
ENSO		0.06	0.07	0.06	0.02	-0.13	0.05	-0.22	ENSO	-0.02	-0.01	0.10	-0.05	-0.21	0.03	-0.15
		p=.67	p=.66	p=.70	p=.90	p=.42	p=.75	p=.16		p=.89	p=.96	p=.60	p=.78	p=.25	p=.89	p=.41

		1980-2002						
		FB0202/B04			B38	B39	FB0702	FB0704
		$\delta^{18}\text{O}$	δD	d excess	$\delta^{18}\text{O}$	$\delta^{18}\text{O}$	$\delta^{18}\text{O}$	$\delta^{18}\text{O}$
SAM		0.53	0.51	-0.28	0.32	0.23	0.13	0.27
		p=.01	p=.02	p=.21	p=.14	p=.30	p=.56	p=.23
ENSO		-0.15	-0.14	0.19	-0.39	-0.62	-0.01	-0.07
		p=.50	p=.55	p=.40	p=.07	p=.00	p=.96	p=.75

Table 5.3: Summer correlation matrices of monthly isotope means from all firn cores from coastal DML and climate forcing modes SAM and ENSO. All statistically significant correlation ($p < 0.1$) are displayed in red. Three selected periods are shown.

6.5 On the potential of the stable water isotopes as proxy for climate-reconstruction: Conclusions, ideas for future research and outlook

In this thesis, it has been demonstrated that isotope composition and physical properties of firn in both high accumulation regions from AP and DML have a great potential to be utilized as a multi-climate proxy. The high accumulation of both regions ensures that snow at the respective locations will not be exposed to the atmosphere for longer time periods. In this way any possible secondary isotopic exchange with the atmosphere (e.g. through sublimation) is avoided and a good conservation of the original atmospheric isotope signal is assured. The detailed stable isotope analysis results in new and significant insight on regional climate dynamics (temperature, moisture transport history and sea ice variability) including amplitudes, rates of change, causes, interactions and temporal patterns of the precipitation history at both until now scarcely-explored regions.

With recent precipitation samples collected at the AP (King George Island and O'Higgins station) and the coastal DML (Neumayer station), the seasonal stable water isotope cycle of the two regions has been studied in depth. Both localities present a strong oceanic influence, which is reflected in the LMWLs (slopes close to 8). Nonetheless, the regions differ in the location of their moisture sources, which were determined by combining circulation models with d excess values. The main moisture source regions of the northern AP region were found at: (a) the South Pacific and (b) the Amundsen-Bellinghousen Sea, whereas DML receives mixed moisture derived mainly from the Weddell Sea and the continental region east of DML (Schlosser et al., 2008). Further difference in the evaporation conditions at the moisture source can be concluded from mean d excess values. Mean d excess values varies from 9‰ at DML, to around 1‰ at the AP, thus implying a difference of the relative humidity of around 10% (Uemura et al., 2008) between both evaporation regions. The stable water isotope datasets of both regions show a good correlation with surface air temperatures. Correlation coefficients between $\delta^{18}\text{O}$ and air temperature are high (around $r=0.7$) for both regions. Moreover, the d excess from the AP shows a significant correlation to air temperature as well. The $\delta^{18}\text{O}$ - air temperature gradient for DML is about $0.6\text{‰ }^{\circ}\text{C}^{-1}$, thus slightly higher than the gradient of the AP of $0.4\text{‰ }^{\circ}\text{C}^{-1}$ for $\delta^{18}\text{O}$ and $0.6\text{‰ }^{\circ}\text{C}^{-1}$ for d excess.

These findings are of major importance, since once the relationship between stable water isotope and the climate variability is proved, this can be transferred to the firn core records retrieved from the same region. Therefore, from 4 different cores retrieved in the hinterland of the Ekströmisen ice-shelf (DML) no significant air temperature trends were concluded for at least the last 50 years in the region, which is supported by the 20 years of meteorological record from the Neumayer station. At the AP, a first firn core retrieved from the ice divide between the east and west

coast (Plateau Laclavere) shows that this location possesses a good potential to study the recent climate variability at this region. However, the $\delta^{18}\text{O}$ of this core does not show any important correlation to air temperatures. This on one hand explained by the restricted air temperature annual oscillation, on the other hand potentially by the shortness of the record. Nonetheless, the d excess of different cores in this region exhibits a better correlation than expected to air temperature oscillation. This occurs because the source of the moisture transported to the regions is situated very close to AP (in the surrounding Southern Pacific and Amundsen Bellingshausen Sea). Moreover, the air temperatures at west AP are highly dependent on sea ice conditions, thus, the isotope compositions of firn cores are a reliable proxy not only for air temperature, but also for the sea ice and sea surface conditions. This is an important finding, since seasonal d excess cycles may be used to date the firn cores.

Contrary to DML, the AP is undergoing a remarkable warming of the air temperature as observed from long-term meteorological data. It was shown that the trend began before the instrumental record (ca. 1950). However, the beginning of the warming trends has been yet not determined for this region. The statistical treatment of the meteorological data shows that warming trends are seasonally biased (stronger for summer and autumn seasons west AP). Moreover, it was demonstrated that the climate variability of the region is greatly modulated by the Southern Annular Mode (SAM). This atmospheric mode has shifted to a marked positive anomaly for the last 50 years, clearly increasing since the 1980s, which coincides with the period of highest temperatures (around 1989AD) of the meteorological record. The d excess composition of shallow firn cores, display a marked correlation to SAM during summer and autumn, showing a SAM influence on precipitation in the region. The interaction of SAM and the climatology at DML, as seen from the correlation with the stable water isotope composition of firn cores, is significant only after 1970 for the summer season, while in winter the isotope composition shows sporadic (negative correlated) connections to SAM. Additionally to the SAM, sporadic connection was found between isotope composition and ENSO. However, this correlation is always weaker and opposite in sign than SAM. Statistically significant ENSO correlations were found only during selected time slices and disappear on a decadal time scale. However, the shortness of the records does not allow to draw a final conclusion of the ENSO/SAM relationship on the regional climate. This relationship varies on a decadal or larger time scales, which is a noticeable difference to the AP, which is much more sensitive to any environmental change.

In general at coastal East Antarctica, a big gap of information exists regarding local and regional mass balance and climate variability at a centennial to millennial time scale. The ice

thickness of the coastal DML region reaches up to 900 m (Steinhage et al., 1999). Therefore, a climate record of up to 2 kyr is potentially available from the ice sheet in the hinterland of Neumayer. In 2007, a field campaign was carried out in the frame of the International Partnerships in Ice Cores Sciences (IPICS) (Brook et al., 2006), with the aim to evaluate the potential of this region to contribute to the IPICS 40k array. However, the new findings presented in this thesis (Fernandoy et al., 2010), especially the high accumulation rates point out that this region most likely contributes to the IPICS 2k array only. The main objective of the IPICS initiative is to contribute to the understanding of the Antarctic climate on a decadal to centennial time scale at a high resolution. For this purpose, a precisely dated record is needed to capture the dominant regional pattern of climate variability (Brook et al., 2006). In the near future, further work in this direction is planned at the Alfred Wegener Institute, with the aim to retrieve a medium - depth core (>300m) most likely at the summit of Halvfarryggen.

According to this thesis, a special focus should be put on the reconstruction of the temporal-spatial climate variability at the northern AP, of the last 150-200 years (or beyond since the ice thickness of the region is still not well known). For this purpose, several shallow firn cores as well as a medium-depth (150-200 m) ice core should be extracted at the Plateau Laclavere region, Antarctic Peninsula. The posterior laboratory work, should include the determination of the basic parameters of ice (density, dielectric properties, isotopic and hydrochemical composition) to date the ice/firn cores (annual layer counting, event-related dating) for climate reconstruction. Moreover, stable water isotope time series should be combined with other geophysical and geochemical tools (e.g.: major ions analysis and tephrochronology) to improve the age model and establish of new methods for climate reconstructions. A good example is the implementation of methanesulphonic acid (MSA), which has successfully used as a sea-ice indicator in the AP region (Abram et al., 2010).

The AP region and its glaciological records are key climate archives for West Antarctica. The climate record from AP accumulated in precipitation, ice and firn of the region provides highly valuable time series that gather to a unique and yet not existing set of information relevant for this area and potentially beyond. It contributes to the key understanding of major Antarctic climate changes of the transition from pre-industrial to the anthropogenic-influenced times. However, these objectives can only be achieved in collaboration with other similar scientific initiatives (e.g.: Polar to Tropical Initiative: <http://www.polartropical.org/>), since the high local climate variability is a key issue to overcome. In order to properly address the regional frame of the recent climate variability and air temperature warming, more data and joint work is needed.

7 References

- Abram, N. J., Anderson, J., Bargelloni, L., Barrett, P., Bentley, M. J., Bertler, N., Chown, S., Clarke, A., Convey, P., Crame, A., Crosta, X., Curran, M., di Prisco, G., Francis, J., Goodwin, I., Gutt, J., Hodgson, D., Massé, G., Masson-Delmotte, V., Mayewski, P., Mulvaney, R., Peck, L., Pörtner, H., Röthlisberger, R., Stevens, M., Summerhayes, C., van Ommen, T., Verde, C., Verleyen, E., Vyverman, W., Wiencke, C., and Zane, L.: Antarctic Climate and environmental history in the pre-instrumental period, in: Antarctic climate change and the environment, edited by: Hodgson, D., Scientific Committee on Antarctic Research, Cambridge, UK., 115-182, 2009.
- Abram, N. J., Thomas, E. R., McConnell, J. R., Mulvaney, R., Bracegirdle, T. J., Sime, L. C., and Aristarain, A. J.: Ice core evidence for a 20th century decline of sea ice in the Bellingshausen Sea, Antarctica, *J. Geophys. Res.*, 115, D23101, doi: 10.1029/2010jd014644, 2010.
- Ackley, S. F., Geiger, C. A., King, J. C., Hunke, E. C., and Comiso, J.: The Ronne polynya of 1997/98: observations of air-ice-ocean interaction, *Ann. Glaciol.*, 33, 425-429, 2001.
- Adams, B., Arthern, R., Atkinson, A., Barbante, C., Bargagli, R., Bergstrom, D., Bertler, N., Bindschadler, R., Bockheim, J., Boutron, C., Bromwich, D., Chown, S., Comiso, J., Convey, P., Cook, A., di Prisco, G., Fahrbach, E., Fastook, J., Forcarda, J., Gili, J., Gugliemin, M., Gutt, J., Hellmer, H., Hennion, F., Heywood, K., Hodgson, D., Holland, D., Hong, S., Huiskes, A., Isla, E., Jacobs, S., Jones, A., Lenton, A., Marshall, G., Mayewski, P., Meredith, M., Metzl, N., Monaghan, A., Naveira-Garabato, A. C., Newsham, K., Orejas, C., Peck, L., Pörtner, H., Rintoul, S., Robinson, S., Roscoe, H., Rossi, S., Scambos, T., Shanklin, J., Smetacek, V., Speer, K., Stevens, M., Summerhayes, C., Trathan, P., Turner, J., Van der Veen, C. J., D.G., V., Verde, C., Webb, D., Wiencke, C., Woodworth, P., Worby, T., Worland, R., and Takashi, Y.: The Instrumental Period, in: Antarctic Climate Change and the Environment, edited by: Turner, J., Scientific Committee on Antarctic Research, Cambridge, U.K., 183-298, 2009.
- Ainley, P., Barrett, P., Bindschadler, R., Clarke, A., Convey, P., Fahrbach, E., Gutt, J., Hodgson, D. A., Meredith, M., Murray, A., Pörtner, H., di Prisco, G., Schiel, S., Speer, K., Summerhayes, C., Turner, J., Verde, C., and Willems, A.: The Antarctic Environment in the Global System, in: Antarctic Climate Change and the Environment, edited by: Summerhayes, C., Scientific Committee on Antarctic Research, Cambridge, 1-32, 2009.
- Aristarain, A., Delmas, R., and Stievenard, M.: Ice-Core Study of the link between Sea-Salt aerosol, Sea-Ice cover and climate in the Antarctic Peninsula Area, *Climatic Change*, 67, 63-86, 2004.
- Bentley, M. J., Hodgson, D. A., Smith, J. A., Cofaigh, C. O., Domack, E. W., Larter, R. D., Roberts, S. J., Brachfeld, S., Leventer, A., Hjort, C., Hillenbrand, C. D., and Evans, J.: Mechanisms of Holocene palaeoenvironmental change in the Antarctic Peninsula region, *Holocene*, 19, 51-69, 2009.
- Bertler, N., Mayewski, P. A., Aristarain, A., Barrett, P., Becagli, S., Bernardo, R., Bo, S., Xiao, C., Curran, M., Qin, D., Dixon, D., Ferron, F., Fischer, H., Frey, M., Frezzotti, M., Fundel, F., Genthon, C., Gragnani, R., Hamilton, G., Handley, M., Hong, S., Isaksson, E., Kang, J., Ren, J., Kamiyama, K., Kanamori, S., Kärkäs, E., Karlöf, L., Kaspari, S., Kreutz, K., Kurbatov, A., Meyerson, E., Ming, Y., Zhang, M., Motoyama, H., Mulvaney, R., Oerter, H., Osterberg, E., Proposito, M., Pyne, A., Ruth, U., Simoes, J., Smith, B., Sneed, S., Teinilä, K., Traufetter, F., Udisti, R., Virkkula, A., Watanabe, O., Williamson, B., Winther, J. G., Li, Y., Wolff, E., Li, Z., and Zielinski, A.: Snow chemistry across Antarctica, *Ann. Glaciol.*, 41, 167-179, 2005.
- Bertler, N. A., Barrett, P. J., Mayewski, P. A., and Fogt, R. L.: El Niño suppress Antarctic warming, *Geophys. Res. Lett.*, 31, 1-4, 10.1029/2004GL020749, 2004.
- Bertler, N. A., Naish, T. R., Mayewski, P. A., and Barrett, P. J.: Opposing oceanic and atmospheric ENSO influence on the Ross Sea Region, Antarctica, *Adv. Geosci.*, 6, 83-86, 2006.
- Blindow, N., Suckro, S., Rückamp, M., Braun, M., Schindler, M., Breuer, B., Saurer, H., Simoes, J., and Lange, M.: Geometry and thermal regime of the King George Island ice cap, Antarctica, from GPR and GPS, *Ann. Glaciol.*, 51, 103-109, 2010.
- Bracegirdle, T. J., Connolley, W. M., and Turner, J.: Antarctic climate change over the twenty first century, *J. Geophys. Res.*, 113, 1-13, doi: 10.1029/2007JD008933, 2008.

- Bromwich, D. H., Chen, B., and Hines, K. M.: Global atmospheric impacts induced by year-round open water adjacent to Antarctica, *J. Geophys. Res.-Atmos.*, 103, 11173-11189, 1998.
- Brook, E., Wolff, E., Dahl-Jensen, D., Fischer, H., and Steig, E. J.: The future of ice coring: International Partnerships in Ice Core Sciences (IPICS), *PAGES news*, 14, 6-10, 2006.
- Carrasco, J., and González, M. (Eds): *Climatología de la Península Antártica y de la Base Presidente Eduardo Frei Montalva*, Dirección Meteorológica de Chile, 2007.
- Carrasco, J. F., Bromwich, D. H., and Monaghan, A. J.: Distribution and characteristics of mesoscale cyclones in the Antarctic: Ross Sea eastward to the Weddell Sea, *Mon. Weath. Rev.*, 131, 289-301, 2003.
- Carsey, F. D.: Microwave Observation of the Weddell Polynya, *Mon. Weath. Rev.*, 108, 2032-2044, 1980.
- Chapman, W. L., and Walsh, J. E.: A Synthesis of Antarctic Temperatures, *J. Climate*, 20, 4096-4117, 2007.
- Chen, J. L., Wilson, C. R., Blankenship, D., and Tapley, B. D.: Accelerated Antarctic ice loss from satellite gravity measurements, *Nat. Geosci.*, 2, 859-862, 2009.
- Clark, I., and Fritz, P., J., S., and A., S. (Eds): *Environmental Isotopes in Hydrogeology*, Lewis, Boca Raton, New York, 311 pp., 1997.
- Cook, A. J., Fox, A. J., Vaughan, D. G., and Ferrigno, J. G.: Retreating Glacier Fronts on the Antarctic Peninsula over the Past Half-Century, *Science*, 308, 541-544, 10.1126/science.1104235, 2005.
- Craig, H.: Isotopic variations in meteoric waters, *Science*, 133, 1702-1703, doi: 10.1126/science.133.3465.1702, 1961.
- Dansgaard, W.: Stable isotopes in precipitation, *Tellus*, 16, 436-468, doi: 10.1111/j.2153-3490.1964.tb00181.x, 1964.
- Davis, C. H., Li, Y., McConnell, J. R., Frey, M. M., and Hanna, E.: Snowfall-Driven Growth in East Antarctic Ice Sheet Mitigates Recent Sea-Level Rise, *Science*, 308, 1898-1901, 10.1126/science.1110662, 2005.
- De Angelis, H., and Skvarca, P.: Glacier Surge After Ice Shelf Collapse, *Science*, 299, 1560-1562, doi: 10.1126/science.1077987, 2003.
- Divine, D. V., Isaksson, E., Kaczmarek, M., Godtliessen, F., Oerter, H., Schlosser, E., Johnsen, S. J., van den Broeke, M., and van de Wal, R. S. W.: Tropical Pacific-high latitude south Atlantic teleconnections as seen in $\delta^{18}\text{O}$ variability in Antarctic coastal ice cores, *J. Geophys. Res.*, 114, 2009.
- Domack, E. W., Leventer, A., Burnett, A., Bindschadler, R., Convey, P., and Kirby, M. (Eds): *Antarctic Peninsula Climate Variability. Historical and Paleoenvironmental Perspectives*, Antarctic Research Series, 79, American Geophysical Union, Washington, D.C., 260 pp., 2003a.
- Domack, E. W., Leventer, A., Root, S., Williams, E., Carlson, D., Hirshorn, E., Wright, W., Gilbert, R., and Burr, G.: Marine sedimentary record of natural environmental variability and recent warming in the Antarctic Peninsula, in: *Antarctic Peninsula Climate Variability: Historical and Paleoenvironmental Perspectives*, edited by: Domack, E. W., Leventer, A., Burnett, A., Bindschadler, R., Convey, P., and Kirby, M., Antarctic Research Series, American Geophysical Union, Washington, D.C., 205-222, 2003b.
- Draxler, R. R., and Hess, G. D.: An Overview of the HYSPLIT-4 modelling system for trajectories, dispersion and deposition, *Aust. Meteorol. Mag.*, 47, 295-308, 1998.
- HYSPLIT (HYbrid Single-Particle Lagrangian Integrated Trajectory) Model access via NOAA ARL READY. NOAA Air Resources Laboratory, Silver Spring, MD. : <http://www.arl.noaa.gov/ready/hysplit4.html>, last access: 2010
- Eisen, O., Frezzotti, M., Genthon, C., Isaksson, E., Magand, O., van den Broeke, M. R., Dixon, D. A., Ekaykin, A., Holmlund, P., Kameda, T., Karlöf, L., Kaspari, S., Lipenkov, V. Y., Oerter, H., Takahashi, S., and Vaughan, D. G.: Ground-based measurements of spatial and temporal variability of snow accumulation in East Antarctica, *Rev. Geophys.*, 46, RG2001, doi: 10.1029/2006rg000218, 2008.
- EPICA community members: Eight glacial cycles from an Antarctic ice core, *Nature*, 429, 623-628, 2004.
- EPICA community members: One-to-one coupling of glacial climate variability in Greenland and Antarctica, *Nature*, 444, 195-198, 2006.

- Fernandoy, F., Oerter, H., Meyer, H., Wilhelms, F., Graf, W., and Schwander, J.: Temporal and spatial variation of stable isotope ratios and accumulation rates in the hinterland of Neumayer Station, East Antarctica, *J. Glaciol.*, 56, 673-687, 2010.
- Fernandoy, F., Meyer, H., Thomas, E. R., Simões, J., and Tonelli, M.: Seasonal to decadal climate variability in the northern Antarctic Peninsula region from 50 years of meteorological records and ice-core time series, in preparation for submission.
- Fernandoy, F., Meyer, H., and Tonelli, M.: Stable water isotopes of precipitation and firn cores from the northern Antarctic Peninsula region as a proxy for climate reconstruction, *The Cryosphere*, Submitted, in review.
- Ferraz-Mello, S.: Estimation of periods from unequally spaced observations, *Astron. J.*, 86, 619-624, 1981.
- Fogt, R., Bromwich, D., and Hines, K.: Understanding the SAM influence on the South Pacific ENSO teleconnection, *Clim Dyn*, 1-22, 10.1007/s00382-010-0905-0, 2010.
- Fogt, R. L., and Bromwich, D. H.: Decadal variability of the ENSO teleconnection to the high-latitude South Pacific governed by coupling with the southern annular mode, *J. Climate*, 19, 979-997, 2006.
- Gat, J. R.: Oxygen and hydrogen isotopes in the hydrological cycle, *Annual Review of Earth and Planetary Sciences*, 24, 225-262, doi:10.1146/annurev.earth.24.1.225, 1996.
- Gillett, N., Kell, T. D., and Jones, P. D.: Regional climate impacts of the Southern Annular Mode, *Geophys. Res. Lett.*, 33, 1-4, 2006.
- Gillett, N. P., Stone, D. A., Stott, P. A., Nozawa, T., Karpechko, A. Y., Hegerl, G. C., Wehner, M. F., and Jones, P. D.: Attribution of polar warming to human influence, *Nat. Geosci.*, 1, 750-754, 2008.
- Gong, D., and Shaowu, W.: Definition of Antarctic oscillation index, *Geophys. Res. Lett.*, 26, 459-462, 0094-8276/1999GL900003, 1999.
- Gordon, A. L., Visbeck, M., and Comiso, J. C.: A possible link between the Weddell Polynya and the Southern Annular Mode, *J. Climate*, 20, 2558-2571, Doi 10.1175/Jcli4046.1, 2007.
- Hall, B.: Holocene glacial history of Antarctica and the sub-Antarctic islands, *Quat. Sci. Rev.*, 28, 2213-2230, 2009.
- Helsen, M. M., van de Wal, R. S. W., van den Broeke, M. R., van As, D., Meijer, H. A. J., and Reijmer, C. H.: Oxygen isotope variability in snow from western Dronning Maud Land, Antarctica and its relation to temperature, *Tellus B*, 57, 423-435, 2005.
- Hines, K. M., Bromwich, D. H., and Marshall, G. J.: Artificial surface pressure trends in the NCEP-NCAR reanalysis over the southern ocean and Antarctica, *J. Climate*, 13, 3940-3952, 2000.
- Hofstede, C. M., van de Wal, R. S. W., Kaspers, K. A., van den Broeke, M. R., Karlöf, L., Winther, J.-G., Isaksson, E., Lappégard, G., Mulvaney, R., Oerter, H., and Wilhelms, F.: Firn accumulation records for the past 1000 years on the basis of dielectric profiling of six cores from Dronning Maud Land, Antarctica, *J. Glaciol.*, 50, 279-291, 2004.
- Holland, D. M.: Explaining the Weddell Polynya - a large ocean eddy shed at Maud Rise, *Science*, 292, 1697-1700, 2001.
- Huybrechts, P., Steinhage, D., Wilhelms, F., and Bamber, J.: Balance velocities and measured properties of the Antarctic ice sheet from a new compilation of gridded data for modelling, *Ann. Glaciol.*, 30, 52-60, 2000.
- Global Network of Isotopes in Precipitations. The GNIP Database.: <http://www-naweb.iaea.org/napc/ih/index.html>, last access: 2010
- Ichiyanagi, K., Numaguti, A., and Kato, K.: Interannual variation of stable isotopes in Antarctic precipitation in response to El Niño-Southern Oscillation, *Geophys. Res. Lett.*, 29, -, doi: 10.1029/2000gl012815, 2002.
- IPCC, Solomon, S., Qin, D., Manning, M., Chen, Z., Marquis, M., Averyt, K. B., Tignor, M., and Miller, H. (Eds): *Climate Change 2007: The Physical Science Basis. Contribution of Working Group I to the Fourth Assessment*

- Report of the Intergovernmental Panel on Climate Change, Cambridge University Press, Cambridge, United Kingdom and New York, USA, 2007.
- Isaksson, E., Kohler, J., Pohjola, V., Moore, J., Igarashi, M., Karlof, L., Martma, T., Meijer, H., Motoyama, H., Vaikmae, R., and van de Wal, R.: Two ice-cores $\delta^{18}\text{O}$ records from Svalbard illustrating climate and sea-ice variability over the last 400 years, *Holocene*, 15, 501-509, 2005.
- Jacobs, S. S., and Comiso, J. C.: Climate Variability in the Amundsen and Bellingshausen Seas, *J. Climate*, 10, 697-709, doi:10.1175/1520-0442(1997)010<0697:CVITAA>2.0.CO;2, 1997.
- Jouzel, J., and Merlivat, L.: Deuterium and Oxygen 18 in Precipitation: Modeling of the Isotopic Effects during Snow Formation, *J. Geophys. Res-Atmos.*, 89, 1749-1757, 1984.
- Jouzel, J., Masson-Delmotte, V., Cattani, O., Dreyfus, G., Falourd, S., Hoffmann, G., Minster, B., Nouet, J., Barnola, J. M., Chappellaz, J., Fischer, H., Gallet, J. C., Johnsen, S., Leuenberger, M., Loulergue, L., Luethi, D., Oerter, H., Parrenin, F., Raisbeck, G., Raynaud, D., Schilt, A., Schwander, J., Selmo, E., Souchez, R., Spahni, R., Stauffer, B., Steffensen, J. P., Stenni, B., Stocker, T. F., Tison, J. L., Werner, M., and Wolff, E. W.: Orbital and Millennial Antarctic Climate Variability over the Past 800,000 Years, *Science*, 317, 793-796, 10.1126/science.1141038, 2007.
- Kalnay, E., Kanamitsu, M., Kistler, R., Collins, W., Deaven, D., Gandin, L., Iredell, M., Saha, S., White, G., Woollen, J., Zhu, Y., Leetmaa, A., Reynolds, R., Chelliah, M., Ebisuzaki, W., Higgins, W., Janowiak, J., Mo, K. C., Ropelewski, C., Wang, J., Jenne, R., and Joseph, D.: The NCEP/NCAR 40-Year Reanalysis Project, *Bulletin of the American Meteorological Society*, 77, 437-471, doi: 10.1175/1520-0477(1996)077<0437:TNYRP>2.0.CO;2, 1996.
- Kanamitsu, M.: Description of the NMC Global Data Assimilation and Forecast System, *Weath. Forecast.*, 4, 335-342, doi: 10.1175/1520-0434(1989)004<0335:DOTNGD>2.0.CO;2, 1989.
- Kawamura, K., Parrenin, F., Lisiecki, L., Uemura, R., Vimeux, F., Severinghaus, J. P., Hutterli, M. A., Nakazawa, T., Aoki, S., Jouzel, J., Raymo, M. E., Matsumoto, K., Nakata, H., Motoyama, H., Fujita, S., Goto-Azuma, K., Fujii, Y., and Watanabe, O.: Northern Hemisphere forcing of climatic cycles in Antarctica over the past 360,000 years, *Nature*, 448, 912-916, 2007.
- Kejna, M.: Trends of air temperature of the Antarctic during the period 1958-2000, *Polish Polar Research*, 24, 99-126, 2003.
- King, J. C.: Recent Climate Variability in the Vicinity of the Antarctic Peninsula, *Int. J. Climatol.*, 14, 357-369, 1994.
- King, J. C., and Comiso, J. C.: The spatial coherence of interannual temperature variations in the Antarctic Peninsula, *Geophys. Res. Lett.*, 30, -, doi: 10.1029/2002gl015580, 2003.
- King, J. C., Turner, J., Marshall, G., Connolley, W. M., and Lachlan-Cope, T.: Antarctic Peninsula climate variability and its causes as revealed by analysis of instrumental records, in: *Antarctic Peninsula Climate Variability. Historical and paleoenvironmental perspectives.*, edited by: Domack, E. W., Leventer, A., Burnett, A., Bindschadler, R., Convey, P., and Kirby, M., Antarctic Research Series, American Geophysical Union, Washington, D.C., 17-30, 2003.
- Koerner, R. M.: Some comments on climatic reconstructions from ice cores drilled in areas of high melt, *J. Glaciol.*, 43, 90-97, 1997.
- Kohshima, S., Nozomu, T., Uetake, J., Shiraiwa, T., Uemura, R., Yoshida, N., Matoba, S., and Godoi, M. A.: Estimation of net accumulation rate at a Patagonian glacier by ice core analyses using snow algae, *Global Planet. Change*, 59, 236-244, 2007.
- König-Langlo, G., and Loose, B.: The Meteorological Observatory at Neumayer Stations (GvN and NM-II) Antarctica, *Ber. Polarforsch. Rep. Pol.*, 76, 19-25, 2007.
- Kwok, R., and Comiso, J. C.: Spatial patterns of variability in antarctic surface temperature: Connections to the Southern Hemisphere Annular Mode and the Southern Oscillation, *Geophys. Res. Lett.*, 29, -, doi: 10.1029/2002gl015415, 2002.
- Legrand, M., and Mayewski, P.: Glaciochemistry of polar ice cores: A review, *Rev. Geophys.*, 35, 219-243, 1997.

- Levitus, S., Antonov, J. I., Boyer, T. P., and Stephens, C.: Warming of the World Ocean, *Science*, 287, 2225-2229, doi: 10.1126/science.287.5461.2225, 2000.
- Levitus, S., Antonov, J., and Boyer, T.: Warming of the world ocean, 1955-2003, *Geophys. Res. Lett.*, 32, -, doi: 10.1029/2004gl021592, 2005.
- Lumpkin, R., and Speer, K.: Global Ocean Meridional Overturning, *Journal of Physical Oceanography*, 37, 2550-2562, doi: 10.1175/JPO3130.1, 2007.
- Marshall, G., Di Battista, S., Naik, S., and Thamban, M.: Analysis of a regional change in the sign of the SAM-temperature relationship in Antarctica, *Clim. Dyn.*, 36, 277-287, doi: 10.1007/s00382-009-0682-9, 2011.
- Marshall, G. J.: Analysis of recent circulation and thermal advection change in the northern Antarctic Peninsula, *International Journal of Climatology*, 22, 1557-1567, 2002.
- Marshall, G. J.: Trends in the Southern Annular Mode from observations and Reanalyses, *J. Climate*, 16, 4134-4143, 2003.
- Marshall, G. J., Orr, A., van Lipzig, N. P. M., and King, J. C.: The Impact of a Changing Southern Hemisphere Annular Mode on Antarctic Peninsula Summer Temperatures, *J. Climate*, 19, 5388-5404, 2006.
- Marshall, G. J.: Half-century seasonal relationships between the Southern Annular Mode and Antarctic temperatures, *Int. J. Climatol.*, 27, 373-383, doi: 10.1002/Joc.1407, 2007.
- Masson-Delmotte, V., Hou, S., Ekaykin, A., Jouzel, J., Aristarain, A., Bernardo, R. T., Bromwich, D., Cattani, O., Delmotte, M., Falourd, S., Frezzotti, M., Gallée, H., Genoni, L., Isaksson, E., Landais, A., Helsen, M. M., Hoffmann, G., Lopez, J., Morgan, V., Motoyama, H., Noone, D., Oerter, H., Petit, J. R., Royer, A., Uemura, R., Schmidt, G. A., Schlosser, E., Simoes, J. C., Steig, E. J., Stenni, B., Stievenard, M., van den Broeke, M. R., van de Wal, R. S. W., van de Berg, W. J., Vimeux, F., and White, J. W. C.: A Review of Antarctic Surface Snow Isotopic Composition: Observations, Atmospheric Circulation, and Isotopic Modeling, *J. Climate*, 21, 3359-3387, 2008.
- Mayewski, P., Maasch, K. A., Yan, Y., Kang, S., Meyerson, E., Sneed, S., Kaspari, S., Dixon, D., Osterberg, E., Morgan, V., van Ommen, T., and Curran, M.: Solar forcing of the polar atmosphere, *Annals of Glaciology*, 41, 147-154, 2005.
- Mayewski, P. A., Meredith, M. P., Summerhayes, C. P., Turner, J., Worby, A., Barrett, P. J., Casassa, G., Bertler, N. A. N., Bracegirdle, T., Naveira Garabato, A. C., Bromwich, D., Campbell, H., Hamilton, G. S., Lyons, W. B., Maasch, K. A., Aoki, S., Xiao, C., and van Ommen, T.: State of the Antarctic and Southern Ocean climate system, *Rev. Geophys.*, 47, RG1003, doi: 10.1029/2007rg000231, 2009.
- Meredith, M., and King, J. C.: Rapid climate change in the ocean west of the Antarctic Peninsula during the second half of the 20th century, *Geophys. Res. Lett.*, 32, 1 - 5, doi: 10.1029/2005GL024042, 2005.
- Merlivat, L., and Jouzel, J.: Global Climatic Interpretation of the Deuterium-Oxygen 18 Relationship for Precipitation, *J. Geophys. Res.*, 84, 5029-5033, 1979.
- Meyer, H., Schönicke, L., Wand, U., Hubberten, H. W., and Friedrichsen, H.: Isotope Studies of Hydrogen and Oxygen in Ground Ice - Experiences with the Equilibration Technique, *Isot. Environ. Health. S.*, 36, 133 - 149, 2000.
- Monaghan, A. J., Bromwich, D. H., Chapman, W., and Comiso, J. C.: Recent variability and trends of Antarctic near-surface temperature, *J. Geophys. Res.*, 113, 1-21, 2008.
- Moore, G. W. K., Alverson, K., and Renfrew, I. A.: A reconstruction of the air-sea interaction associated with the Weddell polynya, *J. Phys. Oceanogr.*, 32, 1685-1698, 2002.
- Mudelsee, M., and Schulz, M.: The Mid-Pleistocene climate transition: onset of 100 ka cycle lags ice volume build-up by 280 ka, *Earth Planet Sc Lett*, 151, 117-123, 1997.
- Naik, S. S., Thamban, M., Laluraj, C. M., Redkar, B. L., and Chaturvedi, A.: A century of climate variability in central Dronning Maud Land, East Antarctica, and its relation to Southern Annular Mode and El Niño-Southern Oscillation, *J. Geophys. Res.*, 115, D16102, doi: 10.1029/2009jd013268, 2010.

- Noone, D., and Simmonds, I.: Sea ice control of water isotope transport to Antarctica and implications for ice core interpretation, *J. Geophys. Res.*, 109, doi: 10.1029/2003jd004228, 2004.
- Noone, D.: The influence of midlatitude and tropical overturning circulation on the isotopic composition of atmospheric water vapor and Antarctic precipitation, *J. Geophys. Res-Atmos.*, 113, -, doi 10.1029/2007jd008892, 2008.
- Oerter, H., Graf, W., Wilhelms, F., Minikin, A., and Miller, H.: Accumulation studies on Amundsenisen, Dronning Maud Land, Antarctica, by means of tritium, dielectric profiling and stable-isotope measurements: first results from the 1995-96 and 1996-97 field seasons, *Ann. Glaciol.*, 29, 1-9, 1999.
- Opel, T., Fritzsche, D., Meyer, H., Schütt, R., Weiler, K., Ruth, U., Wilhelms, F., and Fischer, H.: 115-year ice core data from Akademii Nauk ice cap (Severnaya Zemlya): high resolution record of Eurasian Arctic climate change, *J. Glaciol.*, 55, 21-31, 2009.
- Peel, D. A., Mulvaney, R., and Davison, B. M.: Stable-Isotope/Air-Temperature relationship in ice cores from Dolleman Island and the Palmer Land Plateau, Antarctic Peninsula, *Ann. Glaciol.*, 10, 130-136, 1988.
- Peel, D. A.: Ice core evidence from the Antarctic Peninsula region, in: *Climate since A.D. 1500*, 2 ed., edited by: Bradley, R., and Jones, P., Routledge, London, New York, 706, 1995.
- Pritchard, H. D., and Vaughan, D. G.: Widespread acceleration of tidewater glaciers on the Antarctic Peninsula, *J. Geophys. Res.*, 112, F03S29, doi: 10.1029/2006jf000597, 2007.
- Rau, F., and Braun, M.: The regional distribution of the dry-snow zone on the Antarctic Peninsula north of 70S, *Ann. Glaciol.*, 34, 95-100, 2002.
- Rayner, N. A., Parker, D. E., Horton, E. B., Folland, C. K., Alexander, L. V., Rowell, D. P., Kent, E. C., and Kaplan, A.: Global analyses of sea surface temperature, sea ice, and night marine air temperature since the late nineteenth century, *J. Geophys. Res-Atmos.*, 108, -, doi: 10.1029/2002jd002670, 2003.
- Rignot, E., and Thomas, R. H.: Mass Balance of Polar Ice Sheets, *Science*, 297, 1502-1506, 10.1126/science.1073888, 2002.
- Rignot, E., Casassa, G., Gogineni, P., Krabill, W., Rivera, A., and Thomas, R.: Accelerated ice discharge from the Antarctic Peninsula following the collapse of Larsen B ice shelf, *Geophys. Res. Lett.*, 31, 2004.
- Rignot, E., Casassa, G., Gogineni, S., Kanagaratnam, P., Krabill, W., Pritchard, H., Rivera, A., Thomas, R., Turner, J., and Vaughan, D.: Recent ice loss from the Fleming and other glaciers, Wordie Bay, West Antarctic Peninsula, *Geophys. Res. Lett.*, 32, 2005.
- Rignot, E.: Changes in ice dynamics and mass balance of the Antarctic ice sheet, *Philosophical Transactions of the Royal Society A: Mathematical, Physical and Engineering Sciences*, 364, 1637-1655, 10.1098/rsta.2006.1793, 2006.
- Robertson, R., Visbeck, M., Gordon, A. L., and Fahrbach, E.: Long-term temperature trends in the deep waters of the Weddell Sea, *Deep-Sea Res. Pt. II*, 49, 4791-4806, pii: S0967-0645(02)00159-5, 2002.
- Rotschky, G., Holmlund, P., Isaksson, E., Mulvaney, R., Oerter, H., Van Den Broeke, M. R., and Winther, J.-G.: A new surface accumulation map for western Dronning Maud Land, Antarctica, from interpolation of point measurements, *J. Glaciol.*, 53, 385-398, 2007.
- Rozanski, K., Araguás-Araguás, L., and Gonfiantini, R.: Isotopic Patterns in Modern Global Precipitation, in: *Climate Change in Continental Isotopic Records*, edited by: Swart, P. K., Lohman, K. C., McKenzie, J., and Savin, S., American Geophysical Union, Washington, USA, 1993.
- Rückamp, M., Blindow, N., Suckro, S., Braun, M., and Humbert, A.: Dynamics of the ice cap on King George Island, Antarctica: field measurements and numerical simulations, *Ann. Glaciol.*, 51, 80-90, 2010.
- Satake, H., and Kawada, K.: The quantitative evaluation of sublimation and the estimation of original hydrogen and oxygen ratios of a firn core at East Queen Maud Land, Antarctica, *Bulletin of Glacier Research*, 15, 93-97, 1997.
- Scambos, T. A., Hulbe, C., Fahnestock, M., and Bohlander, J.: The link between climate warming and break-up of ice shelves in the Antarctic Peninsula, *J. Glaciol.*, 46, 516-530, 2000.

- Scher, H. D., and Martin, E. E.: Timing and climatic consequences of the opening of Drake Passage, *Science*, 312, 428-430, 2006.
- Schlosser, E., Oerter, H., and Graf, W.: Snow Accumulation on Ekströmis, Antarctica, 1980-1996, *Ber. Polarforsch. Rep. Pol.*, 313, 1-29, 1999.
- Schlosser, E., and Oerter, H.: Seasonal variations of accumulation and the isotope record in ice cores: a study with surface snow samples and firn cores from Neumayer station, Antarctica, *Ann. Glaciol.*, 35, 97-101, 2002a.
- Schlosser, E., and Oerter, H.: Shallow firn cores from Neumayer, Ekströmis, Antarctica: a comparison of accumulation rates and stable-isotope ratios, *Ann. Glaciol.*, 35, 91-96, 2002b.
- Schlosser, E., van Lipzig, N., and Oerter, H.: Temporal variability of accumulation at Neumayer station, Antarctica, from stake array measurements and a regional atmospheric model, *J. Glaciol.*, 48, 87-94, 2002.
- Schlosser, E., Reijmer, C., Oerter, H., and Graf, W.: The influence of precipitation origin on the $\delta^{18}\text{O}$ -T relationship at Neumayer station, Ekströmis, Antarctica, *Ann. Glaciol.*, 39, 41-48, 2004.
- Schlosser, E., Oerter, H., Masson-Delmotte, V., and Reijmer, C.: Atmospheric influence on the deuterium excess signal in polar firn: implications for ice-core interpretation, *J. Glaciol.*, 54, 117-124, 2008.
- Schneider, D. P., Steig, E. J., van Ommen, T. D., Dixon, D. A., Mayewski, P. A., Jones, J. M., and Bitz, C. M.: Antarctic temperatures over the past two centuries from ice cores, *Geophys. Res. Lett.*, 33, 1-5, doi: 10.1029/2006GL027057, 2006.
- Schulz, M., and Stattegger, K.: SPECTRUM: Spectral analysis of unevenly spaced paleoclimatic time series, *Comput Geosci*, 23, 929-945, 1997.
- Schulz, M., and Mudelsee, M.: REDFIT: estimating red-noise spectra directly from unevenly spaced paleoclimatic time series, *Comput Geosci*, 28, 421-426, 2002.
- Schwerdtfeger, W.: Effect of Antarctic Peninsula on Temperature Regime of Weddell Sea, *Mon. Weath. Rev.*, 103, 45-51, 1975.
- Sharp, Z. (Eds): *Principles of Stable Isotope Geochemistry*, 1st ed., Pearson/Prentice Hall, Upper Saddle River, NJ, 344 pp., 2007.
- Shepherd, A., Wingham, D., and Rignot, E.: Warm ocean is eroding West Antarctic Ice Sheet, *Geophys. Res. Lett.*, 31, 1-4, 2004.
- Sime, L. C., Marshall, G. J., Mulvaney, R., and Thomas, E. R.: Interpreting temperature information from ice cores along the Antarctic Peninsula: ERA40 analysis, *Geophys. Res. Lett.*, 36, L18801, doi: 10.1029/2009gl038982, 2009.
- Simmonds, I.: Regional and Large-Scale Influence on Antarctic Peninsula Climate, in: *Antarctic Peninsula Climate Variability. Historical and paleoenvironmental perspectives.*, edited by: Domack, E. W., Leventer, A., Burnett, A., Bindshadler, R., Convey, P., and Kirby, M., Antarctic Research Series, American Geophysical Union, Washington, D.C., 31-42, 2003.
- Simões, J., Ferron, F., Bernardo, R., Aristarain, A., Stievenard, M., Pourchet, M., and Delmas, R.: Ice core study from the King George Island, South Shetlands, Antarctica., *Pesquisa Antártica Brasileira*, 4, 9-23, 2004a.
- Simões, J., Goßmann, H., Delmas, R., and Moskalevsky, M.: Glaciological research in King George Island: missions and developments in the 1990s, *Pesquisa Antártica Brasileira*, 4, 1-8, 2004b.
- Simões, J. C., Bremer, U. F., Aquino, F. E., and Ferron, F. E.: Morphology and variations of glacial drainage basins in the King George Island ice field, Antarctica, *Ann. Glaciol.*, 29, 220-224, 1999.
- Smith, S. R., Legler, D. M., and Verzone, K. V.: Quantifying uncertainties in NCEP reanalyses using high-quality research vessel observations, *J. Climate*, 14, 4062-4072, 2001.
- Steig, E. J., Schneider, D. P., Rutherford, S. D., Mann, M. E., Comiso, J. C., and Shindell, D. T.: Warming of the Antarctic ice-sheet surface since the 1957 International Geophysical Year, *Nature*, 457, 459-462, 2009.

- Steinhage, D., Nixdorf, U., Meyer, U., and Miller, H.: New maps of the ice thickness and subglacial topography in Dronning Maud Land, Antarctica, determined by means of airborne radio-echo sounding, *Ann. Glaciol.*, **29**, 267-272, 1999.
- Stenni, B., Buiron, D., Frezzotti, M., Albani, S., Barbante, C., Bard, E., Barnola, J. M., Baroni, M., Baumgartner, M., Bonazza, M., Capron, E., Castellano, E., Chappellaz, J., Delmonte, B., Falourd, S., Genoni, L., Iacumin, P., Jouzel, J., Kipfstuhl, S., Landais, A., Lemieux-Dudon, B., Maggi, V., Masson-Delmotte, V., Mazzola, C., Minster, B., Montagnat, M., Mulvaney, R., Narcisi, B., Oerter, H., Parrenin, F., Petit, J. R., Ritz, C., Scarchilli, C., Schilt, A., Schupbach, S., Schwander, J., Selmo, E., Severi, M., Stocker, T. F., and Udisti, R.: Expression of the bipolar see-saw in Antarctic climate records during the last deglaciation, *Nature Geosci.*, **4**, 46-49, doi: 10.1038/ngeo1026, 2010a.
- Stenni, B., Masson-Delmotte, V., Selmo, E., Oerter, H., Meyer, H., Röthlisberger, R., Jouzel, J., Cattani, O., Falourd, S., Fischer, H., Hoffmann, G., Iacumin, P., Johnsen, S. J., Minster, B., and Udisti, R.: The deuterium excess records of EPICA Dome C and Dronning Maud Land ice cores (East Antarctica), *Quat. Sci. Rev.*, **29**, 146-159, 2010b.
- Tedesco, M., Abdalati, W., and Zwally, H. J.: Persistent surface snowmelt over Antarctica (1987-2006) from 19.35 GHz brightness temperatures, *Geophys. Res. Lett.*, **34**, -, doi: 10.1029/2007gl031199, 2007.
- Thomas, E. R., Marshall, G. J., and McConnell, J. R.: A doubling in snow accumulation in the western Antarctic Peninsula, *Geophys. Res. Lett.*, **35**, 1-5, doi: 10.1029/2007GL032529, 2008.
- Thomas, E. R., and Bracegirdle, T. J.: Improving ice core interpretation using in situ and reanalysis data, *J. Geophys. Res.*, **114**, D20116, doi: 10.1029/2009jd012263, 2009.
- Thomas, E. R., Dennis, P. F., Bracegirdle, T. J., and Franzke, C.: Ice core evidence for significant 100-year regional warming on the Antarctic Peninsula, *Geophys. Res. Lett.*, **36**, -, doi: 10.1029/2009gl040104, 2009.
- Thompson, D. W. J., and Solomon, S.: Interpretation of Recent Southern Hemisphere Climate Change, *Science*, **296**, 895-899, doi: 10.1126/science.1069270, 2002.
- Traufetter, F., Oerter, H., Fischer, H., Weller, R., and Miller, H.: Spatio-temporal variability in volcanic sulphate deposition over the past 2 kyr in snow pits and firn cores from Amundsenisen, Antarctica, *J. Glaciol.*, **50**, 137-146, 2004.
- Trenberth, K. E.: The Definition of El Niño, *B. Am. Soc. Meteorol. Soc.*, **78**, 2771-2777, doi:10.1175/1520-0477(1997)078<2771:TDOENO>2.0.CO;2, 1997.
- Trenberth, K. E., and Caron, J. M.: The Southern Oscillation Revisited: Sea Level Pressures, Surface Temperatures, and Precipitation, *Journal of Climate*, **13**, 4358-4365, doi:10.1175/1520-0442(2000)013<4358:TSORSL>2.0.CO;2, 2000.
- Trenberth, K. E., and Stepaniak, D. P.: Indices of El Niño Evolution, *J. Climate*, **14**, 1697-1701, doi:10.1175/1520-0442(2001)014<1697:LIOENO>2.0.CO;2, 2001.
- Trenberth, K. E., Jones, P. D., Ambenje, P., Bojariu, R., Easterling, D., Tank, A. K., Parker, D., Rahimzadeh, F., Renwick, J. A., Rusticucci, M., Soden, B., and Zhai, P.: Observations: Surface and Atmospheric Climate Change, in: *Climate Change 2007: The Physical Science Basis. Contribution of Working Group I to the Fourth Assessment Report of the Intergovernmental Panel on Climate Change*, edited by: Solomon, S., Qin, D., Manning, M., Chen, Z., Marquis, M., Averyt, K. B., Tignor, M., and Miller, H. L., Cambridge University Press, Cambridge, United Kingdom and New York, NY, USA, 237-336, 2007.
- Turner, J., Lachlan-Cope, T., Marshall, G. J., Morris, E. M., and Mulvaney, R.: Spatial variability of Antarctica Peninsula net surface mass balance, *J. Geophys. Res.*, **107**, 2002.
- Turner, J.: Review: The El Niño-Southern Oscillation and Antarctica, *Int. J. Climatol.*, **24**, 1-31, 2004.
- Turner, J., Colwell, S. R., Marshall, G. J., Lachlan-Cope, T. A., Carleton, A. M., Jones, P. D., Lagun, V., Reid, P. A., and Iagovkina, S.: The SCAR READER project: Toward a high-quality database of mean Antarctic meteorological observations, *J. Climate*, **17**, 2890-2898, 2004.
- Turner, J., Colwell, S. R., Marshall, G. J., Lachlan-Cope, T. A., Carleton, A. M., Jones, P. D., Lagun, V., Reid, P. A., and Iagovkina, S.: Antarctic climate change during the last 50 years, *Int. J. Climatol.*, **25**, 279-294, 2005.

- Turner, J., Bindschadler, R., Convey, P., di Prisco, G., Fahrbach, E., Gutt, J., Hodgson, D., Mayewski, P., and Summerhayes, C. (Eds): Antarctic Climate Change and the Environment, 1st ed., Scientific Committee on Antarctic Research, Cambridge, 2009.
- Tymofeyev, V.: On the role of tropospheric circulation in recent climate changes in the Antarctic Peninsula region, *Bulletin of Geography - physical geography series*, 63-75, 2009.
- Uemura, R., Matsui, Y., Yoshimura, K., Motoyama, H., and Yoshida, N.: Evidence of deuterium excess in water vapor as an indicator of ocean surface conditions, *J. Geophys. Res.*, 113, 1-10, 2008.
- Uemura, R., Abe, O., and Motoyama, H.: Determining the $^{17}\text{O}/^{16}\text{O}$ ratio of water using a water- CO_2 equilibration method: Application to glacial-interglacial changes in ^{17}O -excess from the Dome Fuji ice core, *Antarctica, Geochimica Et Cosmochimica Acta*, 74, 4919-4936, doi: 10.1016/j.gca.2010.05.007, 2010.
- van den Broeke, M.: Strong surface melting preceded collapse of Antarctic Peninsula ice shelf, *Geophys. Res. Lett.*, 32, L12815, doi: 10.1029/2005gl023247, 2005.
- van den Broeke, M., van de Berg, W. J., and van Meijgaard, E.: Snowfall in coastal West Antarctica much greater than previously assumed, *Geophys. Res. Lett.*, 33, L02505, doi: 10.1029/2005gl025239, 2006.
- van den Broeke, M. R.: The semi-annual oscillation and Antarctic climate. Part 1: Influence on near surface temperatures (1957-79), *Antarct. Sci.*, 10, 175-183, 1998.
- van den Broeke, M. R., van Lipzig, N. P. M., and van Meijgaard, E.: Momentum Budget of the East Antarctic Atmospheric Boundary Layer: Results of a Regional Climate Model, *Journal of the Atmospheric Sciences*, 59, 3117-3129, 2002.
- van den Broeke, M. R., and van Lipzig, N. P. M.: Factors Controlling the Near-Surface Wind Field in Antarctica, *Mon. Weath. Rev.*, 131, 733-743, 2003.
- van den Broeke, M. R., and van Lipzig, N. P. M.: Changes in Antarctic temperature, wind and precipitation in response to the Antarctic Oscillation, *Ann. Glaciol.*, 39, 119-126, 2004.
- van Lipzig, N. P. M., King, J. C., Lachlan-Cope, T. A., and van den Broeke, M. R.: Precipitation, sublimation, and snow drift in the Antarctic Peninsula region from a regional atmospheric model, *J. Geophys. Res.*, 109, D24106, doi: 10.1029/2004jd004701, 2004.
- van Ommen, T. D., and Morgan, V.: Calibrating the ice core paleothermometer using seasonality, *J. Geophys. Res-Atmos.*, 102, 9351-9357, 1997.
- Vaughan, D. G., Marshall, G. J., Connolley, W. M., Parkinson, C., Mulvaney, R., Hodgson, D. A., King, J. C., Pudsey, C. J., and Turner, J.: Recent Rapid Regional Climate Warming on the Antarctic Peninsula, *Climatic Change*, 60, 243-274, 2003.
- Weatherly, J. W., Walsh, J. E., and Zwally, H. J.: Antarctic Sea Ice Variations and Seasonal Air-Temperature Relationships, *J. Geophys. Res-Oceans*, 96, 15119-15130, 1991.
- Wei, W. C.: Opening of the Australia-Antarctica Gateway as dated by nannofossils, *Mar. Micropaleontol.*, 52, 133-152, 2004.
- Weiler, K., Fischer, H., Fritzsche, D., Ruth, U., Wilhelms, F., and Miller, H.: Glaciochemical reconnaissance of new ice core from Severnaya Zemlya, Eurasian Arctic, *J. Glaciol.*, 51, 64-74, 2005.
- Wen, J. H., Kang, J. C., Han, J. K., Xie, Z. C., Liu, L. B., and Wang, D. L.: Glaciological studies on the King George Island ice cap, South Shetland Islands, Antarctica, *Ann. Glaciol.*, 27, 105-109, 1998.
- Wesche, C., Riedel, S., and Steinhage, D.: Precise surface topography of the grounded ice ridges at the Ekströmisen, Antarctica, based on several geophysical data sets, *ISPRS Journal of Photogrammetry and Remote Sensing*, 64, 381-386, 2009.
- White, W. B., and Peterson, R. G.: An Antarctic circumpolar wave in surface pressure, wind, temperature and sea-ice extent, *Nature*, 380, 699-702, 1996.
- Wilhelms, F.: Messung dielektrischer Eigenschaften polarer Eiskerne, *Ber. Polarforsch. Rep. Pol.*, 367, 1-171, 2000.

- Wilhelms, F.: Explaining the dielectric properties of firn as a density-and-conductivity mixed permittivity (DECOMP), *Geophys. Res. Lett.*, 32, doi: 10.1029/2005gl022808, 2005.
- Zazulie, N., Rusticucci, M., and Solomon, S.: Changes in Climate at High Southern Latitudes: A Unique Daily Record at Orcadas Spanning 1903-2008, *J. Climate*, 23, 189-196, doi:10.1175/2009JCLI3074.1, 2010.
- Zhou, S., Nakawo, M., Hashimoto, S., and Sakai, A.: The effect of refreezing on the isotopic composition of melting snowpack, *Hydrological Processes*, 22, 873-882, 2008.